Dielectric Spectroscopy of Colloidal Quantum Dots in Apolar Liquids

Universiteit Utrecht

ISBN 978-90-393-6075-0
Subject headings: Quantum dots / colloids / dipole moment / electric double layer / dielectric spectroscopy / electroacoustics.

Dielectric Spectroscopy of Colloidal Quantum Dots in Apolar Liquids

Diëlektrische Spectroscopie van Colloïdale Quantum Dots in Apolaire Vloeistoffen

(met een samenvatting in het Nederlands)

Proefschrift

ter verkrijging van de graad van doctor aan de
Universiteit Utrecht op gezag van de rector magnificus,
prof. dr. G. J. van der Zwaan, ingevolge het besluit van het
college voor promoties in het openbaar te verdedigen
op woensdag 15 januari 2014 des middags te 2.30 uur

door

Robert Jan Kortschot

geboren op 25 juni 1985 te Gorinchem

Promotor: Prof. dr. A.P. Philipse

Co-promotor: Dr. B.H. Erné

Het in dit proefschrift beschreven onderzoek werd gefinancierd door het gebied chemische wetenschappen (CW) van de Nederlandse Organisatie voor Wetenschappelijk Onderzoek (NWO).

Contents

1

General Introduction

1.1. Colloidal Quantum Dots

Colloidal quantum dots (QDs) are 2 - 10 nm particles of a semiconductor material, consisting typically of a few thousand atoms [1]. These particles are able to absorb and emit light, and their luminescent color depends not only on the material itself, but also on their size. Photoluminescence in a semiconductor occurs after an absorbed photon excites an electron from the valence band to the conduction band. The excited electron is delocalized from its atom within a typical Bohr radius of a few nanometers. In a quantum dot with a radius smaller than the Bohr radius, an excited electron is confined by the boundaries of the particle, and the bandgap is size dependent. This quantum confinement effect resembles the quantum mechanical particle-in-a-box model [2, 3].

Due to their high photoluminescence and tunability, the particles find various electronic and optoelectronic applications [4], such as in light emitting devices, solar cells, television screens, telecommunication devices, and photodetectors. Quantum dots also act as building blocks themselves for the formation of new materials such as superlattices, whose properties are also tunable, for instance by varying the size ratio, or by using different types of nanoparticles.

The most popular way to synthesize monodisperse colloidal nanoparticles is the hot injection method, which involves the quick injection of organometallic precursors into a hot apolar solvent [5, 6]. Rapid nucleation is followed by a drop in temperature, quenching the nucleation, and the nuclei are allowed to grow to the desired size. Organic ligands cover the surface of the particles and provide steric stabilization against aggregation. Additionally, these ligands passivate

electronic surface traps and thus improve photoluminescence. Further advances in synthesis have led to a variety of shapes and different materials.

The interest in the electrical properties of QDs, in particular their permanent dipole moment and their net charge, is threefold. An internal electric field due to a dipole moment or net charge influences the electronic structure and transition rules. Furthermore, they play an important role in understanding colloidal interactions between QDs in self-assembly processes. And they are crucial for directed assembly using electric fields. The main topic of this thesis is the characterization of dipole moments and net charges using dielectric spectroscopy.

1.2. CHARGES

A polar liquid consists of molecules that, though overall charge neutral, have their charge asymmetrically distributed. This permanent electric dipole moment is important for electrostatic screening, reflected in a high dielectric constant compared to apolar liquids, whose molecules have no or only a small dipole moment. A direct consequence is that monovalent electrolytes dissociate easily into free ions in a polar liquid, such as water (dielectric constant ϵ_s = 80), whereas in an apolar liquid ($\epsilon_s < 5$), dissociation of a salt is energetically unfavorable, hence ions do not dissolve or they form neutral ion pairs [7]. The influence of the dielectric constant on the solvation of ions depends on the Coulombic interaction free energy $w(r) = q^2/(4\pi\epsilon_0\epsilon_s r)$ between two ions with charge q at a distance r. Additionally, large ions are better separated as an ion pair, hence they dissolve more easily than small ions. Colloidal quantum dots in apolar solvents are usually assumed to be charge neutral and symmetric. This turns out to be an idealistic picture.

1.3. DIELECTRIC SPECTROSCOPY

Dielectric spectroscopy is in fact electrical impedance spectroscopy of a dielectric medium between two electrodes. The dielectric response of a system is measured when subjected to a small sinusoidal voltage with frequency f (or angular frequency $\omega = 2\pi f$) [8]. The relation between the applied voltage and the measured current provides information on the system under study. The response of the system can be expressed in various ways; most common is the impedance $Z(\omega) = V(\omega)/I(\omega)$, the ratio between the applied voltage $V(\omega)$ and measured current $I(\omega)$. A different expression for the response is the complex permittivity, which will be defined in Chapter 2. The impedance is either expressed by its amplitude and phase or as a complex quantity consisting of a real and an imaginary part. This is illustrated in Fig. 1.1 for two examples. The solvent with dielectric

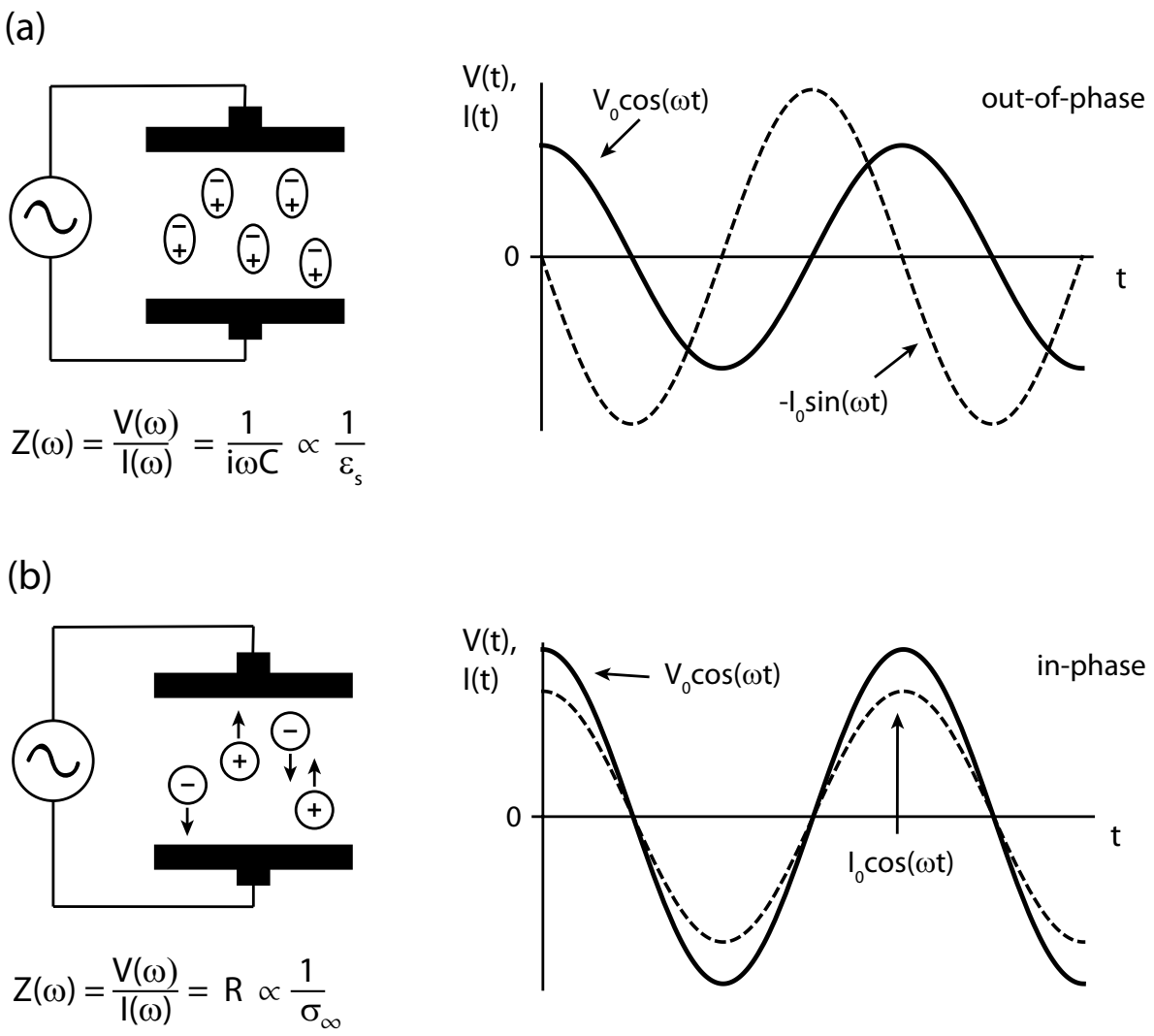

FIGURE 1.1. Illustration of two typical responses measured with dielectric spectroscopy. In (a), induced dipoles give rise to a current $I(\omega)$ that is out-of-phase with the applied voltage $V(\omega)$, and its impedance $Z(\omega)$ is inversely proportional to the dielectric constant. In (b), charges migrate and give rise to a current that is in-phase with the applied voltage, and the impedance is inversely proportional to the conductivity.

constant ϵ_s in Fig. 1.1a conducts a current that is shifted by a phase of 90 degrees compared to the applied voltage. The voltage and current are 'out-of-phase' and the impedance is an imaginary number, inversely proportional to ϵ_s. The electrical charges in Fig. 1.1b, for instance ions, conduct a current that has the same phase as the voltage. The voltage and current are 'in-phase' and the impedance is a real number; it is the resistance, inversely proportional to the conductivity σ_∞.

Sinusoidal voltages and currents are often expressed as complex numbers for mathematical convenience; however, they are truly physical quantities. In the time domain, they are always represented by the real part of their complex function. Thus, in Fig. 1.1a the complex voltage $V_0 e^{i\omega t}$ represents the real voltage $Re[V_0 e^{i\omega t}] = V_0 \cos(\omega t)$, and the complex current $i\omega C V_0 e^{i\omega t}$ represents the current $Re[i\omega C V_0 e^{i\omega t}] = -C V_0 \sin(\omega t)$. Generally, the measured signal is the sum of an in-phase and an out-of-phase component. The response of a system can be compared to a physical model or to an equivalent circuit, which is an electronic circuit of resistors, capacitors, inductors, and/or other circuit elements.

1.4. ELECTROSTATIC DOUBLE LAYERS

When a charged wall is in contact with an ionic solution, an excess of ions of opposite charge will reside near the wall, resulting in what is called an electrical double layer. In dielectric spectroscopy measurements, double layers form at low frequencies, when charged species are present and migrate to the electrodes. In the case of colloidal particles in a polar liquid, they usually acquire a net charge spontaneously, due to for instance dissociation of surface chemical groups or specific absorption. The double layers that surround colloidal particles are crucial for their colloidal stability. Overlapping double layers of two adjacent particles exert a repulsive osmotic pressure, which prevents them from aggregation, as described by the DLVO theory [9,10]. The characteristics of electrical double layers are often inferred from electrokinetic phenomena, that is either the motion of particles or fluid in an electric field, or the generation of a voltage or current due to particle or liquid motion [11, 12]. The mobility of a charged colloidal particle in an electric field depends strongly on its surrounding ionic cloud, which exerts an opposing force on the particle. Interpretation of the mobility in terms of the surface charge or surface potential, though, is complicated due to the strong dependence on the thin layer close to the surface.

A commonly used and convenient method to measure the electrophoretic mobility is laser Doppler electrophoresis [13], which measures the electrophoretic velocity from the Doppler shift of the scattered light of a laser beam. A less common method is electroacoustics [14]. This technique applies a sound wave to generate colloidal motion based on the density difference between particle and solvent, and this motion is detected as an electrical current if the particles are charged. Laser Doppler electrophoresis and electroacoustics are thus two complementary techniques which measure the same phenomenon but are based on different effects.

1.5. THIS THESIS

The main topic of this thesis is the study of the electrical properties of colloidal quantum dots in an apolar liquid measured with dielectric spectroscopy. This non-optical technique was chosen in view of the sensitivity of QDs to light. The dielectric measurements are performed with a homebuilt differential complex permittivity setup, described in **Chapter 2**. Rather than the total permittivity, this setup measures only the contribution of the quantum dots to the complex permittivity, to measure at the highest sensitivity. It is typically observed in such measurements that at low frequencies the electrodes are polarized by charged species. Electrode polarization is studied in **Chapter 3** for several electrolytes in both polar and apolar solvents, with specific attention to the effect of ionic strength. Then, in **Chapter 4**, the response of colloidal PbSe and CdSe quantum dots is measured, to obtain information on their dipole moment, net charge, and interparticle interactions. Another non-optical technique, electroacoustics, is explored in **Chapter 5**, using a model system of charged silica colloids in ethanol. A comparison is made between the electrophoretic mobility measured with laser Doppler electrophoresis and the dynamic mobility measured with electroacoustics.

2

Differential Dielectric Spectroscopy Setup to Measure the Electric Dipole Moment and Net Charge of Colloidal Quantum Dots

ABSTRACT

A sensitive dielectric spectroscopy setup is built to measure the response of colloidal quantum dots dispersed in a liquid to an alternating electric field over a frequency range from 10^{-2} to 10^{7} Hz. The measured complex permittivity spectrum records both the rotational dynamics due to a permanent electric dipole moment and the translational dynamics due to net charges. The setup consists of a half-transparent capacitor in a bridge circuit, which is balanced on pure solvent only, using a software-controlled compensating voltage. In this way, the measured signal is dominated by the contributions of the quantum dots rather than by the solvent. We demonstrate the performance of the setup with measurements on a dispersion of colloidal CdSe nanoparticles.

2.1. INTRODUCTION

Two essential electric properties of colloidal semiconductor nanoparticles, so-called quantum dots, are their net charge and permanent electric dipole moment. They affect their optical properties [15] and colloidal interactions [16, 17], for instance enabling controlled assembly of particles on a substrate using electric fields [18]. The electric properties can be determined from the complex permittivity spectrum when the particles are dispersed in a liquid [19, 20]. Dilute dispersions have the advantage of avoiding interparticle interactions and of limiting the required amount of precious particles, but the relative contribution of the nanoparticle dipole moments to the permittivity spectrum is weak. To optimize sensitivity, we built a complex dielectric spectroscopy setup whose output signal can be nullified in the absence of nanoparticles, so that after they are added to the liquid, their contribution dominates the measured signal.

Both dipole moment and charge of colloidal quantum dots can be determined by dielectric spectroscopy. The permanent electric dipole moment of particles with a hydrodynamic radius on the order of 2 to 8 nm dispersed in a liquid with a viscosity of about 1 mPa·s is observable in the permittivity spectrum as a Debye relaxation in the 10^5 - 10^7 Hz frequency range [19, 20]. Net charge on the particles gives rise to conductivity of the dispersion and polarization of the electrodes [20, 21], with a relaxation frequency of typically 10^{-1} - 10^3 Hz, a function of cell geometry, ion concentration, and mobility of the charged particles. Either the dipole moment or the net charge can also be measured by other techniques. Dipole moments have been measured using optical spectroscopy [22] or with transient electric birefringence (for rod-like particles) [23]. Net charges have been determined by transient current analysis [24] and laser Doppler electrophoresis [25]. Additionally, it has been shown by electrostatic force microscopy that quantum dots can acquire a net charge upon illumination [26]. Here, by measuring the permittivity spectrum from 10^{-2} - 10^7 Hz using a transparent capacitor, we want to make it possible to measure both the net charge and permanent dipole moment in the dark and under illumination in a single setup.

Dielectric spectroscopy is well-known in soft matter science and has been applied to many materials, for instance polymers [27], proteins [28], and colloids [29]. Commercial analyzers for dielectric spectroscopy generally include automatic balancing bridges and frequency response analysis [30, 31]. The bridge achieves balance by automatically adjusting capacitive and resistive components [32–34], and the permittivity at a particular frequency is calculated from the circuit components in the balanced situation. Phase-dependent voltages are measured using gain-phase analyzers, vector voltmeters, or lock-in amplifiers. A

broad frequency range can be accessed thanks to measurement resistors whose values can be selected on a logarithmic scale [35]. The end result is the total permittivity of the sample. Our own objective is to measure directly the *excess* permittivity from the differential signal of a bridge circuit. Background signal is removed using a software-controlled phase-dependent compensating voltage [36–38]. The bridge is balanced on pure solvent, and upon addition of colloidal nanoparticles, the complex excess permittivity is measured at the highest possible sensitivity of the lock-in amplifier.

This chapter is organized as follows: the experimental setup is presented in section 2.2, followed by its characterization and calibration in section 2.3. Example permittivity spectra are shown in section 2.4, and conclusions are drawn in section 2.5.

2.2. EXPERIMENTAL SETUP

2.2.1. General Principle

A differential impedance bridge is used, in which two capacitors are compared (Fig. 2.1) to measure the complex excess permittivity $\epsilon^{\mathrm{ex}}(\omega)$:

$$\epsilon^{\mathrm{ex}}(\omega) = \epsilon(\omega) - \epsilon_s \tag{2.1}$$

where $\epsilon(\omega)$ is the permittivity of the colloidal dispersion, ϵ_s is the permittivity of the solvent, and $\omega = 2\pi f$ is the angular frequency. Capacitor C_A is a reference capacitor with capacitance C_A or C, and capacitor C_B contains either dispersion or solvent and has capacitance C_B. The voltage $V_{\mathrm{A-B}}$ is proportional to the difference ΔC in capacitance between sample and reference capacitors. Ideally, the reference capacity is such that ΔC is zero at each frequency for a background measurement (ΔC_{bg}), i.e., the sample capacitor filled with pure solvent. Then, the excess complex capacitance or permittivity can be measured with a sample measurement (ΔC_s), i.e., the sample capacitor filled with a dispersion. In practice, the bridge is never exactly balanced and ΔC_{bg} is neither zero nor frequency independent. To measure at the highest sensitivity, not limited by any offset, a compensating voltage V_{comp} is applied in both the sample and the background measurement. This is similar to the approach that we followed to develop a differential magnetic susceptibility setup [36]. A sample capacitor with one transparent ITO electrode was constructed to allow measurements under illumination.

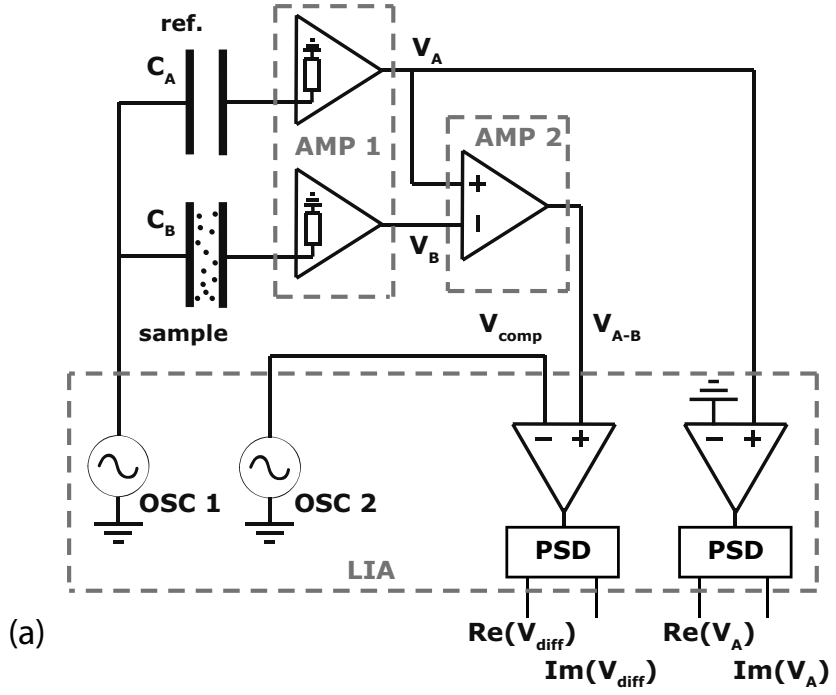

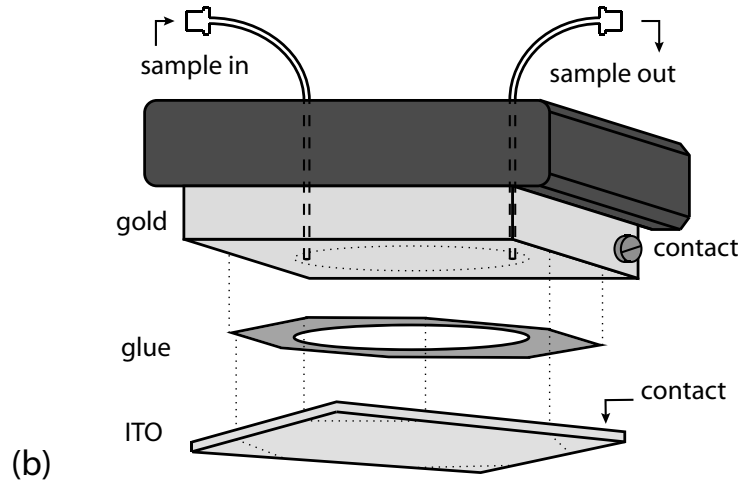

FIGURE 2.1. Schematic diagrams of (a) the differential permittivity measurement circuit and (b) the transparent capacitor.

2.2.2. Hardware

The setup consists of a Zurich Instruments HF2LI differential lock-in amplifier (LIA) with two oscillation outputs (OSC1/OSC2), and two external Zurich Instruments HF2CA current pre-amplifiers (AMP1/AMP2).

The signals of the reference and sample branches, V_{A} and V_{B}, respectively, are measured with the two independent amplification channels of the first amplifier (AMP1), which has a 10^1 - 10^6 Ω selectable measurement resistor. These signals

are subtracted using the second amplifier (AMP2), yielding $V_{\mathrm{A-B}}$. A second output (OSC2) is used to apply a compensating voltage (V_{comp}), to reduce any offset if the impedance bridge is not perfectly balanced at a particular frequency. This voltage is subtracted from $V_{\mathrm{A-B}}$ by the LIA, yielding V_{diff}. The voltage of the reference branch V_{A} is also measured separately, providing magnitude and phase of the reference capacitor.

The transparent capacitor consists of one gold-plated electrode (25 mm $\times$ 25 mm $\times$ 7.5 mm) and one indium tin oxide (ITO) coated glass electrode (25 mm $\times$ 25 mm $\times$ 1.1 mm, surface resistivity 8-12 Ω/sq, Sigma Aldrich). Both square electrodes are glued together on the edges with adhesive (Araldite, AW2101/HW2951), through which 75 μm diameter glass spacer beads (Sigma Aldrich) are mixed. Two PTFE syringe tubes (Sigma Aldrich) are glued in two holes (diameter = 1 mm) through the gold electrode to fill the capacitor with dispersion. Conductive silver epoxy (SPI, #05062) is used for electrical contact with the ITO electrode.

An adjustable capacitor with aluminum electrodes and teflon spacer was used as reference capacitor. Its capacitance was measured independently with an HP4192A impedance analyzer. The circuit was placed in an electrically grounded and thermally insulated box with internal copper walls in contact with copper tubing thermostatized using liquid pumped from a Julabo F25 thermostatic bath ($\pm$ 0.01 °C).

2.2.3. Measurement Procedure

Determination of the excess capacitance C^{ex} requires measurement of V_{diff} and V_{A}, both for a sample measurement on dispersion and a background measurement on pure solvent. Additionally, the nullification procedure is necessary to determine and to apply a compensating voltage V_{comp}. All measurement procedures were implemented on a PC using LABVIEW software.

The measurement procedure is as follows. First, the capacitor is filled with a sample and the voltage $V_{\mathrm{A\text{-}B}}$ is measured directly without compensating voltage, starting with the least sensitive range of the LIA, and switching successively to more sensitive ranges if no overload is expected [36]. Second, a compensating voltage V_{comp} is applied, which is set equal to the measured voltage $V_{\mathrm{A\text{-}B}}$, and the remnant signal V_{diff} is measured. Third, since V_{diff} is not necessarily zero, V_{comp} is adjusted by an iterative procedure as discussed below, to further reduce V_{diff}. Finally, the capacitor is filled with pure solvent and, while the optimal V_{comp} is applied, V_{diff} is measured at the highest sensitivity. Independently from this nullification procedure, the voltage V_{A} is measured.

The compensating voltage V_{comp} necessary to nullify V_{diff}, in order to reduce any offset, was determined by an iterative nullification procedure that we developed for this setup [38]. This procedure rapidly converges to the noise-limited minimum by taking into account the instrumental damping and phase shifting of V_{comp} in terms of an empirical complex constant $\tilde{\alpha}$. According to this procedure, the output of the circuit is determined in the n-th step of the iteration by $V_{\mathrm{diff}}^{\mathrm{n}} = V_{\mathrm{A-B}} - \tilde{\alpha} V_{\mathrm{comp}}^{n}$. After the initializing step, in which $V_{\mathrm{comp}}^{0} = V_{\mathrm{A-B}}$, the compensating voltage is then determined by:

$$V_{\mathrm{comp}}^{n+1} = \frac{V_{\mathrm{A-B}}}{\tilde{\alpha}} = \frac{V_{\mathrm{comp}}^{n}}{1 - (V_{\mathrm{diff}}^{n}/V_{\mathrm{A-B}})} \tag{2.2}$$

As explained in reference [36], it is preferred to perform the nullification procedure during the sample measurement and to apply the same compensating voltage again during the background measurement, instead of the other way around.

The selectable measurement resistors of AMP1 are chosen to be as large as possible, but with the restriction $\omega RC < 0.015$, where R is the measurement resistance. AC coupling is selected for AMP1 and AMP2 at frequencies above 100 kHz. An oscillating voltage of 1 V was applied, unless stated otherwise. Usually, 10 data points are averaged at each frequency. Calibration of the setup was performed at 22.0 °C with toluene (J.T. Baker), cyclohexane (Interchema) and diethyl ether (Biosolve).

2.2.4. Calculation of the Permittivity

The electric circuit allows calculation of the difference between capacitances, $\Delta C = C_{\mathrm{B}} - C$, by measuring the voltage over the reference resistor, V_{A}, and the voltage difference between the two resistors, $V_{\mathrm{A-B}}$. In the case of $\omega RC \ll 1$:

$$\Delta C = -C \frac{V_{\mathrm{A-B}}}{V_{\mathrm{A}}} \tag{2.3}$$

To exclude any additional capacitance resulting from an imperfectly balanced bridge, the increment in capacitance due to the sample is determined from a sample measurement (s, with sample) and a background measurement (bg, without sample):

$$C^{\mathrm{ex}} = \Delta C^{\mathrm{s}} - \Delta C^{\mathrm{bg}} = -C \left(\frac{V_{\mathrm{A-B}}^{\mathrm{s}}}{V_{\mathrm{A}}^{\mathrm{s}}} - \frac{V_{\mathrm{A-B}}^{\mathrm{bg}}}{V_{\mathrm{A}}^{\mathrm{bg}}} \right) \tag{2.4}$$

provided that $\omega RC \ll 1$ and $\omega RC \cdot V_{\mathrm{A-B}}/V_{\mathrm{A}} \ll 1$.

The nullification procedure applies a compensating voltage to cancel any remaining signal, which is required in the case that the sample signal is smaller than the additional capacitance due to an imperfectly balanced bridge. In this

case, one measures $V_{\mathrm{diff}} = V_{\mathrm{A-B}} - V_{\mathrm{comp}}$ and C^{ex} is determined from:

$$C^{\mathrm{ex}} = -C\left(\frac{V_{\mathrm{diff}}^{\mathrm{s}}}{V_{\mathrm{A}}^{\mathrm{s}}} - \frac{V_{\mathrm{diff}}^{\mathrm{bg}}}{V_{\mathrm{A}}^{\mathrm{bg}}}\right) \tag{2.5}$$

provided that $\omega RC \ll 1$ and $\omega RC \cdot V_{\mathrm{diff}}/V_{\mathrm{A}} \ll 1$.

Measurements of electrode polarization at lower frequencies require less sensitivity, and alternatively, V_{B} can be measured directly. In this case, the reference branch is disconnected, and C_B is obtained from:

$$C_B = \frac{V_{\mathrm{B}}}{i\omega R V_{\mathrm{app}}} \tag{2.6}$$

with V_{app} the applied voltage.

The complex excess relative permittivity due to the nanoparticles ϵ^{ex} is given by:

$$C^{\mathrm{ex}} = K_{\mathrm{c}}\epsilon^{ex} \approx \frac{A}{d}\epsilon_0\epsilon^{ex} \tag{2.7}$$

with K_{c} the cell constant of the capacitor, A the surface area of the capacitor, d the spacing between the capacitor plates, and ϵ_0 the vacuum permittivity.

2.3. CHARACTERIZATION AND CALIBRATION

The setup is characterized and calibrated with organic solvents of known permittivity and low conductivity. The results are used to determine the cell constant of the capacitor.

The impedance spectra of the transparent capacitor with different solvents (Fig. 2.2a) resemble that of a capacitor and resistor in parallel, though not perfectly. When measured with the differential setup in the 10^2 - 10^7 Hz frequency range with a reference capacitor of 185.4 pF, it becomes clear that $Re(\Delta C)$, the component of ΔC that is in phase with the reference capacitor, is not constant (Fig. 2.2b), but it decreases approximately linearly with the logarithm of frequency. Concurrently, the out-of-phase component $Im(\Delta C)$ is nonzero (Fig. 2.2c). Despite this nonideal behavior, which we ascribe to dissipation of the glue spacer, accurate measurements are possible. Empirically we find, when calculating the excess capacity C^{ex} compared to toluene, that the capacity scales linearly with the permittivity of the solvents (Fig. 2.2d). $Im(C^{ex})$ shows effects of nonzero conductivity and approaches zero at higher frequencies (Fig. 2.2e), while above 1 MHz inductive effects become visible, proportional to $Re(C^{ex})$. To calibrate the setup and to determine the cell constant of the capacitor, $Re(C^{ex})$ is averaged over the 10^3 - 10^6 Hz frequency range for each solvent and plotted against the relative permittivity of the solvent, known from the literature [39] (Fig. 2.2f). The slope in this plot is equal to the cell constant K_c = 28.70 $\pm$ 0.10 pF. The surface

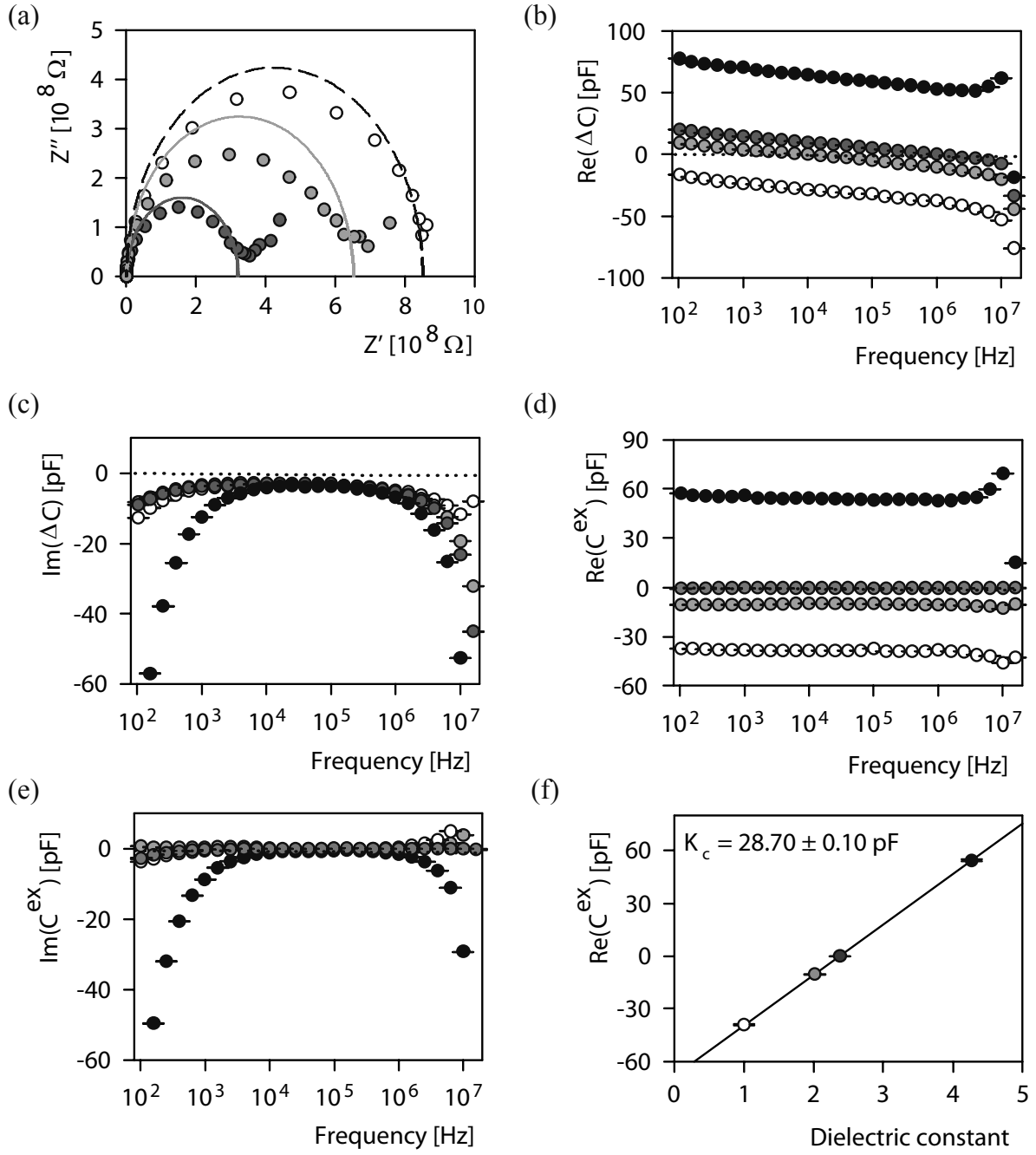

FIGURE 2.2. Calibration in the $10^2 - 10^7$ Hz range with different solvents (diethyl ether ●, toluene ●, cyclohexane ●) and air (○): (a) Impedance spectrum $Z = Z' - iZ''$, (b) Re(ΔC), (c) Im(ΔC), (d) Re(C^{ex}), and (e) Im(C^{ex}) as a function of frequency, and (f) Re(C^{ex}) as a function of solvent permittivity to determine the cell constant K_c.

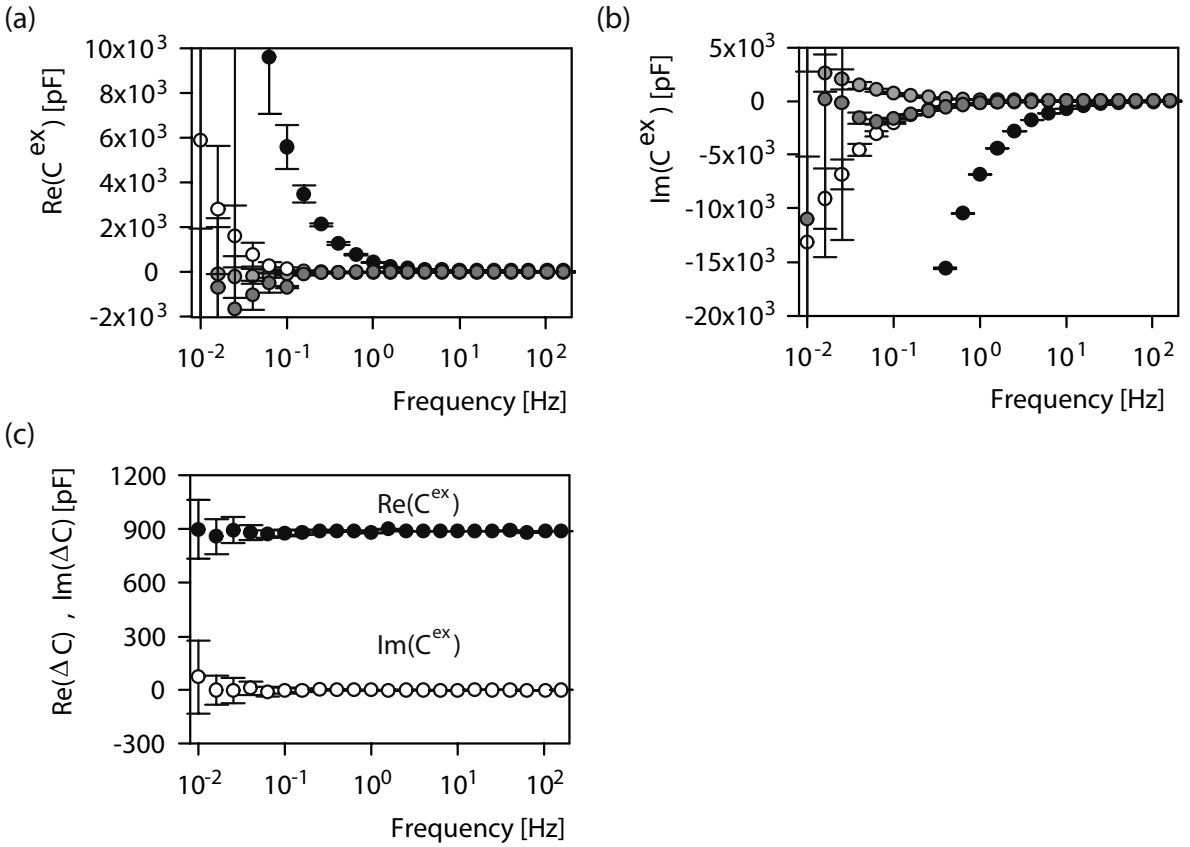

FIGURE 2.3. Calibration in the $10^{-2}-10^{2}$ Hz range with different solvents (diethyl ether •, toluene •, cyclohexane •) and air (○): (a) Re(C^{ex}) and (b) Im(C^{ex}) as a function of frequency, and (c) calibration with an air capacitor (C^{ex} = 900 pF).

area of the capacitor was determined from a digital photograph of the capacitor (A = 3.07 cm^2). Using eq. 2.7, the distance between the electrodes is estimated to be d = 94.6 μm, slightly larger than the average diameter of the silica glass beads (75 μm) used as spacer.

At lower frequencies ($10^{-2} - 10^{2}$ Hz) C^{ex} goes up dramatically (Fig. 2.3a,2.3b), due to electrode polarization. Apparently, charged impurities are present in the solvents, be it at very low concentrations ($\sim$ nM for diethyl ether, $<$ nM for toluene and cyclohexane). Calibration with an air capacitor (C^{ex} = 900 pF) shows that our setup operates properly in this frequency range (Fig. 2.3c). No attempts were made to measure at even lower frequencies, despite the hardware low frequency cut-off at 1 μHz.

The sensitivity of the setup was probed by measuring the capacitance of two separate aliquots of toluene and comparing the difference C^{ex}. Care was taken to refill the capacitor without disturbing the circuit, and to keep the circuit well thermostatized. A resolution down to $\epsilon^{ex} \approx 10^{-3}$ (corresponding to 0.01 % of total

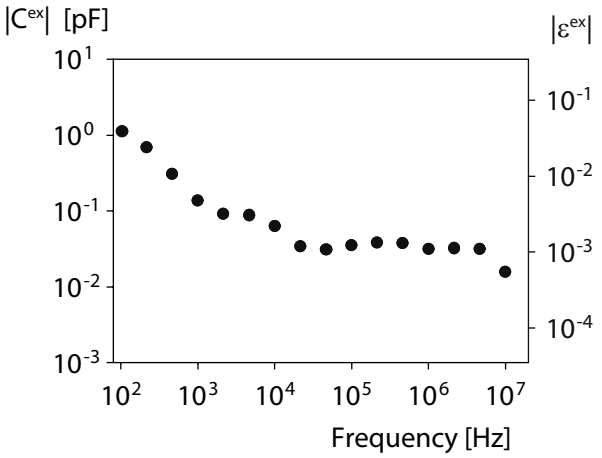

FIGURE 2.4. Differential measurement between two aliquots of toluene.

capacitance) was achieved in the frequency range of $10^4 - 10^7$ Hz (Fig. 2.4), where dipole relaxations are expected for nanoparticles. A higher resolution is expected to be possible, by reducing the measurement time, which reduces drift.

2.4. PERMITTIVITY SPECTRA

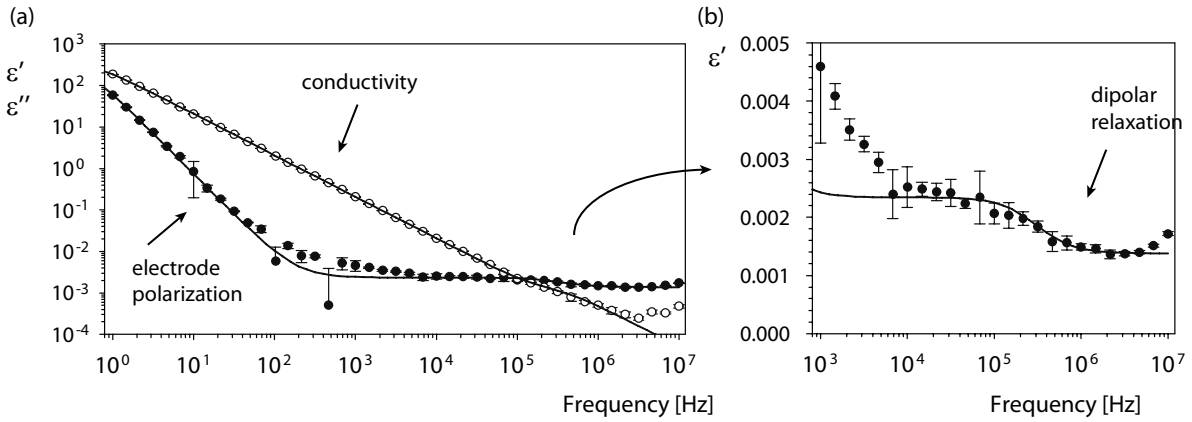

FIGURE 2.5. The real (black) and the imaginary (white) parts of the excess permittivity spectrum of CdSe quantum dots dispersed in decalin.

As a demonstration of the setup, the excess complex permittivity spectrum was measured of a dispersion of CdSe quantum dots with a 4 nm core diameter dispersed in decalin. The real part of the spectrum (Fig. 2.5) shows dipolar relaxation in the 10^4 - 10^6 Hz frequency range, and charged species are present, indicated by the conductivity in ϵ'' and the large increase in the permittivity at low frequencies. Further details of this system, and a detailed analysis of the dielectric spectra of colloidal quantum dots follows in Chapter 4. After fitting of the electrode polarization and the dipolar relaxation, a small shoulder is observed in

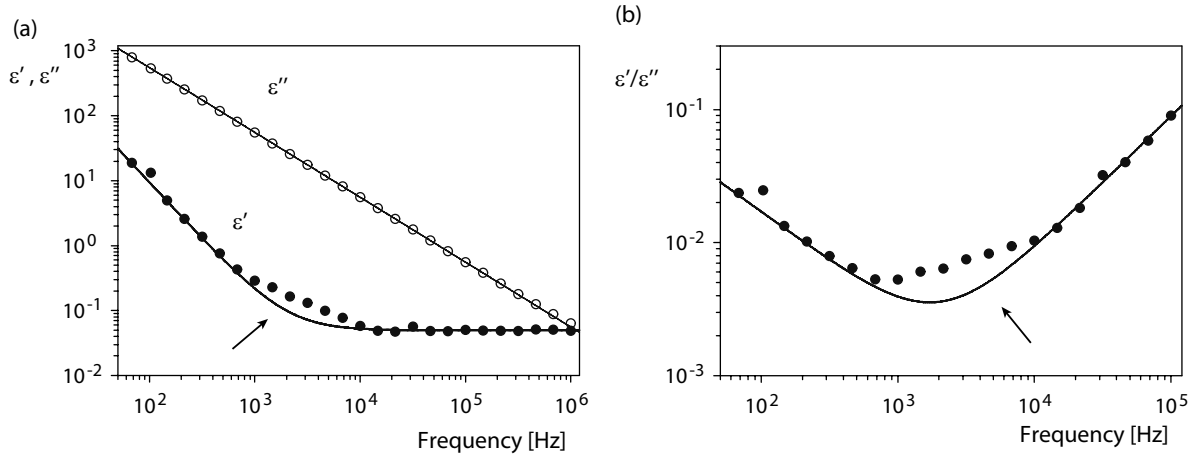

FIGURE 2.6. Permittivity spectrum of tertbutylammonium tertphenylborate salt in hexanol (described in Chapter 3) and fitted for electrode polarization. The part of the real permittivity in (a) that is not fitted well, as indicated by the arrow, corresponds to the frequency range where the ratio ϵ'/ϵ'' in (b) is the smallest.

the real part of the permittivity in the 10^2 - 10^4 Hz frequency range. This shoulder is likely an artifact. Exactly in this frequency range is the ratio ϵ'/ϵ'' the smallest ($\epsilon'/\epsilon'' < 0.01$), hence ϵ' is the most susceptible for, for instance, a small systematic error in the phase angle in the measured impedance. As indicated in Fig. 2.6, this shoulder is also observed in the permittivity spectrum of tertbutylammonium tertphenylborate salt in hexanol, which is studied in Chapter 3. This shoulder does not obstruct the observation of the dipolar relaxation.

2.5. CONCLUSIONS

The described setup successfully measures the complex excess permittivity of liquid dispersions of colloidal quantum dots in the 10^{-2} - 10^7 Hz frequency range, using a differential circuit with background compensating voltage. Measurement on a CdSe quantum dot dispersion demonstrate sufficient sensitivity to measure the dipolar relaxation due to a permanent dipole moment and the conductivity and electrode polarization due to particles with a net charge.

2.6. ACKNOWLEDGEMENTS

Bonny Kuipers and Emile Bakelaar are greatly acknowledged for their contributions to this setup. CdSe quantum dots were kindly provided by Relinde van Dijk-Moes. Ernst van Faassen en Casper van der Wel are acknowledged for useful discussions.

3

Influence of Ionic Strength on the Frequency Dispersion of Electrode Polarization

Abstract

The electrical impedance spectrum is measured of simple ionic solutions in a parallel plate capacitor at small applied ac voltage. The electric double layers at the electrodes that appear at low frequencies have a frequency-dependent capacitance. The influence of the ionic strength is investigated using several electrolytes at different concentrations in solvents of different dielectric constants. At moderate ionic strength, the transport of ions is in agreement with a model based on the Poisson-Nernst-Planck (PNP) equations. At low ionic strength, double layer dynamics deviate from the PNP model, and the deviation is well described by an empirical function with only one fit parameter. This deviation from the PNP equations increases systematically with increasing Debye length, possibly caused by the long-range Coulomb interaction.

3.1. INTRODUCTION

The accumulation of charged species near an electrode, so-called electrode polarization, occurs in and complicates dielectric spectroscopy measurements of for instance biological materials [40], solids [41], and colloidal dispersions [42]. Additionally, it is also a fundamental process for applications such as fuel cells [43], supercapacitors [43], and electrophoretic displays [44], and it can be used for the manipulation and characterization of red blood cells [45].

Measurements of electrode polarization often exhibit 'capacitance dispersion', that is, the double layer capacitance appears to be frequency dependent [46–49]. A satisfying physical model to describe this effect, however, is still lacking. Experimental data of relaxation behavior are often described by (semi-)empirical functions [50, 51], and capacitance dispersion is usually modeled by a constant phase element (CPE). This equivalent element in an electric circuit has an impedance $Z^{-1} = A_\alpha (i\omega)^\alpha$, with $0 < \alpha \leq 1$ and A_α a constant with units Ω^{-1} s$^\alpha$. The presence of fractal units when $\alpha < 1$ complicates the physical interpretation of a CPE [52]. Whether the term 'double layer capacitance' then still applies to a CPE response has been debated [53–58].

Our objective here is to improve the physical and quantitative understanding of the frequency dependence of the double layer capacitance. Our approach is to perform a systematic study of electrode polarization of simple ionic solutions with several electrolytes of known diffusion coefficients in solvents with different dielectric constants. The electrical impedance is measured in the limit of a small applied voltage. In particular, we examine how capacitance dispersion is affected by the ionic strength, and we focus on electrode polarization in the frequency range above the characteristic frequency of double layer relaxation. Our data are compared with a simple model that takes into account diffusion and drift [59] and an empirical extension of this model with a specific form of a CPE [60].

This chapter starts with a theoretical discussion of electrode polarization in section 3.2 and a description of our experimental methods in section 3.3. Then data are presented and fitted in section 3.4. Finally, a general discussion is made in section 3.5 and conclusions are drawn in section 3.6.

3.2. THEORY

As a simple model for electrode polarization, we consider the response of a symmetric electrolyte in an isotropic solvent, confined between two blocking electrodes of a parallel plate capacitor, to which a small AC voltage is applied. Ionic transport in the direction perpendicular to the electrodes (z-axis) as a function of time t is assumed to occur according to the Poisson-Nernst-Planck (PNP) model,

which consists of the following three equations. First, the fluxes $J_\pm$ of positive or negative ions with concentrations $n_\pm(z,t)$ are due to diffusion in a concentration gradient $\partial n_\pm(z,t)/\partial z$ and drift in a gradient of the electrostatic potential $\partial V(z,t)/\partial z$:

$$J_\pm(z,t) = -D\left(\frac{\partial n_\pm(z,t)}{\partial z} \pm \frac{q}{kT} n_\pm(z,t)\frac{\partial V(z,t)}{\partial z}\right) \tag{3.1}$$

Second, the gradient in the electric field is determined by the Poisson equation:

$$\frac{\partial^2 V(z,t)}{\partial z^2} = -\frac{q}{\epsilon_0 \epsilon_s}\Big(n_+(z,t) - n_-(z,t)\Big) \tag{3.2}$$

Third, conservation of particles is formulated in the equation of continuity:

$$\frac{\partial n_\pm(z,t)}{\partial t} = -\frac{\partial J_\pm(z,t)}{\partial z} \tag{3.3}$$

In these equations, k is the Boltzmann constant, T the temperature, q the absolute ion charge, D the diffusion coefficient, ϵ_0 the vacuum permittivity, and ϵ_s the dielectric constant of the solvent.

The response of the electric cell can be defined as the impedance $Z^*(\omega)$, or alternatively as a complex capacity $C^*(\omega)$ or a complex relative permittivity $\epsilon^*(\omega)$:

$$Z^*(\omega) = \frac{1}{i\omega C^*(\omega)} = \frac{d}{i\omega A \epsilon_0 \epsilon^*(\omega)} \tag{3.4}$$

with $i = \sqrt{-1}$, $\omega = 2\pi f$ the angular frequency, A the surface area of the electrodes, and d the distance between the electrodes. The frequency response of the PNP model was first derived, in a more general form, by Macdonald [59], through linearization of the ion concentrations and assuming blocking electrodes and conservation of the number of ions (derivation in appendix A, section 3.8):

$$\epsilon^*(\omega) \equiv \epsilon'(\omega) - i\epsilon''(\omega) = \frac{\frac{1}{2} d \epsilon_s \lambda^2}{(\kappa^2/\lambda)\tanh(\lambda d/2) + i(\omega d/2D)} \tag{3.5}$$

with κ^{-1} the Debye length, for a symmetric electrolyte:

$$\kappa^{-1} = \sqrt{\epsilon_0 \epsilon_s kT/(2nq^2)} \tag{3.6}$$

and with $2n$ the average free ion number density and $\lambda = \sqrt{\kappa^2 + i\omega/D}$. The frequency dependent conductivity is defined as $\sigma(\omega) = \omega\epsilon_0\epsilon''(\omega)$. In the limit of high frequency, the conductivity converges to a constant value σ_∞. For a symmetric electrolyte, the conductivity $\sigma_\infty = 2nq\mu_i$ with μ_i the ionic mobility can conveniently be written as $\sigma_\infty = \epsilon_0\epsilon_s D\kappa^2$, where the Einstein relation $D = \mu_i kT/q$ was used. Equation 3.5 is plotted in terms of $\epsilon'(\omega)/\epsilon_\infty$ and $\sigma(\omega)/\sigma_\infty$ as a function of frequency in Fig. 3.1 (solid lines), corresponding to the equivalent circuit in Fig. 3.2a. In this representation, absence of electrode polarization at high frequencies is characterized by $\epsilon'(\omega)/\epsilon_\infty = \sigma(\omega)/\sigma_\infty = 1$, hence the permittivity is equal to that of the solvent, $\epsilon'_\infty = \epsilon_s$, and the conductivity is σ_∞. In the limit

of low frequency, ions of one type accumulate at one electrode. The flux of ions due to diffusion and the flux due to drift cancel, and an equilibrium ionic double layer is present at each electrode, which strongly enhances the permittivity: $\epsilon'_{\omega\to 0}/\epsilon_s = \kappa d/2$.

Above the double layer relaxation frequency, electrode polarization of order 1 or more ($\epsilon'/\epsilon_\infty - 1 \geq 1$) occurs with a ω^{-2} frequency dependence [61], as indicated in Fig. 3.1 by the slope of -2. In the limit of high frequency, a very small contribution to the permittivity ($\epsilon'/\epsilon_\infty - 1 \ll 1$) is present with a $\omega^{-3/2}$ frequency dependence [61], though it is not visible in Fig. 3.1. Experimental observations of strong electrode polarization with a $\omega^{-3/2}$ frequency dependence have on occasion been ascribed to the PNP model, but this is incorrect, as was recently commented on by Hollingsworth [62].

The exact solution (eq. (3.5)) is, for $\kappa^{-1} \ll d$, to a very good approximation equal to the Debye relaxation function [63, 64]:

$$\epsilon^*(\omega) = \epsilon_s + \frac{\Delta\epsilon}{1 + i\omega\tau} \tag{3.7}$$

with $\Delta\epsilon = \epsilon_s\kappa d/2$ and the double layer relaxation time $\tau = d/(2D\kappa)$. The response of this Debye function can also be produced by the equivalent electronic circuit shown in Fig. 3.2b. In this circuit, $C_{dl} = A\epsilon_0\epsilon_s\kappa/2$ accounts for the double layers at both electrodes, $R_\infty = d/(A\sigma_\infty)$ accounts for the electrolyte conductivity, and $C_\infty = A\epsilon_0\epsilon_s/d$ accounts for the dielectric response of the solvent.

One empirical model in particular [60], an extension of the PNP model just presented, appears successful in describing our experimental data. It has been found useful before to fit electrode polarization data [65], and here, it is tested for a wider set of dielectric constants and ionic strengths. This model is, to a very good approximation, equal to an equivalent circuit (Fig. 3.2c) of electrode polarization in which the double layer capacitance is replaced by a CPE with an impedance of the specific form:

$$Z_{CPE}^{-1}(\omega) = \frac{C_{dl}}{\tau_\infty}(i\omega\tau_\infty)^\alpha \tag{3.8}$$

with $0 < \alpha \leq 1$ and $\tau_\infty = R_\infty C_\infty = \epsilon_0\epsilon_s/\sigma_\infty$ the Maxwell-Wagner relaxation time. The total impedance of the equivalent circuit (Fig. 3.2c) is then given by:

$$Z^*(\omega) = \frac{Z_{CPE} + R_\infty}{1 + i\omega C_\infty(Z_{CPE} + R_\infty)} \tag{3.9}$$

and the corresponding complex permittivity, using equation 3.4, by:

$$\epsilon^*(\omega) = \epsilon_s + \frac{\Delta\epsilon}{(i\omega\tau_\infty)^{1-\alpha} + i\omega\tau} \tag{3.10}$$

In the case of $\alpha = 1$, the CPE reduces to a double layer capacitance, and the equivalent circuit reduces to that of the Debye function (eq. 3.7). The responses

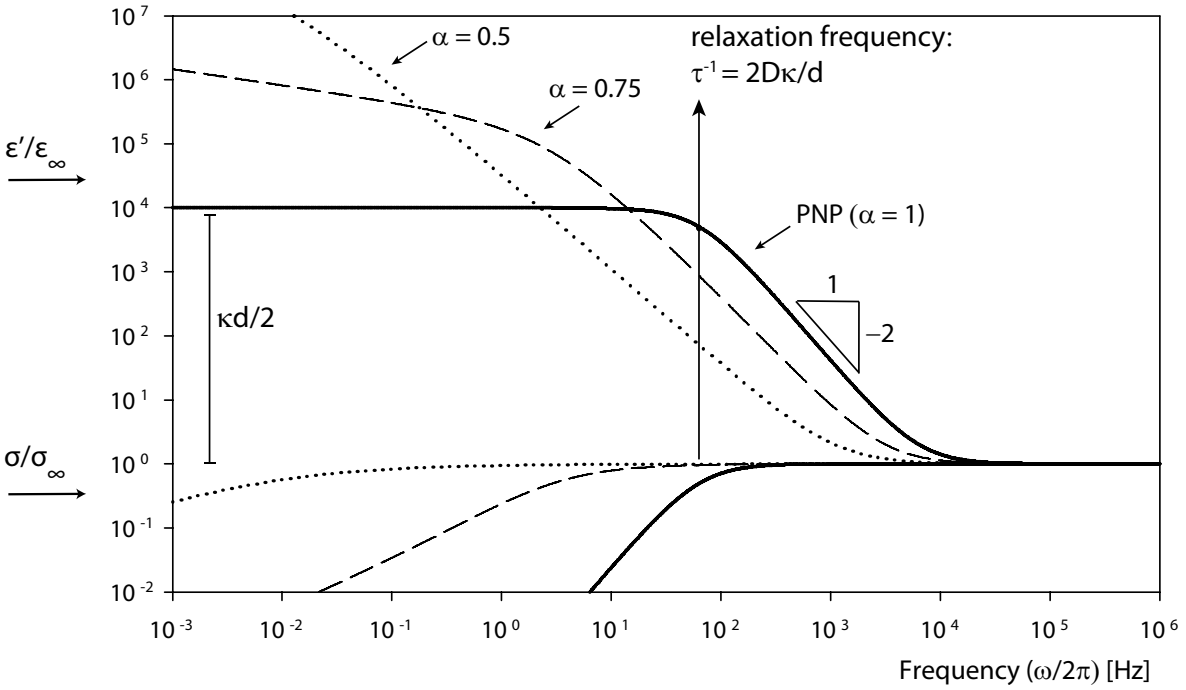

FIGURE 3.1. Theoretical response of a monovalent electrolyte with diffusion coefficient $D = 1 \times 10^{-10}$ m^2 s^{-1}, Debye length $\kappa^{-1} = 5$ nm, and electrode spacing d = 100 μm according to the PNP model (eq. 3.7) (solid line), or that of the empirical model (eq. 3.10) with α = 0.75 (dashed line), or α = 0.5 (dotted line).

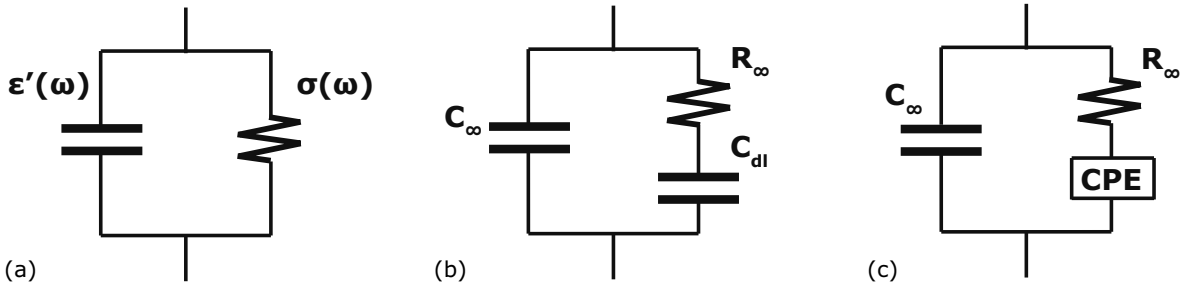

FIGURE 3.2. Schematic overview of equivalent circuits of: a) the complex permittivity in terms of frequency-dependent parameters $\epsilon'(\omega)$ and $\sigma(\omega)$, b) the PNP model (eq. 3.7), and c) the empirical model (eq. 3.10).

for $\alpha = 0.5$ and $\alpha = 0.75$ are plotted in Fig. 3.1. Decreasing the CPE exponent α leads to an apparent slower build up of the double layer; above the double layer relaxation frequency τ^{-1}, ϵ' shows a $\omega^{-1-\alpha}$ frequency dependence. At even lower frequencies ϵ' does not level off to a constant value but remains frequency dependent with a $\omega^{\alpha-1}$ frequency dependence.

3.3. EXPERIMENTAL METHODS

Ionic solutions were prepared from weighed amounts of KCl (99+ %, Acros), $MgSO_4 \cdot 7H_2O$ (>99.5 %, Fluka), $LiNO_3$ (99+ %, Merck), tertbutylammonium tertphenylborate (TBATPB, ≥99.0 %, Fluka), demineralized water (Millipore), ethanol (p.a., Merck), 1-hexanol (98 %, Sigma-Aldrich), and butyl acetate (99+ %, Janssen Chimica). Ethanol was deionized with resin prior to use (BioRad, AG 501-X8 20-50 mesh (D)). TBATPB solutions were sonicated for an hour. All solutions were prepared at least 24 hours before performing the measurements.

Two capacitors were used for the measurements, which were calibrated with solvents of known dielectric constant. One capacitor has a gold and an ITO electrode (which has also been used in Chapter 2), glued together on the edges with adhesive (Araldite, AW2101/HW2951), through which 75 μm glass beads (Sigma-Aldrich) are mixed. This capacitor has a cell constant K_c = 28.70 pF ($C_\infty = K_c \epsilon_s$) and a surface area A = 3.066 cm^2, from which we calculate the electrode spacing d = 94.6 μm. The other capacitor has two gold electrodes, separated by a teflon sheet. This capacitor has a cell constant K_c = 24.03 pF and a surface area A = 14.95 cm^2, from which we calculate the electrode spacing d = 551 μm.

Dielectric spectra were recorded with the complex permittivity setup and measurement procedures described in Chapter 2. Since electrode polarization dominates the signal, the setup was not used in its differential mode, but the voltage was measured over a measurement resistor in series with the capacitor directly. Measurements were performed upon applying a voltage of 25 mV in the frequency range of 10^{-1} to 10^6 Hz at a temperature of either 293 K or 295 K. It was verified that the response was independent of the applied voltage; deviations were only observed at a voltage of ≤1 V, and in this case only at the lowest frequencies (< 1 Hz). For each measurement, the capacitor was filled with fluid and was allowed to equilibrate. Dielectric spectra did not change over time and were reproducible upon refilling with the same sample.

3.4. RESULTS

The complex permittivity was measured for various electrolytes with known diffusion coefficients in solvents of different dielectric constants, each at different concentrations: KCl in water (Fig. 3.3a), $MgSO_4$ in water (Fig. 3.3b), tertbutylammonium tertphenylborate (TBATPB or $(Bu_4N)^+(Ph_4B)^-$) in butyl acetate (Fig. 3.4a), TBATPB in hexanol (Fig. 3.4b), and $LiNO_3$ in ethanol (Fig. 3.5). All dielectric spectra exhibit the same features. At high frequencies the spectra converge to a constant conductivity σ_∞ and to a real permittivity which corresponds

to the dielectric constant of the solvent. At low frequencies, $\epsilon'(\omega)$ increases and $\sigma(\omega)$ decreases due to electrode polarization.

The fits shown in the Fig. 3.3 - 3.5 were obtained in three steps. First, for each electrolyte, the average diffusion coefficient was calculated from literature data (Table 3.1). Then for each sample the Debye length κ^{-1} was calculated from the conductivity $\sigma_\infty = \epsilon_0 \epsilon_s D \kappa^2$. Finally, the value of α in equation 3.10 was adjusted for an optimal fit.

The average diffusion coefficients in Table 3.2 are the average of positive and negative ions $D = (D_+ + D_-)/2$ and were calculated from the data in Table 3.1. The ionic conductivity in the limit of low salt concentration c_s is $\Lambda^0 = \sigma_\infty / c_s |z|$, with $|z|$ the absolute ion valency. From the Einstein relation $D_i = \mu_i kT/q_i$, the average diffusion coefficient is $D = \sigma_\infty/(\epsilon_0 \epsilon_s \kappa^2) = (D_+ + D_-)/2 = kT|z|(\Lambda_+ + \Lambda_-)/(2N_A q^2)$, with N_A the Avogadro constant. Tertbutylammonium and tertphenylborate ions do not have a solvation shell in organic solvents, hence the Stokes radii a_H are independent of the solvent [66] and the diffusion coefficient is calculated using $D = kT/6\pi\eta a_H$, with η the solvent viscosity. TBATPB in butyl acetate or hexanol does not fully dissociate into free ions, due to the low dielectric constant of the solvents. Instead, many neutral ion pairs are present, which do not contribute to the conductivity. Experimental conductivities of tertbutylammonium salts have been shown to be in good agreement with theory and simulations that describe the equilibrium between free ions and ion pairs [67]. The use of the average diffusion coefficient is justified in appendix B (section 3.9), where it is shown that the complex permittivity of an asymmetric electrolyte hardly varies for different D_+/D_- ratios while keeping the average diffusion coefficient D constant. Beside the diffusion coefficients, the dielectric constants and electrode spacings are also given in Table 3.2. Since the empirical model did not exactly match the data over the whole frequency range, data were fitted in the frequency range above the double layer relaxation frequency $\tau^{-1} = 2D\kappa/d$. The PNP model (eq. 3.5), corresponding to $\alpha = 1$, was unable to fit most of our data. The deviation from the PNP model with the data is most dramatic for the TBATPB electrolyte, for which the deviation is indicated in Fig. 3.4. Pure solvents were fitted as well for comparison, but since the diffusion coefficient of the ions still present in these solvents is unknown, these results are omitted in the discussion of our results.

3.5. DISCUSSION

Remarkably, the empirical model based on equation 3.10 describes the high frequency region of all our data with just one adjustable fit parameter, α. This parameter appears to be strongly dependent on the ionic strength, as illustrated

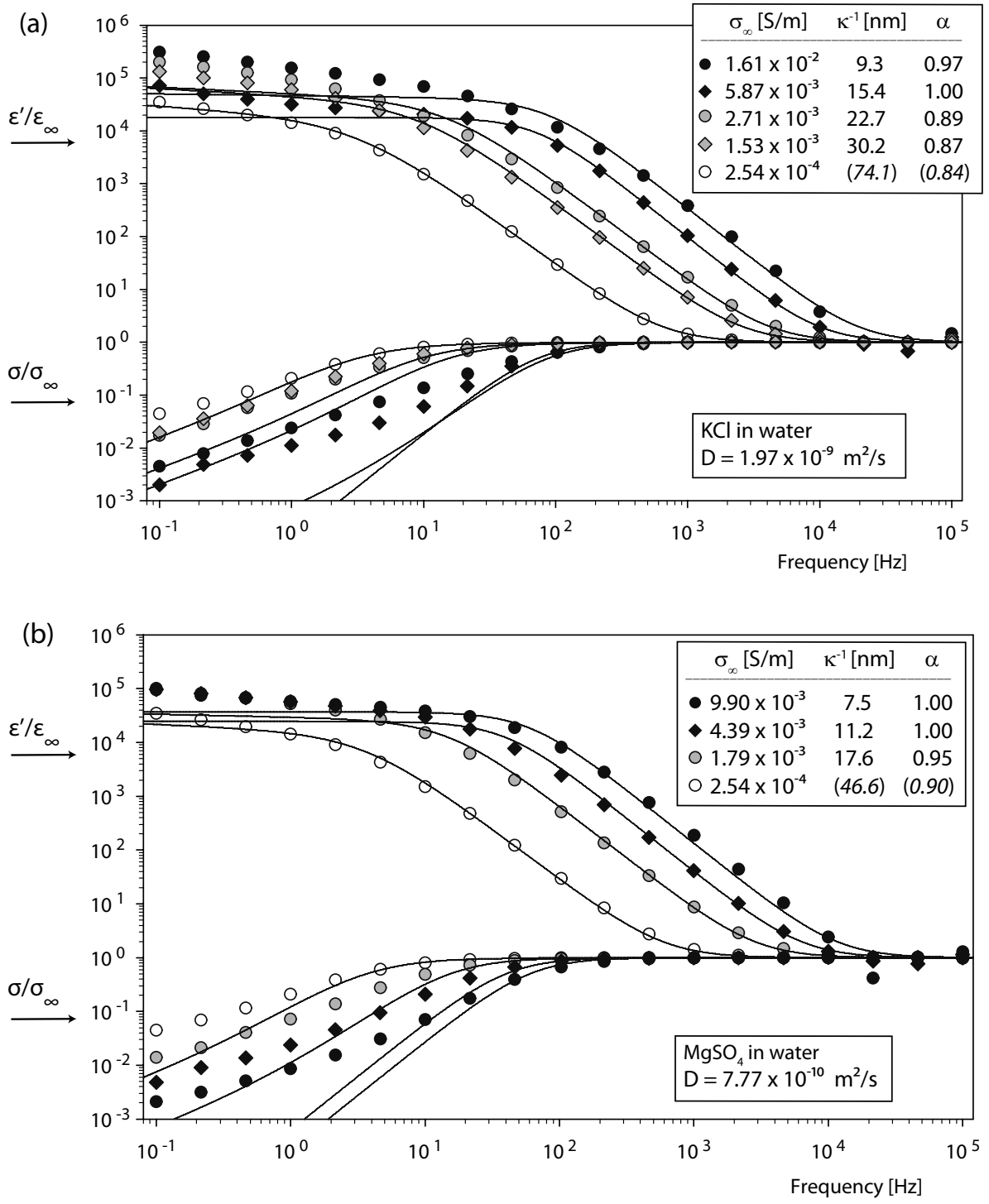

FIGURE 3.3. Dielectric spectra of (a) KCl and (b) $MgSO_4$ in water. Symbols denote experimental data at different concentrations; (○) is pure solvent. Solid lines are fits using equation 3.10 and fit parameters as given in the figure.

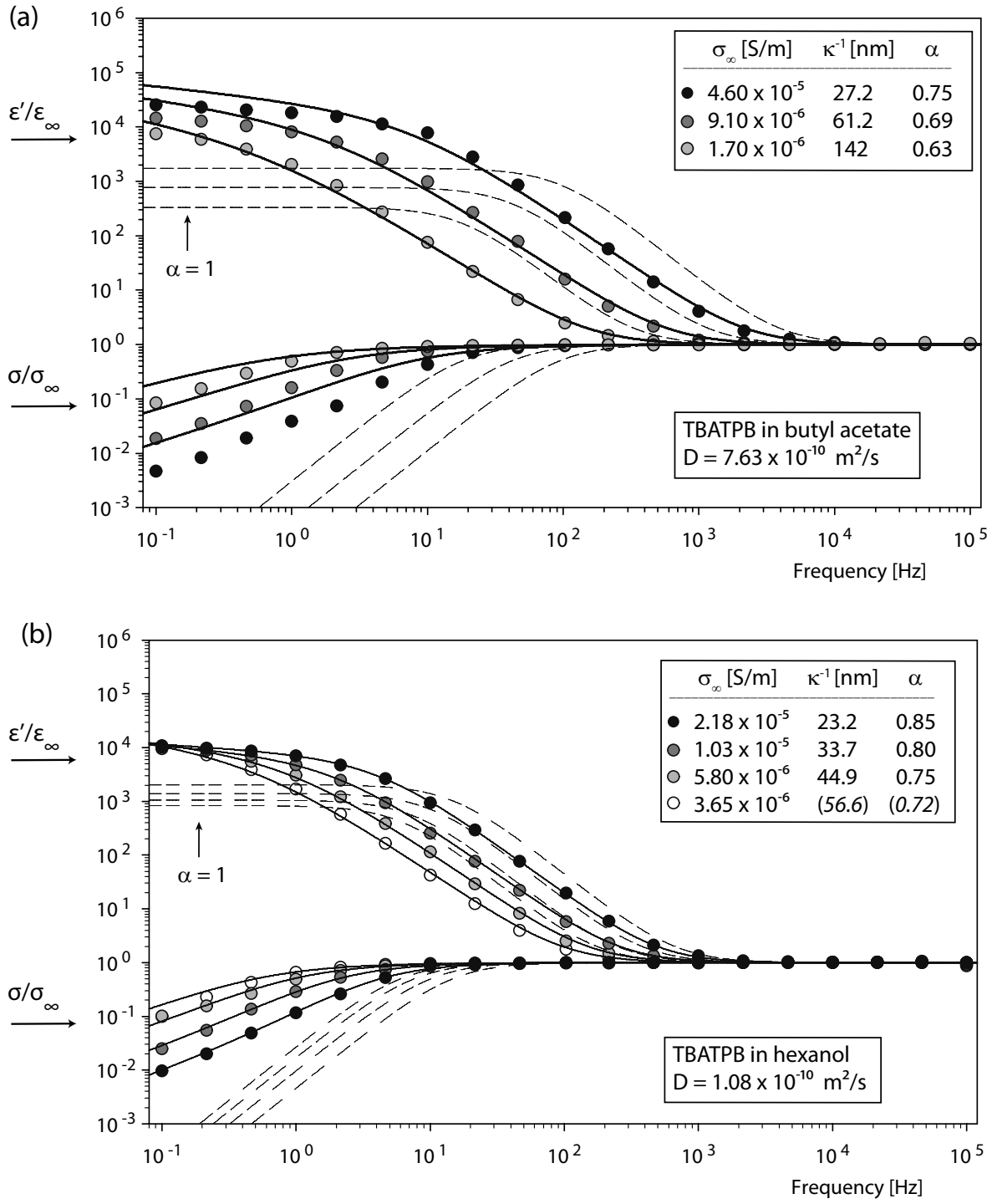

FIGURE 3.4. Dielectric spectra of TBATPB in (a) butyl acetate and (b) hexanol. Symbols denote experimental data at different concentrations; (○) is pure solvent. Solid lines are fits using equation 3.10 and fit parameters as given in the figure. For comparison, spectra for the same parameters are also shown corresponding to $\alpha = 1$.

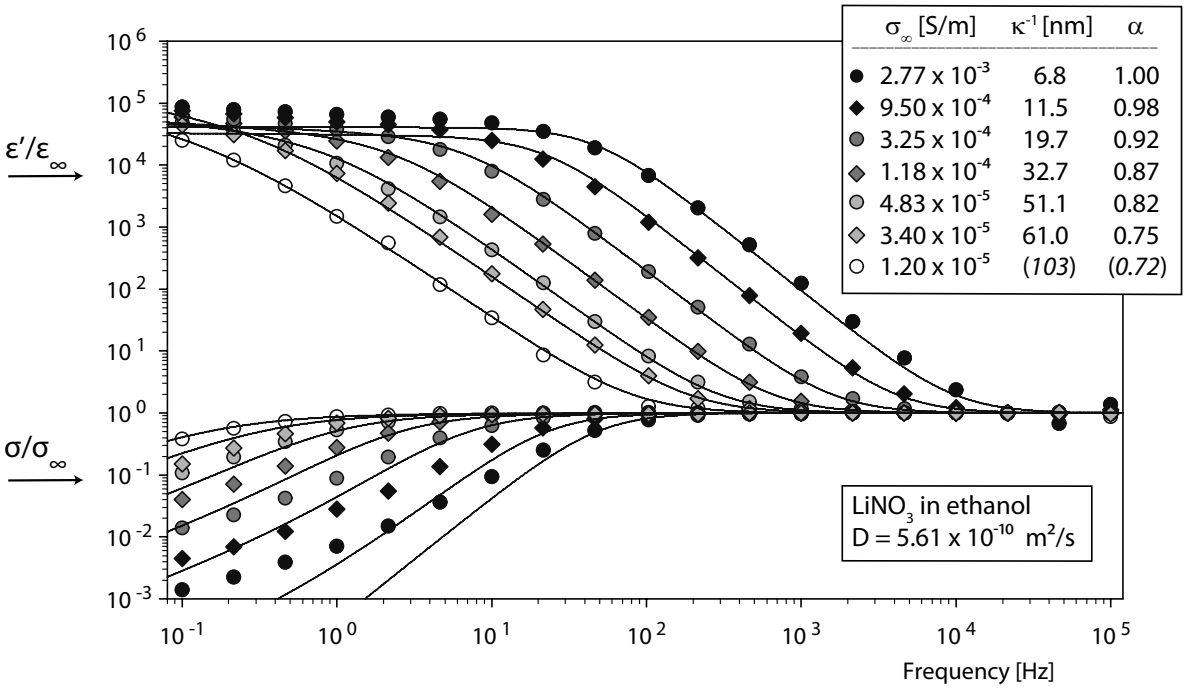

FIGURE 3.5. Dielectric spectra of $LiNO_3$ in ethanol. Symbols denote experimental data at different concentrations; (○) is pure solvent. Solid lines are fits using equation 3.10 and fit parameters as given in the figure.

electrolyte / solvent	Λ_0 [S cm^2 mol^{-1}]		ref.
KCl / water	(K^+)	73.52 [1]	[68]
	(Cl^-)	76.34 [1]	[68]
$MgSO_4$ / water	($\frac{1}{2}Mg^{2+}$)	47.99 [2]	[69]
	($\frac{1}{2}SO_4^{2-}$)	70.47 [2]	[69]
$LiNO_3$ / ethanol	($LiNO_3$)	42.74 [1]	[70]

	a_H [Å]	
$(Bu_4N)^+$	3.84	[66]
$(Ph_4B)^-$	4.08	[66]

TABLE 3.1. Limiting equivalent conductivities Λ_0 and hydrodynamic radii a_H of the used electrolytes as obtained from the cited references at 25 °C [1] and at 20 °C [2].

in Fig. 3.6, where α is plotted versus the Debye length κ^{-1}. Aqueous and ethanolic solutions at concentrations above 0.25 mM are well fitted with $\alpha = 1$, hence they show the expected response of the PNP model (equation 3.5). This is in

electrolyte / solvent	$D = (D_+ + D_-)/2$ [m^2/s]	T [K]	ϵ_s [39]	d [μm]
KCl / water	1.97×10^{-9}	293	80.15	551
$MgSO_4$ / water	7.77×10^{-10}	293	80.15	551
$LiNO_3$ / ethanol	5.61×10^{-10}	293	25.45	551
TBATPB / hexanol	1.02×10^{-10}	293	12.99	94.6
TBATPB / butyl acetate	7.63×10^{-10}	295	5.04	94.6

TABLE 3.2. Measurement parameters.

agreement with other reports of measurements at similar ionic strengths using a parallel plate capacitor [21, 71] or cylindrical capacitor [72]. Decreasing ionic strength leads to a decrease of α, down to $\alpha = 0.6 - 0.7$ for the lowest ionic strengths. Others find at even lower ionic strength in apolar solvents a $\omega^{-3/2}$ frequency dependence of $\epsilon'(\omega)$ [19, 73–76], corresponding to $\alpha = 0.5$, which is consistent with our observations as well. A quantitative relation to physical parameters, however, was not given in these studies, and the observed frequency dependence was incorrectly ascribed to the PNP model, as explained by Hollingsworth [62].

At lower frequencies, below the double layer relaxation frequency τ^{-1}, the agreement of the model with the data varies per measurement. Nevertheless, the model captures the general trend, especially for the lowest ionic strengths. In this frequency range, double layers are strongly charged due to an increased counterion concentration at the electrodes, amplifying the electric field at the electrodes by a factor of $|\epsilon'(\omega)/\epsilon_\infty| \approx 10^4 - 10^5$ compared to the electric field without electrode polarization, $E_0 = V_0/d$, with V_0 the applied potential. Avoiding possible nonidealities related to the increased electric field and ion concentrations in the double layer at the lowest frequencies, we focus on the higher frequency range above $\tau^{-1} = 2D\kappa/d$, where the double layer is not yet fully charged.

In finding a rationale for the ionic strength dependence of α and the specific form of the CPE, a first important point to be noticed is that deviations from the PNP model start already at high frequencies when $\epsilon'/\epsilon_\infty < 10$. In this situation the electric field in the capacitor is still relatively homogeneous, and the variation in ion concentrations is small. Therefore, no effect of ion association or dissociation on the response [59] is expected; this is further illustrated in appendix A (section 3.8). In our experiments there is no large difference in the behavior of the strongly associated TBATPB and strongly dissociated electrolytes (KCl, $MgSO_4$, $LiNO_3$), except for the continuing trend of decreasing α with decreasing ionic strength. The rate of electrolyte dissociation is expected to increase above an electric field strength of $10^6 - 10^7$ V/m [77], but this occurs at much higher field

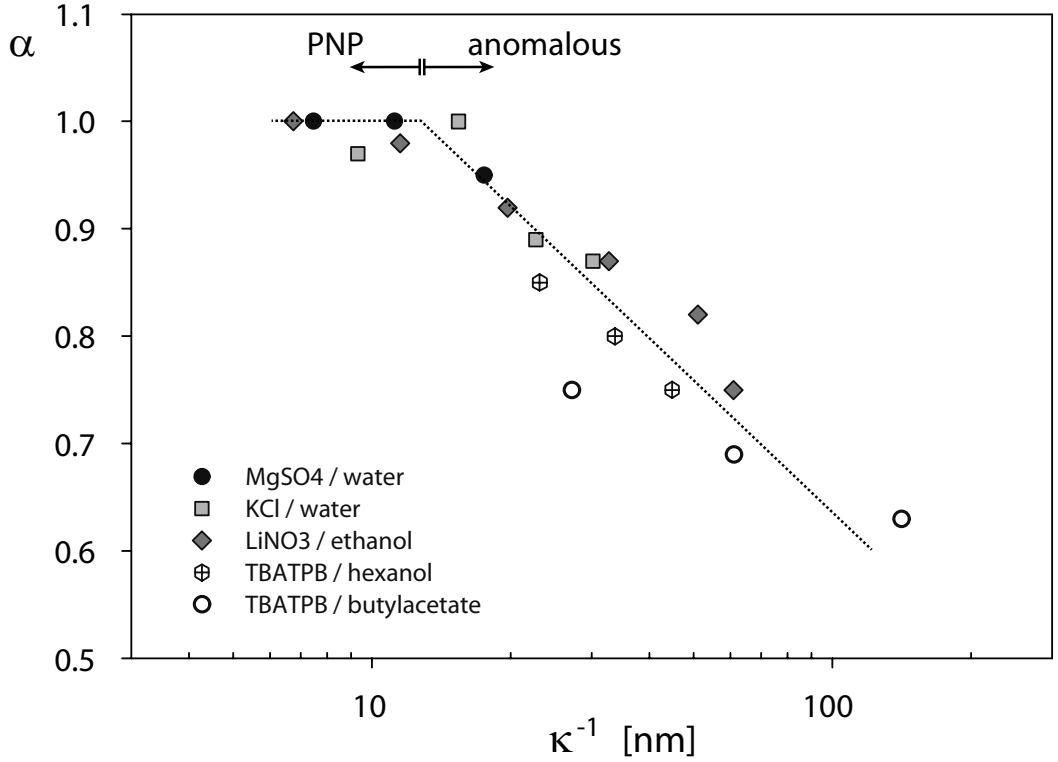

FIGURE 3.6. CPE exponent α as a function of Debye length κ^{-1} for dielectric constants from 5 to 80 and ion concentrations from 0.3 μM to 1 mM. The dotted line is a guide to the eye. Below $\kappa^{-1} \approx$ 10-20 nm experimental data is in agreement with the Poisson-Nernst-Planck (PNP) model, whereas at larger Debye lengths anomalous behavior is observed.

strengths than the field $V_0/d \approx 250$ V/m applied here. It should be kept in mind, however, that the field near the electrodes is amplified by a factor $|\epsilon^*(\omega)/\epsilon_\infty|$, hence the dissociation rate might increase at lower frequencies, when the electrodes are strongly polarized. A second point to notice is that the apparent double layer formation is slower than expected, rather than being faster. This excludes the absorption of ions onto the electrodes as major cause of capacitance dispersion. Adsorption of ions onto the electrodes will lead to an additional increase of the permittivity [78], which might occur at low frequency. It will, however, not lead to a slower double layer formation, but it will accelerate the process.

It has been suggested that capacitance dispersion is caused by electrode roughness and that the CPE exponent is related to the fractal dimension of the rough electrode surface [79–81]. Experiments, however, suggest that there is no correlation between electrode roughness and the CPE exponent [82,83]. Furthermore, thin double layers are expected to follow the surface curvature better than thick

double layers, thus they are expected to show a stronger effect of surface roughness, contrary to our observation of $\alpha < 1$ for thick double layers. Alternatively, it has been suggested that capacitance dispersion might be caused by physicochemical heterogeneities on the electrode surface [83–85].

We measured the response of both strongly dissociated and associated electrolytes, both monovalent and divalent ions, and solvents of different dielectric constants. The trend in the dependence of α on κ^{-1} (Fig. 3.6) suggests that the underlying cause is not specific for one particular system, but general. At low ionic strength, for a double layer thickness $\kappa^{-1} >$ 10 - 20 nm, double layer dynamics become markedly different. The PNP equations describe transport of ions without an effect of interactions between ions. Decreasing the ionic strength would only increase the average distance between the ions, and therefore an effect of the magnitude of the ion interactions is not be expected. At lower ionic strength, however, the range of interaction does increase. The Coulomb interaction potential in ionic solutions is screened by an ionic cloud and effectively short range ($U(r) \propto e^{-\kappa r}/r$), but within a Debye length κ^{-1} the potential decays slowly with distance ($U(r) \propto 1/r$). The double layer dynamics, here relaxation towards equilibrium in the presence of an external field, could be related to the long-range nature of the Coulombic interaction. Effects of the long-range Coulomb interaction become apparent in nonequilibrium plasmas, where non-Maxwellian or power-law electron velocity distributions have been observed [86–88]. Possibly related are unexplained observations in dispersions of charged colloids at low ionic strength, for which their double layers are crucial [89–91]. One approach to include the influence of interactions between ions on their transport is to consider diffusion to be anomalous, by varying the time dependence of the mean square displacement [92]. Responses of an electrolyte under the assumption of anomalous diffusion have been calculated recently [93, 94] (by which also the time dependence of drift was modified via the Einstein relation), but these could not describe our data in a consistent way. Modification of the PNP equations, such that anomalous diffusion is assumed in the double layer only, might yield transport equations that describe our data. While the empirical model of our data is specific for the geometry of the parallel plate capacitor, the modified equations could be tested for different geometries as well.

While we have focussed on the frequency domain, similar measurements have been performed in the time domain, where the current of charged micelles in apolar solvents was measured after the application of a step voltage [95, 96]. Apart from exponentially decaying current, also power law behavior was observed [95]. We evaluated the time response of the equivalent circuit in Fig. 3.2c (derivation in appendix C, section 3.10) and, for $\alpha < 1$, observe power law behavior as

well. The CPE response of the double layer is likely to apply as well to these measurements in the time domain.

3.6. CONCLUSIONS

For moderate to high salt concentrations (≥ 0.25 mM), the frequency dependence of electrode polarization at frequencies above the double layer relaxation frequency is in excellent agreement with the Poisson-Nernst-Planck (PNP) model that accounts for diffusion and drift without ion interactions. At lower ionic strength, however, the measurements deviate from this model and exhibit capacitance dispersion. We find empirically that the response of the double layer capacitance C_{dl} can be described well as a CPE with impedance $Z^{-1}=(C_{dl}/\tau_\infty)(i\omega\tau_\infty)^\alpha$. Our experiments highlight the influence of the ionic strength on the frequency dispersion of electrode polarization through the parameter α. Double layer dynamics become markedly different above a Debye length of 10 - 20 nm, which is possibly related to the long-range nature of the Coulomb interaction.

3.7. ACKNOWLEDGEMENTS

I would like to acknowledge Andrew Hollingsworth, René van Roij, Andrei Petukhov, Jan Groenewold, Alwin Verschueren, and Casper van der Wel for useful discussions.

3.8. APPENDIX A

A derivation is given of equation 3.5, describing the response of a symmetric electrolyte according to the Poisson-Nernst-Planck (PNP) model when submitted to a small AC voltage $V_0e^{i\omega t}$. This is based on the work of Macdonald [59] and uses the parameterization of ref. 97.

Consider a capacitor with two electrodes of surface area A separated by distance d, placed at $z=\pm d/2$, containing a symmetric electrolyte in a solvent with dielectric constant ϵ_s. The two types of ions have an opposite charge of the same magnitude $q_i=|z_i|e$, with the average number densities $\langle n_+\rangle=\langle n_-\rangle=n$. Both ions have the same diffusion constant $D_+=D_-=D$ and the same ionic mobility $\mu_+=\mu_-=\mu$, satisfying the Einstein relation $D_i=\mu_i kT/q_i$. It is assumed that the electrodes are 'blocking', i.e., the particle flux $J(z,t)$ vanishes at the electrodes:

$$J_\pm(\pm d/2,t)=0 \tag{3.11}$$

Also, there is no recombination of the ions, hence there is conservation of the number of ions:

$$\frac{1}{d}\int_{-d/2}^{d/2} n_\pm(z,t)dz=n \tag{3.12}$$

It is assumed that there are no interactions between the ions, such that the transport of ions is governed by the PNP equations (eq. 3.1-3.3). Small deviations are assumed, such that the ion concentrations can be linearized (with $\eta_\pm \ll n$):

$$n_\pm(z,t) = n + \eta_\pm(z)e^{i\omega t} \tag{3.13}$$

and

$$V(z,t) = \phi(z)e^{i\omega t} \tag{3.14}$$

with the boundary condition:

$$\phi(\pm d/2) = \pm V_0/2 \tag{3.15}$$

Under these assumptions, the Poisson equation (3.2) becomes:

$$\phi''(z) = -\frac{q}{\epsilon_0\epsilon_s}\Big(\eta_+(z) - \eta_-(z)\Big) \tag{3.16}$$

and ion fluxes (3.1) become:

$$J_\pm(z,t) = -D\left(\frac{d\eta_\pm(z)}{dz} \pm \frac{qn}{kT}\frac{d\phi(z)}{dz}\right)e^{i\omega t} \tag{3.17}$$

Substitution of (3.16) and (3.17) in the continuity equation (3.3) yields:

$$\eta''_\pm(z) = \left(\frac{\kappa^2}{2} + i\frac{\omega}{D}\right)\eta_\pm(z) - \frac{\kappa^2}{2}\eta_\mp(z) \tag{3.18}$$

where the Debye length κ^{-1} is given by $\kappa^2 = 2nq^2/(\epsilon_0\epsilon_s kT)$. The solution of this linear system of second order differential equations is:

$$\eta_\pm = \pm c_1 \sinh(\lambda z) \tag{3.19}$$

with c_1 a constant, and its eigenvalue:

$$\lambda = \sqrt{\kappa^2 + i\frac{\omega}{D}} \tag{3.20}$$

Substitution of the ion concentrations (3.19) in the Poisson equation (3.16), and double integration yields the potential profile

$$\phi(z) = \frac{-2q}{\epsilon_0\epsilon_s\lambda^2}c_1\sinh(\lambda z) + c_2 z + c_3 \tag{3.21}$$

It follows from the use of symmetry, $\phi(d/2) = -\phi(-d/2)$, that $c_3 = 0$. Additionally, the use of boundary conditions (3.11) and (3.15) yields the two constants c_1 and c_2:

$$c_1 = \frac{-nq\lambda/(2kT)}{(\kappa^2/\lambda)\sinh(\lambda d/2) + i(\omega d/2D)\cosh(\lambda d/2)}V_0 \tag{3.22}$$

$$c_2 = \frac{(i\omega/2D)\cosh(\lambda d/2)}{(\kappa^2/\lambda)\sinh(\lambda d/2) + (i\omega d/2D)\cosh(\lambda d/2)}V_0 \tag{3.23}$$

Gauss's law relates the charge on the capacitor plates $Q(t)$ to the electric field $E(z,t) = -\phi'(z)e^{i\omega t}$ at the electrodes:

$$Q(t) = A\epsilon_0\epsilon_s E(-d/2,t) = -A\epsilon_0\epsilon_s\phi'(-d/2)e^{i\omega t} \tag{3.24}$$

After differentiation of (3.21) and substitution in (3.24), the complex relative permittivity $\epsilon^*(\omega)$ follows from its definition $Q(\omega) = C(\omega)V(\omega) = \frac{A\epsilon_0}{d}\epsilon^*(\omega)V_0e^{i\omega t}$:

$$\epsilon^*(\omega) = \frac{\frac{1}{2}d\epsilon_s\lambda^2}{(\kappa^2/\lambda)\tanh(\lambda d/2) + i(\omega d/2D)} \tag{3.25}$$

which is equation 3.5. The deviation of the ion concentration relative to the average ion concentration, $\eta_\pm/n$, is given by:

$$\left|\frac{\eta_\pm(z)}{n_0}\right| = \frac{(q\lambda/2kT)\sinh(\lambda z)}{(\kappa^2/\lambda)\sinh(\lambda d/2) + i(\omega d/2D)\cosh(\lambda d/2)}V_0 \tag{3.26}$$

The influence of association or dissociation of charge carriers has also been modeled by Macdonald [59]; however, its influence on the response in the frequency range above the double layer relaxation time is very small. The equilibrium between the concentration of ions n_+, n_- and the concentration of neutral ion pairs n_0 could be described by an equilibrium constant $K = n_+n_-/n_0^2$. According to the PNP model without association or dissociation (equations 3.13, 3.19, and 3.26), the (absolute) product $n_+(z)n_-(z) = (n+\eta_+(z))(n+\eta_-(z)) = n^2 - \eta_+^2(z)$ is the largest near the electrodes at $z = \pm d/2$. At the double layer relaxation frequency τ^{-1} this product $n_+(z)n_-(z) = 0.88\ n^2$ is close to the product of the average concentrations for typical values of D = 10^{-9} m^2/s, κ^{-1} = 10 nm, V_0 = 25 mV, and d = 100 μm. At a frequency higher by a factor of 10, the product $n_+(d/2)n_-(d/2) = 0.998\ n^2 \approx n^2$ becomes almost spatially and frequency independent and a shift in the equilibrium is not expected.

3.9. APPENDIX B

The response of an asymmetric electrolyte, with unequal diffusion coefficients $D_+ \neq D_-$, was also considered in the work of Macdonald [59]. Analogous to the derivation of appendix A (section 3.8), but with $D_+ \neq D_-$, while $q_+ = q_-$ and the Einstein relation still applies, the complex permittivity is given by:

$$\frac{\epsilon^*(\omega)}{\epsilon_s} = \left[\lambda_+\cosh(\frac{\lambda_+ d}{2}) + \chi\lambda_-\cosh(\frac{\lambda_- d}{2})\right] / \left[\left(\chi\lambda_- - \frac{\kappa^2}{2}\frac{\chi(1-\gamma^-)}{\lambda_-}\right)\cosh(\frac{\lambda_- d}{2}) + \left(\lambda_+ - \frac{\kappa^2}{2}\frac{1-\gamma^+}{\lambda_+}\right)\cosh(\frac{\lambda_+ d}{2}) + \frac{\kappa^2}{d}\left(\frac{1-\gamma^+}{\lambda_+^2}\sinh(\frac{\lambda_+ d}{2}) + \frac{\chi(1-\gamma^-)}{\lambda_-^2}\sinh(\frac{\lambda_- d}{2})\right)\right] \tag{3.27}$$

with

$$\lambda_\pm^2 = \frac{1}{2}\left(\kappa^2 + \frac{i\omega}{D_+} + \frac{i\omega}{D_-}\right) \pm \frac{1}{2}\sqrt{\kappa^4 - \left(\frac{\omega}{D_+} - \frac{\omega}{D_-}\right)^2} \tag{3.28}$$

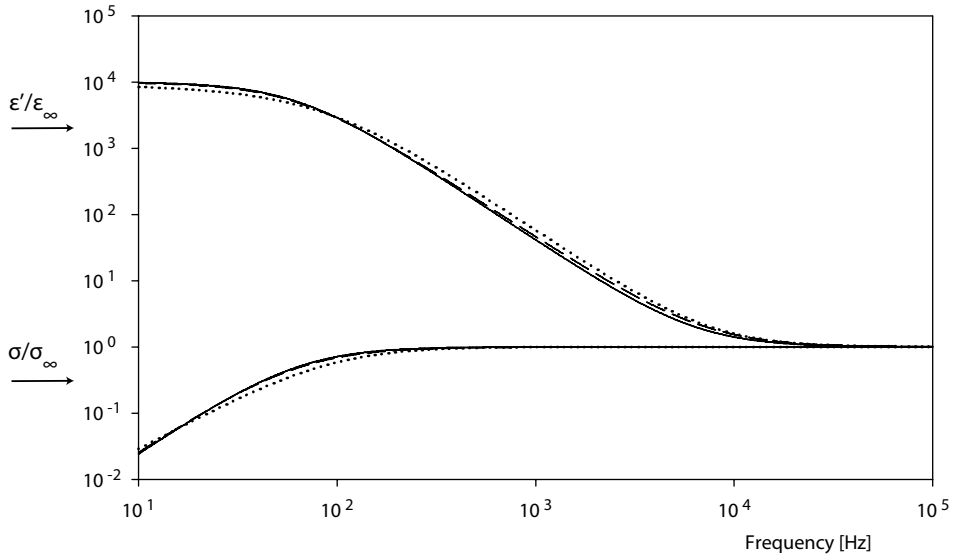

FIGURE 3.7. Response of an asymmetric electrolyte (using equation 3.27) for three different diffusion coefficient ratios: $D_+/D_- = 1$ (solid line), $D_+/D_- = 10^{-2}$ (dashed line), $D_+/D_- = 10^{-4}$ (dotted line) with average diffusion coefficient $D = (D_+ + D_-)/2 = 10^{-10}$ m^2 s^{-1}, $\kappa^{-1} = 5$ nm, and d = 100 μm.

$$\gamma^{\pm} = -\frac{2}{\kappa^2}(\lambda_{\pm}^2 - \kappa^2/2 - i\frac{\omega}{D_+}) \tag{3.29}$$

$$\chi = \frac{-\lambda_+(1+\gamma^+)\cosh(\lambda_+ d/2)}{\lambda_-(1+\gamma^-)\cosh(\lambda_- d/2)} \tag{3.30}$$

This function for an asymmetric electrolyte is plotted in Fig. 3.7 for three different D_+/D_- ratios, while keeping the average diffusion coefficient D, and hence the conductivity σ_∞, constant. The response hardly depends on the D_+/D_- ratio. Therefore, it seems justified to use the average diffusion coefficient in the empirical model, equation 3.10. For comparison, the value of the average diffusion coefficient, rather than the ratio, has a much stronger influence on the response, as is shown in Fig. 3.8.

3.10. APPENDIX C

The response of the equivalent circuit in Fig. 3.2c, which corresponds well with our experimental data, is evaluated in the time domain, with the use of the Laplace transform, defined by $\mathcal{L}\{f(t)\} \equiv \int_0^\infty e^{-st} f(t)dt = F(s)$. The current $i(t)$, with Laplace transform $\mathcal{L}\{i(t)\} = I(s)$, is calculated when a step input voltage $v(t) = V_0$ for $t \geq 0$ is applied, with Laplace transform $\mathcal{L}\{v(t)\} = V(s) = V_0/s$. The impedance $Z(s) = V(s)/I(s)$ of the resistor in series with the CPE element is

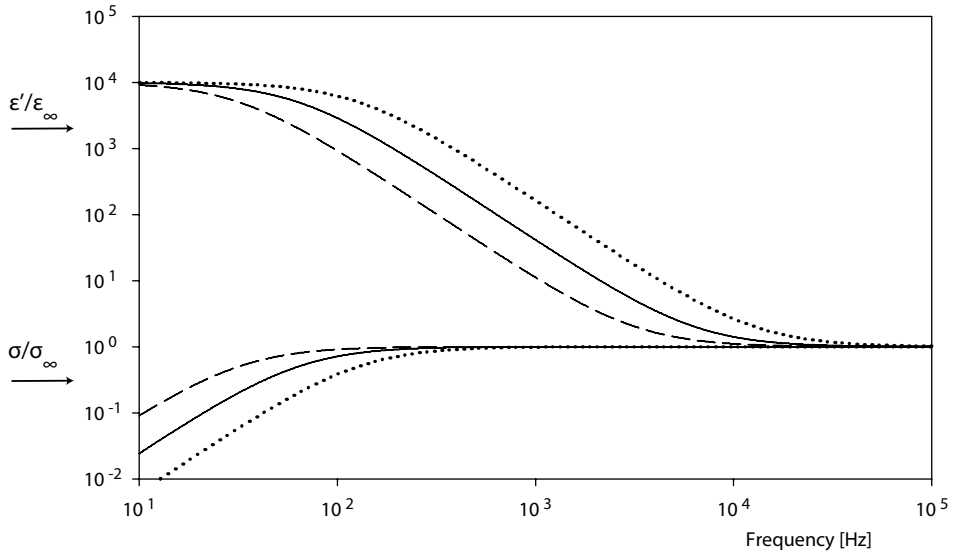

FIGURE 3.8. Response of a symmetric electrolyte (using equation 3.11) for $D = 1 \times 10^{-10}$ m^2 s^{-1} (solid line), $D = 0.5 \times 10^{-10}$ m^2 s^{-1} (dashed line), $D = 2 \times 10^{-10}$ m^2 s^{-1} (dotted line), with $\kappa^{-1} = 5$ nm, and d = 100 μm.

given by:

$$Z(s) = R + \left(\frac{\tau^{1-\alpha}}{C_{dl}}\right) s^{-\alpha} \tag{3.31}$$

Then, the current $i(t)$ is:

$$i(t) = \mathcal{L}^{-1}\left\{\frac{V(s)}{Z(s)}\right\} = \mathcal{L}^{-1}\left\{\frac{V_0/s}{R + (\tau^{1-\alpha}/C_{dl})s^{-\alpha}}\right\} = \frac{V_0}{R} \cdot \mathcal{L}^{-1}\left\{\frac{1}{s} \cdot \frac{s^\alpha}{s^\alpha + \tau_\infty^{1-\alpha}/RC_{dl}}\right\} \tag{3.32}$$

To solve the inverse Laplace transform $\mathcal{L}^{-1}$, the following Laplace transform is used [98]:

$$\mathcal{L}\{E_{\alpha,1}[-at^\alpha]\} = \frac{1}{s}\left(\frac{s^\alpha}{s^\alpha + a}\right) \tag{3.33}$$

where the generalized Mittag-Leffner function is given by:

$$E_{\alpha,\beta}[x] = \sum_{k=0}^{\infty} \frac{x^k}{\Gamma(\alpha k + \beta)} \tag{3.34}$$

where α and β are positive real constants and Γ is the gamma function. A special case of the Mittag-Leffner function is $E_{1,1}[x] = \sum_{k=0}^{\infty} x^k/k! = e^x$. The current is obtained by using equation 3.33 and substitution of the double layer relaxation time $\tau = RC_{dl}$:

$$i(t) = \frac{V_0}{R} E_{\alpha,1}\left[-(\tau_\infty^{1-\alpha}/\tau)t^\alpha\right] = \frac{V_0}{R}\sum_{k=0}^{\infty} \frac{(-\tau_\infty^{1-\alpha}/\tau)^k t^{\alpha k}}{\Gamma(\alpha k + 1)} \tag{3.35}$$

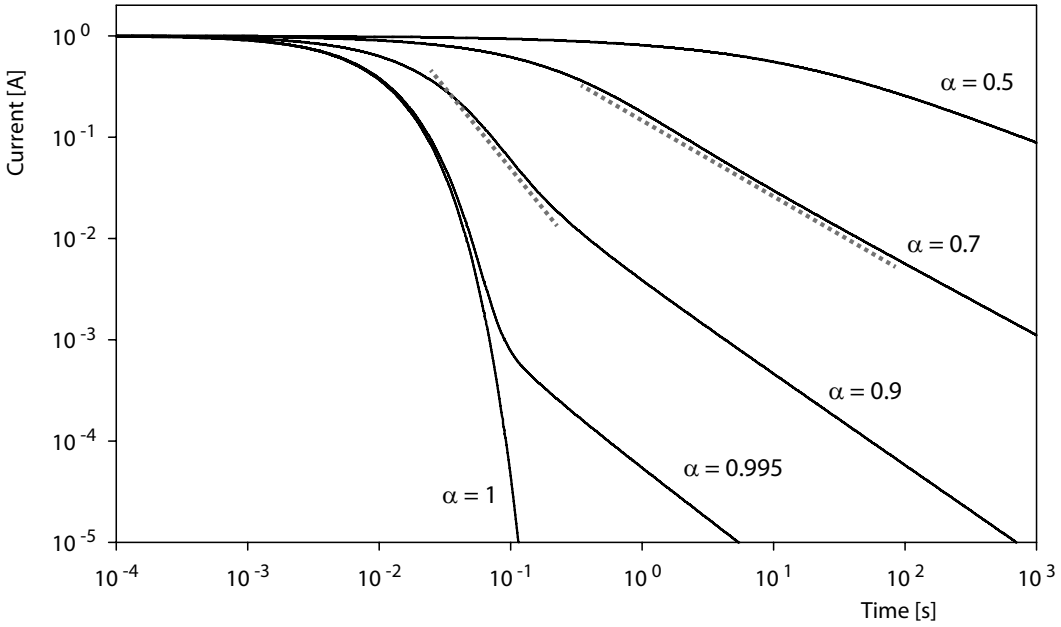

FIGURE 3.9. Time response of the equivalent circuit in Fig. 3.2c. The current $i(t)$ is shown as a function of time t after application of a step voltage, calculated for different values of α, with $\tau = 10^{-2}$ s, $\tau_\infty = 4 \cdot 10^{-6}$ s, and normalized with $V_0/R = 1$ A. Power law behavior is indicated by the dashed gray lines.

For $\alpha = 1$, the CPE element reduces to an ideal capacitor, and the current decays exponentially:

$$i(t) = \frac{V_0}{R} \sum_{k=0}^{\infty} \frac{(-t/\tau)^k}{k!} = \frac{V_0}{R} e^{-t/\tau} \tag{3.36}$$

The response is evaluated for a few values of α in Fig. 3.9. For lower values of α, the formation of the double layer is slower, equivalent to the frequency domain.

4

Dielectric Spectroscopy of PbSe and CdSe Quantum Dots in Apolar Liquid

Abstract

Dielectric spectra of PbSe and CdSe colloidal quantum dots dispersed in an apolar liquid are measured from 1 Hz to 10 MHz. At frequencies of 10 kHz - 1 MHz, Brownian rotation of nanoparticles with a permanent electric dipole moment is detected. At the lowest concentrations ($\sim$ 0.1 %-vol.), the nanoparticles rotate independently of each other and their dipole moment is on the order of 40 - 50 D. At higher concentrations ($\geq$ 0.3 %-vol.), the dipolar relaxation becomes slower, indicating the presence of nanoparticle structures not expected from the weak dipole moment. At lower frequencies, the conductivity and electrode polarization indicate that $\sim$ 1 % of the quantum dots carries a single elementary charge.

4.1. INTRODUCTION

The electric properties of colloidal quantum dots (QDs), in particular their permanent electric dipole moment and net charge, are important for understanding both their optical properties and their colloidal interactions in a liquid. A permanent dipole moment gives rise to an internal electric field that influences the electronic structure and optical selection rules. The presence of a dipole moment for CdSe QDs has been inferred from optical spectroscopy measurements [99], and it has been measured directly by dielectric spectroscopy [19, 20] and optical birefringence measurements [23]. For PbSe QDs, the interpretation of one- and two-photon absorption spectroscopy proved to be difficult [100–105]; breaking of the inversion symmetry due to an internal electric field is suggested to be necessary for a complete understanding of the absorption spectra of both PbSe and PbS QDs [101]. Direct measurements of a dipole moment of PbSe QDs, however, have not been reported.

Initial studies attributed the permanent dipole moment of CdSe quantum dots to its wurtzite crystal structure [19, 23, 106], which has a non-centrosymmetric unit cell, that is, the centers of the positive and negative ion sublattices do not coincide. The bulk unit cell is not necessarily the determining factor for a dipole moment, but also the surface region should be considered, and even the presence of polar facets, which are terminated with only one type of ion, do not necessarily imply the presence of a dipole moment [107–109]. Indeed, also QDs of ZnSe, which has a symmetric zinc-blende unit cell, have a dipole moment, comparable in magnitude to CdSe QDs [20], and this was attributed to the presence of surface charges. Calculations [110] and simulations [111] show that the CdSe dipole moment is strongly reduced by surface reconstruction and relaxation. Minor deviations of the tetrahedral shape of CdS [112] and CdTe [113] nanoparticles lead to varying dipole moments. A strong influence of surface termination on the dipole moment has also been found in calculations for GaAs [114], CdSeCdS [115], and ZnO [116] nanorods.

The dipole moment has also been suggested to play a role in interparticle interactions [16, 117, 118]. In solution, ligand-covered QDs form linear chains, as observed in 2D vitrified thin films of dispersion by cryogenic transmission electron microscopy (cryo-TEM) [16]. The interaction strength could be obtained from statistical analysis of the equilibrium distributions of linear chains. The existence of predominantly linear chains, rather than isotropic clusters, points to a directional interaction. However, the dipole moment calculated from the interaction strength was an order of magnitude larger than those measured with dielectric spectroscopy [19, 20]. Linear chains were also observed in dispersions

of magnetic nanoparticles [119, 120], as well as the effect of these chains on the dipolar relaxation in magnetic susceptibility spectra [121] and on the shape of magnetization curves [122]. Similarly, it might be expected that chains or structures of QDs affect the dipolar relaxation in the complex permittivity spectrum, but such effects have not been observed in previous dielectric spectroscopy measurements [19, 20].

In this chapter, dielectric spectra of both CdSe and PbSe QDs in an apolar liquid are measured, and the dipolar relaxation is studied as a function of volume fraction. The contribution of dipolar relaxation to the permittivity is small. Therefore the complex permittivity spectrum was measured using the setup developed and described in Chapter 2, which directly measures the excess permittivity. First, the theoretically expected contributions to the complex permittivity are discussed (section 4.2), and the experimental methods are explained (section 4.3). Then the results are presented and discussed in section 4.4, and conclusions are drawn in section 4.5.

4.2. THEORY

Several contributions are expected in the frequency-dependent complex relative permittivity $\epsilon(\omega) = \epsilon'(\omega) - i\epsilon''(\omega)$ of colloidal quantum dots in a liquid, where $\omega = 2\pi f$ is the angular frequency. Relative means that the vacuum permittivity ϵ_0 has been divided out. Since the dipolar contribution of the nanoparticles is typically much smaller than the dielectric contribution of the solvent, we built a setup to measure the excess permittivity directly (see Chapter 2), that is, the difference between the permittivity of the dispersion and the dielectric constant of the solvent: $\epsilon^{ex}(\omega) = \epsilon(\omega) - \epsilon_s$. The expected contributions to the excess permittivity are due to dipolar relaxation $\epsilon_d(\omega)$, electrode polarization $\epsilon_{\mathrm{EP}}(\omega)$, and the mismatch in dielectric constant of the quantum dots and solvent ϵ_∞^{ex}:

$$\epsilon^{ex}(\omega) = \epsilon_d(\omega) + \epsilon_{\mathrm{EP}}(\omega) + \epsilon_\infty^{ex} \tag{4.1}$$

These three contributions are discussed in this section.

4.2.1. Relaxation of Permanent Dipoles

The alignment of permanent electric dipoles in an electric field competes with thermal motion and is frequency dependent [123, 124]. In a static electric field, the average dipole moment in the direction of the electric field (z-direction) is obtained from averaging the dipole moment with a Boltzmann weight over all directions, and the result is the Langevin equation:

$$\langle \mu_z \rangle = \mu \left(\coth(x) - \frac{1}{x} \right) \tag{4.2}$$

where $x = \mu E/(kT)$, E is the electric field strength, k is the Boltzmann constant, and T is the absolute temperature. The experiments in this chapter are performed in the limit of a low electric field, when $x \ll 1$, and the dipoles are aligned only to a small extent, such that:

$$\langle \mu_z \rangle = \frac{\mu^2}{3kT} E \tag{4.3}$$

With a contribution to the permittivity given by $\Delta\epsilon_d = n\mu^2/(3kT\epsilon_0)$ in the low frequency limit, the frequency response of spherical particles with a permanent dipole moment is given by the Debye relaxation:

$$\epsilon_d(\omega) = \frac{\Delta\epsilon_d}{1 + i\omega\tau_d} \tag{4.4}$$

On the assumption that Brownian rotation of monodisperse single particles in the solvent is rate limiting, the dipolar relaxation time τ_d is:

$$\tau_d = \frac{4\pi\eta a_H^3}{kT} \tag{4.5}$$

with η the viscosity of the solvent and a_H the hydrodynamic radius of the particles.

4.2.2. Relaxation of Particle Chains

The dipolar relaxation described by eq. (4.4) is only valid for dilute dispersions, when the rotation is independent of other particles. At higher concentrations, interactions between the particles may influence dipolar relaxation. Here, a simple model for chain formation is used to describe the effect of particle interactions on the dipolar relaxation [17, 120].

It is assumed that chains of length q are in equilibrium with q single particles:

$$qA \leftrightharpoons A_q \tag{4.6}$$

This implies the following equality of chemical potentials:

$$q\widetilde{\mu}_1 = \widetilde{\mu}_q \tag{4.7}$$

where $\sim$ is used to distinguish the chemical potential $\widetilde{\mu}$ from the dipole moment μ. In the dilute regime, the chemical potential is:

$$\widetilde{\mu}_q = \widetilde{\mu}_q^0 + kT \ln \phi_q \tag{4.8}$$

with $\widetilde{\mu}_q^0$ the standard chemical potential and ϕ_q the volume fraction of chains of q particles. Then,

$$\phi_q = \phi_1^q e^{-\Delta G_q^0/kT} \tag{4.9}$$

where $\Delta G_q^0 = \widetilde{\mu}_q^0 - q\widetilde{\mu}_1^0$ is the standard Gibbs free energy of a chain of q particles. Furthermore, it is assumed that ΔG_q^0 is determined by the number of contacts

between particles in a chain times a contact free energy of two particles equal to the free energy formation of a dimer, such that for a linear chain:

$$\Delta G_q^0 = (q-1)\Delta G_2^0 \tag{4.10}$$

In terms of the total volume fraction $\phi_{tot} = \sum_q \phi_q$, the volume fraction of chains of q particles is then, by substitution of eq. (4.10) in eq. (4.9):

$$\phi_q = \left(\frac{\phi_{tot}}{\phi_{tot} + e^{\Delta G_2^0/kT}}\right)^q e^{\Delta G_2^0/kT} \tag{4.11}$$

with the use of the series $\sum_{i=1}^{\infty} x^i = x/(1-x)$, valid for $x < 1$.

As an estimate for the rotational relaxation time τ_q of a chain of q particles, the following relation (for $q \geq 2$) is used, which has successfully been applied to model the relaxation of dipolar chains of magnetic nanoparticles [121]:

$$\tau_q = \tau_d \cdot \frac{q^3/3}{(\ln(q) - 0.662 + 0.917q^{-1} - 0.050q^{-2})} \tag{4.12}$$

where τ_d is the rotational relaxation time of a single particle. This relation is based on the rotational diffusion coefficient of spherocylinders [125–127] with an aspect ratio $L/d \geq 2$, with L the rod length and d the width. The L/d ratio is interpreted as a measure for q.

For the dipole moment μ_q of a chain of length q it will be assumed either that all dipoles are aligned within the chain, such that it is equal to q times the dipole moment of a single particle $\mu_q = q\mu$, or that all dipoles are randomly distributed within the chain, such that the average dipole moment of chains is $\mu_q = \sqrt{q} \cdot \mu$.

The end result is that particle chains, whose length distribution is determined by equation (4.11), give the following contribution of dipolar relaxation to the permittivity:

$$\epsilon_d(\omega) = \sum_{q=1}^{\infty} \frac{n_q \mu_q^2}{3\epsilon_0 kT} \cdot \frac{1}{1 + i\omega\tau_q} \tag{4.13}$$

with $n_q = \phi_q/(q(4/3)\pi a_H^3)$ the number density of chains with length q.

4.2.3. Electrode Polarization

Any charged species present in dispersion migrates in an electric field and, at low frequencies, accumulates as an electrostatic double layer near the electrodes. This phenomenon has been studied in detail for ionic solutions in Chapter 3, and the frequency response of a symmetric electrolyte was found to obey the empirical model:

$$\epsilon_{\mathrm{EP}}(\omega) = \frac{\Delta\epsilon_{\mathrm{EP}}}{(i\omega\tau_\infty)^{1-\alpha} + i\omega\tau} \tag{4.14}$$

where $\Delta\epsilon_{\mathrm{EP}} = \epsilon_s \kappa d/2$ reflects the double layer capacitance, $\kappa^{-1} = \sqrt{\epsilon_0 \epsilon_s kT/(2nq^2)}$ is the Debye length, n is the number density of charged species with charge q,

$\tau = d/(2D\kappa)$ is the double layer relaxation time, $\tau_\infty = \epsilon_0\epsilon_s/\sigma_\infty$ the Maxwell-Wagner relaxation time, and α is an empirical constant. At frequencies above the double layer relaxation frequency τ^{-1}, in absence of electrode polarization, the conductivity is defined by $\sigma_\infty = \omega\epsilon_0\epsilon''_{\mathrm{EP}}$. For α = 1, charge transport obeys the Poisson-Nernst-Plank (PNP) equations (eq. (3.1) - (3.3)); however, in Chapter 3 it was found that for Debye lengths $\kappa^{-1} > 10$ - 20 nm, double layer dynamics are different. The deviation from the PNP equations is indicated by $\alpha < 1$.

4.2.4. High Frequency Contribution

The mismatch between the dielectric constants of the quantum dot and the solvent gives an additional contribution to the total permittivity. This contribution is frequency independent in our experimental range, but it is expected to be observed only at high frequencies above the double layer and dipolar relaxations.

The polarizability of a spherical particle with radius a and dielectric constant ϵ_{QD} dispersed in a solvent with dielectric constant ϵ_s is [124]:

$$\alpha_{\mathrm{QD}} = 4\pi\epsilon_s\epsilon_0 a^3 \left(\frac{\epsilon_{\mathrm{QD}} - \epsilon_s}{\epsilon_{\mathrm{QD}} + 2\epsilon_s}\right) \tag{4.15}$$

With the assumption that the dielectric constants of the surfactant and solvent are equal, the excess permittivity due to the dielectric mismatch is:

$$\epsilon_\infty^{ex} = 3\epsilon_s\phi_{core} \left(\frac{\epsilon_{\mathrm{QD}} - \epsilon_s}{\epsilon_{\mathrm{QD}} + 2\epsilon_s}\right) \tag{4.16}$$

where ϕ_{core} is the volume fraction of quantum dots, taking into account only the quantum dot cores, without the absorbed surfactants.

4.3. EXPERIMENTAL METHODS

4.3.1. PbSe Quantum Dots

PbSe quantum dots were prepared using standard airless techniques (Schlenk line and nitrogen glove box) and the following chemicals: lead chloride ($PbCl_2$, 99.999%, Sigma-Aldrich), oleylamine (OLA, 90 %, Aldrich), $Sn[N(SiMe_3)_2]_2$ (Sigma-Aldrich), trioctylphosphine (TOP, 90%, Sigma Aldrich), oleic acid (OA, 90%, Sigma-Aldrich), decalin (Sigma-Aldrich), methanol (MeOH, Sigma-Aldrich, anhydrous, 99.8%), toluene (Sigma-Aldrich, anhydrous, 99.8%).

The synthesis is based on the method of Heiss et al. [128]. A mixture of $PbCl_2$ (0.95 g) and OLA (17.5 mL) was heated to 140 °C. At this temperature a mixture of Se-TOP (1.2 g in 10 mL) and $Sn[N(SiMe_3)_2]_2$ (1.5 mL) was quickly injected. The mixture was reheated to 120 °C and afterwards it was allowed to cool to room temperature in 30 minutes. OA (15 mL) was slowly added, followed by the addition of methanol (40 mL) to precipitate the particles. After centrifugation

(2500 g, 5 minutes), the supernatant was removed. Finally, the particles were re-dissolved in toluene and stored inside a glove box under nitrogen atmosphere.

4.3.2. CdSe Quantum Dots

CdSe quantum dots were prepared using standard airless techniques (Schlenk line and nitrogen glove box) and the following chemicals: $Cd(Ac)_2$ (Sigma-Aldrich, 99%), oleic acid (OA, Sigma-Aldrich, 90%), octadecene (ODE, Sigma-Aldrich, 90%), octadecene amine (ODA, Siga-Aldrich, 90%) selenium (Strem Chemicals, 99.99%), trioctylphosphine (TOP, Sigma-Aldrich, 90%), trioctylphosphine oxide (TOPO, Sigma-Aldrich, 99%), acetone (Merck), decalin (Sigma-Aldrich), hexane (Sigma-Aldrich, anhydrous, 99.8%), methanol (Sigma-Aldrich, anhydrous, 99.8%), toluene (Sigma-Aldrich, anhydrous, 99.8%).

The synthesis is based on the method of Peng et al. [129]. Prior to the synthesis of the CdSe quantum dots, two precursors were synthesized. A mixture of OA (3.68 g), ODE (25.92 g), and $Cd(Ac)_2$ (0.64 g) was heated to 150 °C, and kept under vacuum for 2 h to form $Cd(OA)_2$. Selenium (4.25 g) was dissolved in TOP (22.5 g) at 50 °C, followed by the addition of ODE (35.7 g). Then, a mixture of TOPO (2.22 g), ODA (6.40 g), and $Cd(OA)_2$-precursor (9.8 g) was heated in a 50 mL three-neck flask. After reaching a temperature of 300 °C, the Se-precursor (10.4 g) was added rapidly. The mixture was kept at 250 °C for 10 minutes, followed by the slow (dropwise) addition of a Cd-Se-precursor mixture (1:1) of 12 g to allow the particles to grow further. The particles were diluted by adding 1 equivalent amount of hexane. The quantum dots were washed by adding 2 equivalents of methanol and collecting the upper hexane layer (colored), and 1 equivalent of acetone was added to precipitate the QDs. The nanoparticles were precipitated once more with methanol, Finally, the nanoparticles were re-dissolved in toluene, precipitated once more with methanol, dispersed in decalin, and stored inside a glove box under nitrogen atmosphere.

4.3.3. Characterization

UV/Vis/IR absorption spectra were measured using a PerkinElmer Lambda 950 UV/Vis/IR Spectrophotometer. The nanoparticle concentration c can be determined from the absorbance A_λ at a wavelength λ using the Lambert-Beer law $A_\lambda = \epsilon_\lambda l c$, with ϵ_λ the extinction coefficient at wavelength λ and l = 1 cm the optical path length. Concentrations are best determined at absorption energies well above the semiconductor bandgap, in which case quantum confinement effects do not play a role and the molar extinction coefficient scales linearly with the nanoparticle volume but is independent of the nanoparticle size [130, 131]. The studied PbSe nanoparticles have their first absorption peak at a wavelength of λ = 1680 nm, corresponding to a bandgap of 0.740 eV. This indicates that the

nanoparticle core has a diameter of 5.71 nm as determined from the bandgap using the following empirical sizing curve [130]:

$$E_g[\mathrm{eV}] = 0.278 + (0.016d^2 + 0.209d + 0.45)^{-1} \tag{4.17}$$

with d the diameter in nm. The concentration of nanoparticles in the stock dispersion was determined from the absorption at 3.1 eV (λ = 400 nm) using the extinction coefficient [130]:

$$\epsilon_{3.1\mathrm{eV}}[\mathrm{cm}^{-1}\mu\mathrm{M}^{-1}] = (0.0277 \pm 0.0005) \cdot d^3 \tag{4.18}$$

The studied CdSe quantum dots have a bandgap at a wavelength of λ = 589 nm (E_g = 2.11 eV). An empirical sizing curve [131] was used to determine the core diameter d = 4.02 nm:

$$E_g[\mathrm{eV}] = 1.858 + (0.220d^2 + 0.008d + 0.373)^{-1} \tag{4.19}$$

The extinction coefficient at 3.1 eV was used to determine the concentration [131]:

$$\epsilon_\lambda[\mathrm{cm}^{-1}\mathrm{M}^{-1}] = (1.52 \pm 0.03) \cdot 10^3 \cdot zV_{\mathrm{QD}}/V_{\mathrm{UC}} \tag{4.20}$$

with, for wurtzite CdSe, the number of unit ion pairs per unit cell z = 2, the volume of one quantum dot V_{QD}, and the volume of the unit cell V_{UC} = $1.296 \cdot 10^{-22}$ cm^3 [131].

The nanoparticles were also imaged with transmission electron microscopy (TEM). The spherical quantum dots have a core diameter of 5.09 $\pm$ 0.44 nm (PbSe) and 4.2 nm (CdSe).

The viscosity of cis/trans-decalin was measured using an Anton-Paar Physica MCR300 rheometer with a cone-plate cell (1° cone angle). A viscosity was measured of 2.26 mPa·s at 23 $^\circ$C, which is in-between that of cis-decalin (3.18 mPa·s) and trans-decalin (2.02 mPa·s) [132].

4.3.4. Dielectric Spectroscopy Measurements

Dielectric spectra ($\epsilon^{ex} = \epsilon^{ex\prime} - i\epsilon^{ex\prime\prime}$) were measured using the differential complex permittivity setup and measurement procedures described in Chapter 2, with the use of the gold/ITO capacitor with cell constant K_c = 28.70 pF and electrode spacing d = 94.6 μm. The capacitor was filled with dispersion in a glove box under nitrogen atmosphere. The frequency range $10^3 - 10^7$ Hz was measured at 1.0 V, with use of a compensating voltage to cancel the remaining background. The frequency range $10^0 - 10^3$ Hz was measured at 0.25 V, without the use of compensating voltage. Measurements were performed at a temperature of 296 K.

4.4. RESULTS AND DISCUSSION

The complex relative permittivity was measured over a broad frequency range for PbSe quantum dots dispersed in toluene (Fig. 4.1) and CdSe quantum dots in cis/trans-decalin (Fig. 4.2). Both types of nanoparticles are sterically stabilized with oleic acid. The characteristics of both dispersions are given in table 4.1. The core diameter was determined from the first absorption peak UV/Vis/IR absorption measurements (see section 4.3). The size-dependent dielectric constant of CdSe is estimated based on theoretical calculations (ϵ_{CdSe} = 9.1) [134]. Whether the dielectric constant of PbSe is also size-dependent is not known; experiments indicate that $\epsilon_{\mathrm{PbSe}} > 100$ at least [133]. Therefore the bulk value ϵ_{PbSe} = 250 is assumed. Dispersions of different QD concentrations were prepared by dilution of a stock dispersion by pure solvent. The concentration of a diluted dispersion was determined from UV/Vis/IR absorption at an absorption energy of 3.1 eV (see section 4.3). The volume fraction of quantum dots was then determined from this concentration and the hydrodynamic radius a_H as determined below.

The different contributions of the quantum dots to the dielectric spectra will be discussed separately: dipolar relaxation is observed in the frequency range 10 kHz - 1 MHz; charged quantum dots give rise to a conductivity in the imaginary part of the permittivity and polarize the electrodes at low frequencies; a contribution is present at the highest frequencies due to the mismatch in dielectric constants of solvent and particle. As discussed in Chapter 2, also a shoulder is observed in the real part of the permittivity ϵ' in the frequency range $10^2 - 10^4$, after fitting for electrode polarization and the dipolar relaxation. This shoulder is an artifact due to a small $\epsilon'/\epsilon'' < 0.01$ ratio, and not due to quantum dots.

	core diameter d [nm]	ϵ_{QD}	solvent	viscosity η [mPa·s] (at 23°C)	ϵ_s (at 23°C)	capping
PbSe	5.71	250 [133]	toluene	0.569 [132]	2.38	oleic acid
CdSe	4.02	9.1 [134]	cis/trans-decalin	2.26	2.2	oleic acid

TABLE 4.1. Overview of physical parameters for the quantum dots and solvents.

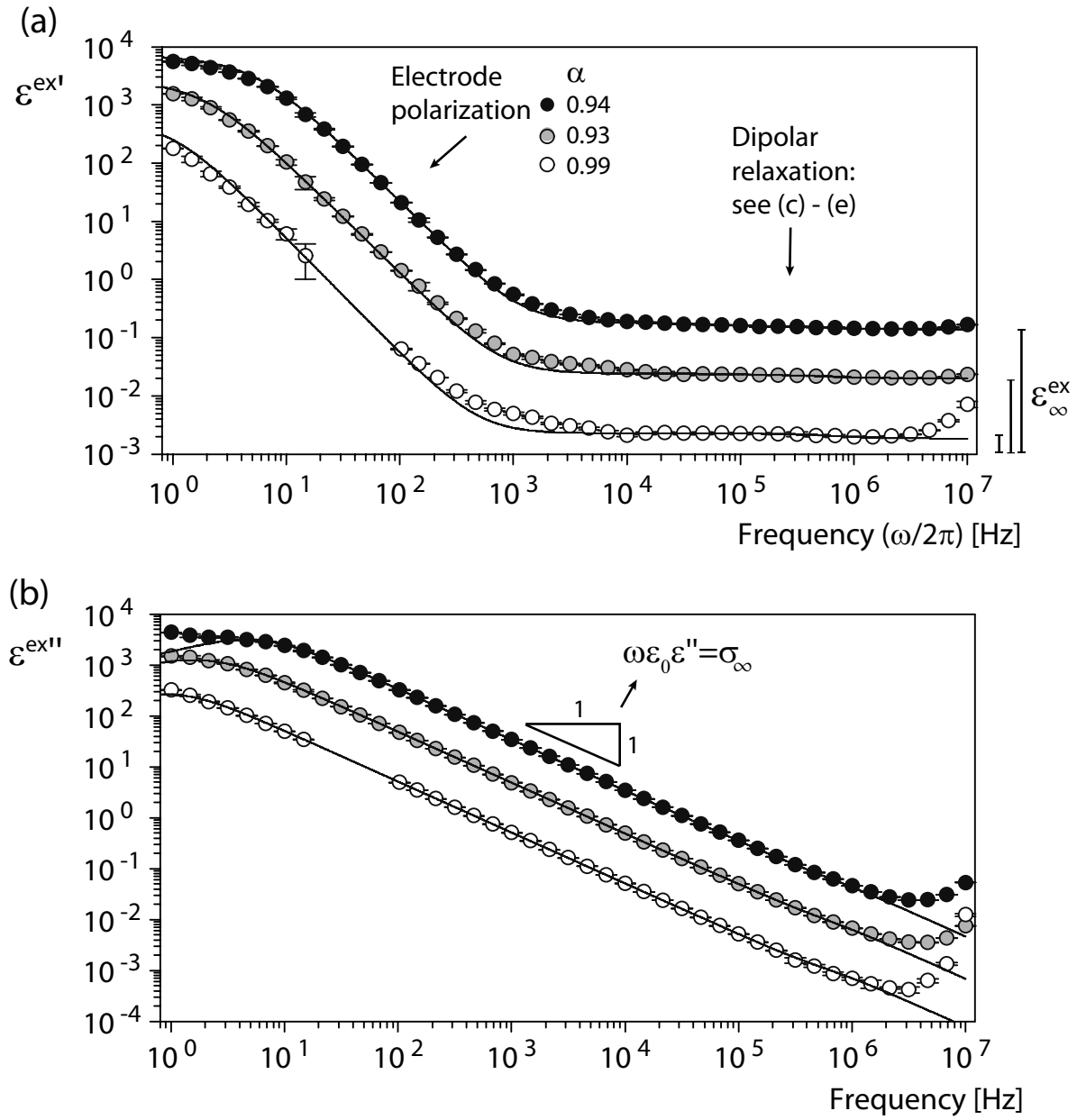

FIGURE 4.1. Dielectric spectra of PbSe quantum dots dispersed in toluene; (a) the real and (b) the imaginary part of the excess permittivity $\epsilon^{ex} = \epsilon^{ex\prime} - i\epsilon^{ex\prime\prime}$. The frequency range where the relaxation of permanent dipole is visible in $\epsilon^{ex\prime}$ is shown enlarged on the next page in (c)-(e) for volume fractions from 0.174 % to 17.4 %. The fits are discussed in the text.

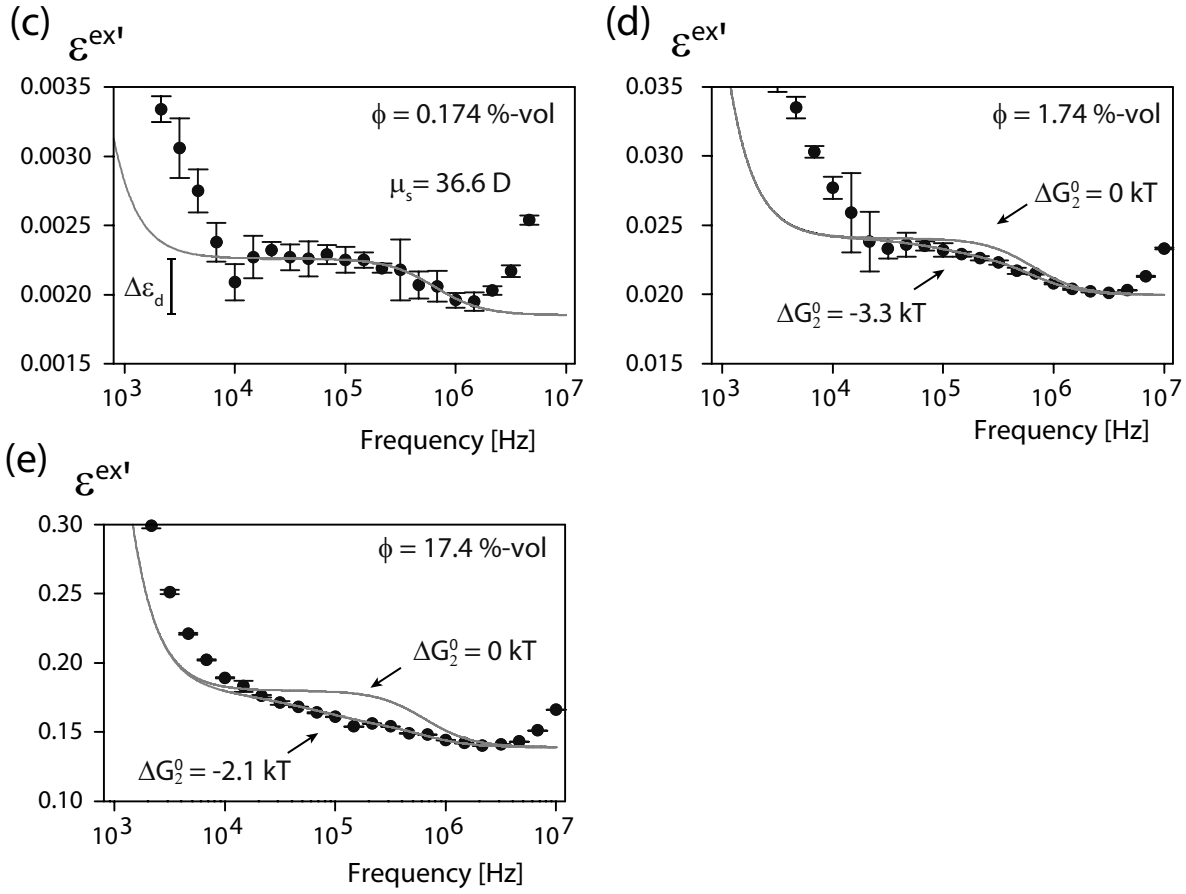

4.4.1. Relaxation of Permanent Dipoles

The relaxation in the frequency range 10 kHz - 1 MHz is shown in more detail in Fig. 4.1c-e and 4.2c-f. At low volume fractions (ϕ = 0.1 %) measurements were fitted on the basis of Brownian rotation of single particles (eqs. (4.4),(4.5)). The hydrodynamic radii, obtained from the relaxation time, are in agreement with those of the single spherical particles, that is, the core radius plus a 2.2 - 2.3 nm oleic acid surfactant shell. From the magnitude of the relaxation, the screened dipole moment for CdSe is μ = 53.1 D, and for PbSe it is μ = 36.6 D. This value for CdSe is comparable with previous dielectric spectroscopy measurements [19,20]. For PbSe, no direct measurements of a permanent dipole moment have been reported before. The presence of a dipole moment is required for understanding of absorption transitions of PbSe QDs [101]. Nanoparticle dispersions always have some size polydispersity, and it seems unlikely that all particles are perfectly symmetrical. To produce such a dipole, only minor variations in the shape of the nanoparticle are necessary, which has been shown for deviations in the truncation of tetrahedral particles [112], or asymmetric distributions of polar facets in facetted cubic particles [117].

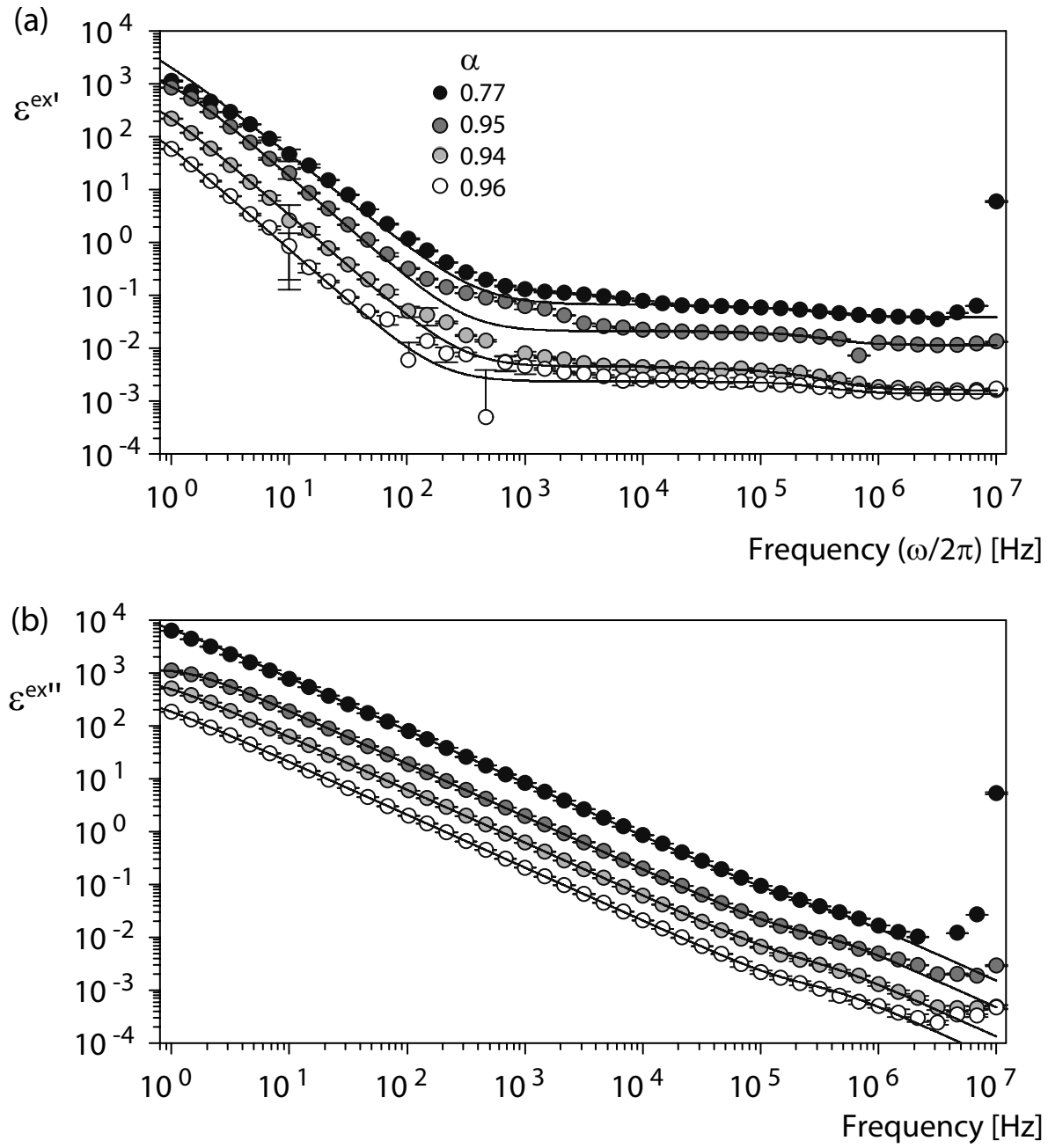

FIGURE 4.2. Dielectric spectra of CdSe quantum dots dispersed in decalin; (a) the real and (b) the imaginary part of the excess permittivity $\epsilon^{ex} = \epsilon^{ex\prime} - i\epsilon^{ex\prime\prime}$. The frequency range where the relaxation of permanent dipole is visible in $\epsilon^{ex\prime}$ is shown enlarged on the next page in (c)-(f) for volume fractions from 0.103 % to 3.09 %. The fits are discussed in the text.

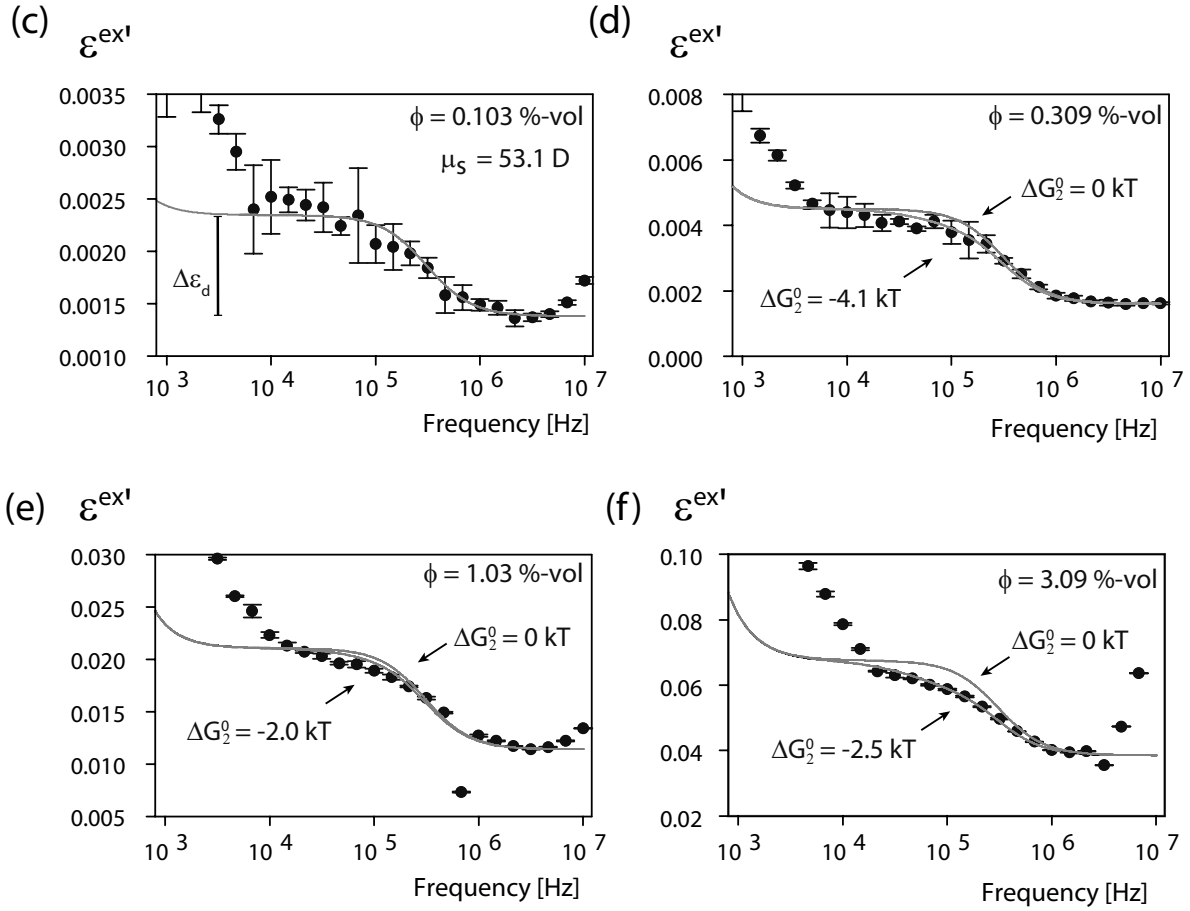

The dipolar relaxation of the concentrated samples is smaller in magnitude and lower in frequency than expected, based on the dilute measurements. The relaxations are fitted to the model that accounts for the presence of chains given by equation (4.13) with the contact free energy ΔG_2^0 as a fit parameter; the total volume fraction of quantum dots ϕ_{tot} is known, and the screened dipole moment μ_s and the dipolar relaxation time τ_d of a single quantum dot are obtained from the dilute measurements. The fits are plotted in Fig. 4.1c-e and 4.2c-f, and the expected response for single particles only is plotted for comparison. Contact free energies are obtained, for both PbSe and CdSe QDs, of $\Delta G_2^0 \approx -2$ to -4 kT. This is also consistent with the dilute measurements, since an interaction of this magnitude does not change the expected response of the dilute measurements due to the low volume fractions. It appears that ΔG_2^0 becomes more negative upon dilution, which might be explained by dissolution of surfactants from the nanoparticle surface such that nanoparticles approach each other more closely upon contact. The chain length distributions, as calculated from the model in equation (4.11) and the experimentally fitted ΔG_2^0, are shown in Fig. 4.4. Apart from single particles, the dipolar relaxations in Fig. 4.1d and 4.2d-f also include the relaxation of dimers and trimers, while Fig. 4.1e includes also longer chains.

The model to describe the dipolar relaxation is rather simple and contains approximations for the chain length distribution, for the rotational relaxation time, and for the dipole moment of a chain. Nevertheless, the contact free energy ΔG_2^0 for PbSe is in quantitative agreement with other reported values for PbSe of similar size obtained from cryo-TEM (ΔG_2^0 = -2 kT), analytical ultracentrifugation, and SAXS measurements [17, 135].

The permanent dipole moments measured for single particles is too weak to explain the chain formation on the basis of dipolar interaction between quantum dots. The attraction between two dipoles is maximal when in contact in the head-to-tail configuration, and the maximum interaction U_{max} is calculated when it is assumed that the dipole consists of two opposite charges placed on opposite sides of the nanoparticle, rather than being present as point-dipole [118]:

$$U_{max} = \frac{-2\mu^2}{4\pi\epsilon_s\epsilon_0\Delta(\Delta^2 - d^2)} \tag{4.21}$$

with Δ the center-to-center distance and d the core diameter. The maximum interaction energy calculated in this way is U_{max} = -0.035 kT for PbSe and U_{max} = -0.14 kT for CdSe. This is much smaller than the coupling free energy ΔG_2^0 of ≈ -2 to -4 kT. In principle, U_{max} should be compared to the coupling free enthalpy ΔH_2^0, rather than the coupling free energy $\Delta G_2^0 = \Delta H_2^0 - T\Delta S_2^0$. Since the entropy $\Delta S_2^0 < 0$ for chain formation, ΔH_2^0 is even more negative than ΔG_2^0. Hence, the interparticle interaction that leads to the observed chain formation is not explained by the interaction between the permanent dipole moments. Since

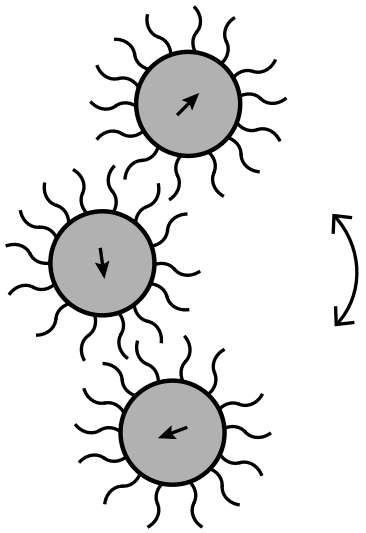

FIGURE 4.3. Schematic illustration of a chain of three quantum dots, where it is assumed that their permanent dipole moments are randomly orientated within the chain.

the interaction of the permanent dipole moment of the quantum dots is weak, it is likely that the dipole moments in a chain are not aligned, but randomly orientated, as illustrated in Fig. 4.3. In fitting the dipolar relaxation above, it was also assumed that the total dipole moment of a chain is given by a random distribution of the dipole moments ($\mu_q = \sqrt{q} \cdot \mu$), and this does give a better fit than assuming the dipoles to be aligned ($\mu_q = q \cdot \mu$).

The origin of the interparticle interaction remains a question, since the permanent dipole moment is too small. When nanoparticle cores are separated by two ligand layers, also van der Waals forces are not expected to be sufficiently strong [135]. The dipole moment, however, might also fluctuate due to atomic motions on a time scale shorter than measured here. A fluctuating dipole moment of ($\sim$ 50 D) has been found in atomistic simulations of PbSe quantum dots, although without a permanent moment [136]. For CdSe nanoparticles, it has been found in calculations for CdSe nanoparticles that, apart from the dipole moment, also higher-order moments exists [110]. At a separation distance comparable to the nanoparticle size, the dipole-quadrupole, dipole-octupole, and quadrupole-quadrupole interactions appear comparable to that of the dipole-dipole interaction. The interparticle interactions possibly result from the sum of several interactions.

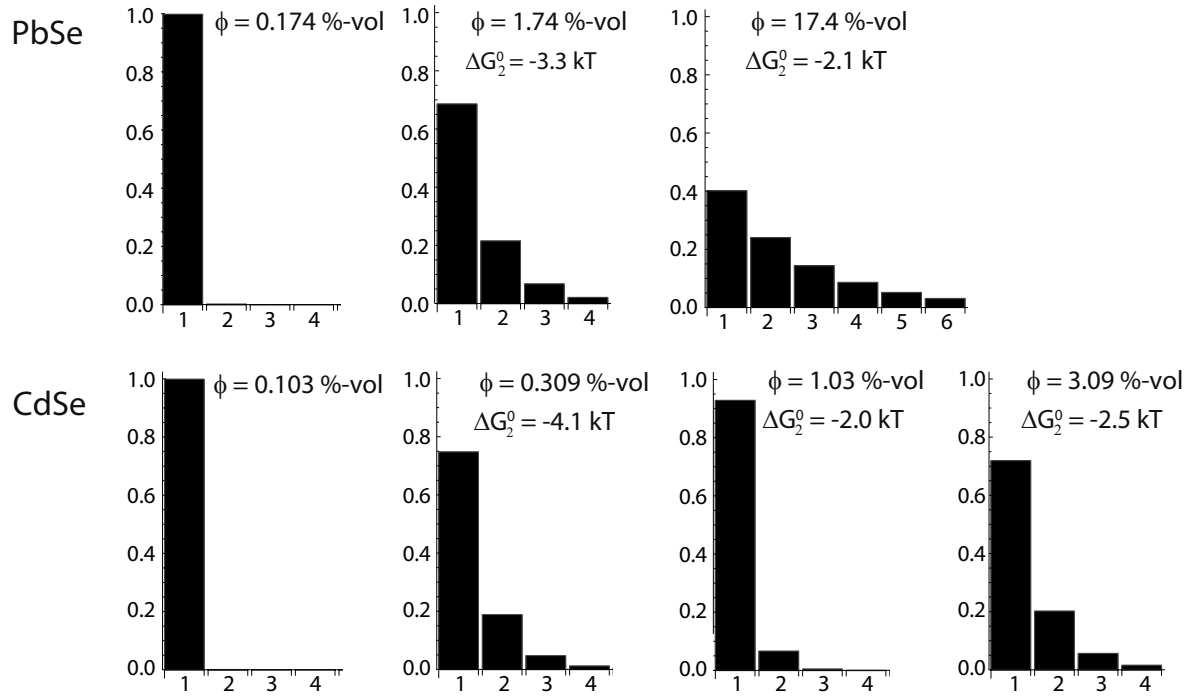

FIGURE 4.4. The relative chain length distributions (ϕ_q/ϕ_{tot} as function of q) for each measurement, as calculated from the model in eq. (4.11) and the experimentally determined coupling free energy ΔG_2^0.

4.4.2. Electrode Polarization

The quantum dot dispersions have a finite conductivity σ_∞, proportional to the concentration of the quantum dots (Fig. 4.5), despite the high electrostatic energy cost of creating net charges in apolar liquids with their low dielectric constant. Shim et al. [20] suggested that the conductivity in their dielectric spectroscopy measurements originated from quantum dots with a net charge, rather than ions or charged surfactants.

Argued along the line of Shim et al. [20] and Cirillo et al. [24], the conductivity is much smaller than when all QDs would carry a charge of $\pm$ 1e, and due to the high charging energy, a QD with a net charge of $\pm$ 2e or larger is rather unlikely. Then charging might be described by the equilibrium QD+QD$\rightleftharpoons$QD$^+$+QD$^-$, which predicts that the conductivity is proportional to the concentration. The charging free energy for this equilibrium is given by [24]:

$$\Delta G^0_{ch} = -kT \cdot \ln\left(\frac{\gamma^2}{(1-2\gamma)^2}\right) \tag{4.22}$$

where γ is the fraction of charged QDs. The measured conductivity ($\sigma_\infty = \epsilon_0 \epsilon_s D \kappa^2$) alone is not sufficient to determine whether the charges originate from QDs, but the electrode polarization at low frequencies, with relaxation time $\tau = d/(2D\kappa)$, does enable to determine both D and κ^{-1}. In our experiments, the electrode polarization and conductivity (Fig. 4.1a and 4.2a) are consistent with a small fraction (PbSe: γ = 1.0 %, CdSe: γ = 1.2 %) of QDs carrying either one positive or one negative net charge ($\pm 1e$), where the electrode polarization is modeled according to eq. (4.14). The parameter α varies little with concentration ($\alpha \approx$ 0.92 - 0.99), with the exception of one measurement.

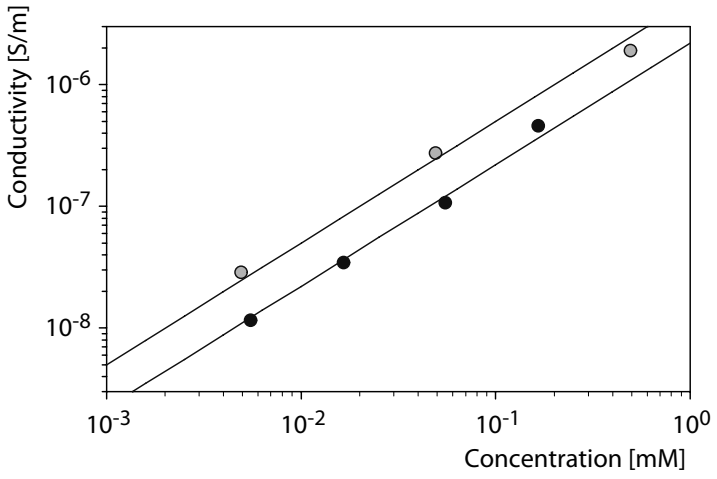

FIGURE 4.5. Conductivity σ_∞ of PbSe QDs in toluene and CdSe QDs in decalin as a function of concentration.

As a simple estimate for the charging energy, the QD core is considered as a homogeneously charged sphere with radius r in a solvent with dielectric constant ϵ_s [24]:

$$E_{ch} = \frac{e^2}{8\pi\epsilon_0\epsilon_s r} \tag{4.23}$$

This estimate predicts $\Delta G^0_{ch} = 2E_{ch}$ = 8.2 kT and 12.7 kT, for respectively the PbSe and CdSe QDs in this study, which is close to the experimental values ΔG^0_{ch} = 9.2 kT and 8.8 kT determined from eq. (4.22). More detailed calculations of the charging energy [20, 24] taking into account screening by the QD core did yield approximately the same values, indicating that the dielectric constant of the solvent is the determining factor for the charging energy.

4.4.3. High Frequency Contribution

The excess permittivity ϵ^{ex}_∞ observed at the highest frequencies, that is, after fitting for electrode polarization and dipolar relaxation, is compared in Fig. 4.6 with the expected contribution to the permittivity from the mismatch in dielectric constant of the particle and solvent, as described by eq. (4.16). It is assumed that the dielectric constant of oleic acid and the apolar solvent are equal. In the case of PbSe, ϵ^{ex}_∞ is proportional to the core volume fraction ϕ_{core}, and the agreement with theory is excellent. Note that, as the dielectric constant of PbSe is much larger than that of the solvent, eq. (4.16) reduces to $\epsilon^{ex}_\infty = 3\epsilon_s\phi_{core}$. In the case of CdSe, ϵ^{ex}_∞ is also proportional to ϕ_{core}, but the experimental values are a factor 3 larger than theory. This discrepancy can not be explained by an unaccounted contribution of the surfactant shell. It is more likely that, for instance, a small fraction of methanol (with dielectric constant $\epsilon_s = 33$) is still present after washing the quantum dots.

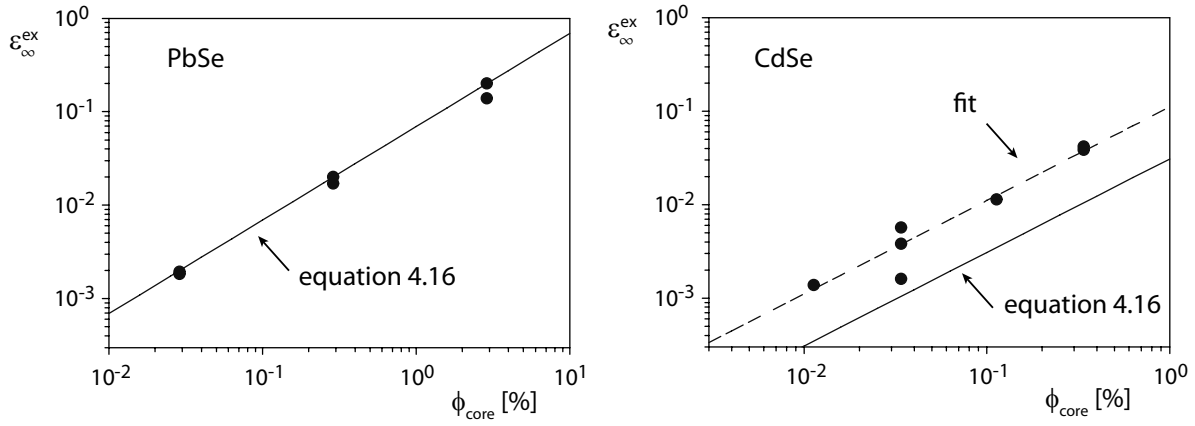

FIGURE 4.6. The excess permittivity ϵ^{ex}_∞ at high frequencies for (a) PbSe and (b) CdSe.

4.5. CONCLUSIONS

Dielectric spectroscopy is a technique that can reveal several electric properties of colloidal quantum dots dispersed in an apolar liquid. Dipolar relaxations have been observed in permittivity spectra of oleic acid capped CdSe and PbSe quantum dots. At low volume fraction ($\phi \approx 0.1$ %-vol) the dipolar relaxation corresponds to that of a single particle. Screened dipole moments have been determined to be 36.6 D for PbSe QDs with a 5.7 nm core diameter and 53.1 D for CdSe QDs with a 4.0 nm core diameter. Direct measurement of a permanent dipole moment of PbSe has not yet been reported before, but it is important when considering the electronic structure. At higher volume fractions ($\phi > 0.3$ %-vol) these relaxations are well fitted by a simple model that takes into account the dipolar relaxation of chains that form due to a net attraction of 2 - 4 kT between the dispersed quantum dots. The found contact free energy is in good agreement with other reported values obtained from cryo-TEM, analytical ultracentrifugation, and SAXS measurements. The maximum interaction energy of ≈ 0.1 kT due to the permanent dipole moment is too small to account for these chains. The interparticle interaction is possibly the sum of different types of interactions, such as multipole interactions.

4.6. ACKNOWLEDGEMENTS

PbSe and CdSe quantum dots were kindly provided by Relinde van Dijk-Moes. I would like to acknowledge Jos van Rijssel, Daniel Vanmaekelbergh and Esther Groeneveld for useful discussions.

5

Comparative Study of Electrophoretic and Dynamic Mobilities of Model Silica Colloids in Ethanol

ABSTRACT

Electroacoustics and laser Doppler electrophoresis were employed to measure the mobility of surface-modified silica colloids in ethanol as a function of the ionic strength. Sufficiently low volume fractions were chosen to exclude effects of interparticle interactions. At high ionic strength, the electrophoretic mobility μ_e is equal to the (electroacoustic) dynamic mobility μ_d at 3.3 MHz. However, the ratio μ_d/μ_e increases significantly to ~ 5 at low ionic strength. This increase may be due to the porous outer-layer of the surface modified silica spheres.

5.1. INTRODUCTION

Electroacoustics is a technique to measure the mobility of colloidal particles using an acoustic effect predicted by Debye [14], and it is an alternative method for the frequently used laser Doppler electrophoresis. Electroacoustics employs ultrasound, as a result of which the colloids move due to a density contrast between colloid and solvent, and the dynamic mobility μ_d is indirectly measured from the resulting colloid vibration current (CVI). Laser Doppler electrophoresis directly measures the electrophoretic mobility μ_e from the velocity of charged particles in an electric field through the frequency (Doppler) shift of scattered laser light. Electroacoustics is of particular interest in two situations when the use of laser Doppler electrophoresis is constrained. Firstly, it allows measurements on colloidal dispersions with high solid volume fractions. In contrast, laser Doppler electrophoresis is limited by multiple scattering to very dilute dispersions, unless special care is taken to minimize the difference in refractive index between the colloid and solvent. Secondly, electroacoustics could be used to study light absorbing colloids, which is more complicated with laser Doppler electrophoresis.

There are two different approaches to obtain the zeta potential from the measured CVI. The first approach uses the dynamic mobility μ_d, which can be obtained from the kinetic coefficients using an Onsager's reciprocal relationship [137–139]:

$$CVI = \mu_d \phi \frac{\rho_p - \rho_s}{\rho_s} \nabla P \tag{5.1}$$

where ϕ is the volume fraction, $\rho_s = \phi\rho_p + (1-\phi)\rho_m$ is the average density, ρ_p and ρ_m are the particle and solvent densities respectively, and ∇P is the gradient of the applied pressure. This dynamic mobility differs from the electrophoretic mobility only in the frequency of the electric field. The dynamic mobility can easily be obtained, but the relation between the dynamic mobility and the zeta potential usually requires knowledge about interparticle interactions. A second approach directly calculates the zeta potential by solving the electrokinetic equations using a cell model [139].

Although a considerable number of electroacoustic measurements have been devoted to aqueous dispersions with a small Debye length κ^{-1} [140–142], rather less attention has been paid to charged colloids in organic solvents with a large Debye length [143]. Monodisperse silica spheres coated with 3-methacryloxypropyltrimethoxysilane (TPM), briefly referred to as TPM-silica,

were designed [144] as model colloids to study charged particles in weakly polar solvents. This system benefits from an important feature of TPM-silica particles and that is the possibility of optical matching up to high volume fractions [91, 145]. TPM-silica colloids have been widely applied in the study of sedimentation [91, 146], hydrodynamic interactions [147, 148], colloidal crystallization [149, 150], scattering dichroism [151], osmotic pressure [152, 153], rheology [154, 155] and electrorheology [156, 157]. Here, we use these spheres to compare the dynamic and electrophoretic mobilities in ethanol as a function of salt concentration. To make this comparison, measurements were performed at low volume fractions (less than 1 %-vol) in absence of double layer overlap and interparticle interactions. $LiNO_3$ is used as an indifferent salt to tune the dispersion between low and high ionic strength.

In this chapter a description of the experimental methods (section 5.2) will be followed by the results of laser Doppler electrophoresis (section 5.3) and electroacoustics (section 5.4), respectively. Next, the comparison between the dynamic and electrophoretic mobilities is discussed in section 5.5, and conclusions are drawn in section 5.6.

5.2. EXPERIMENTAL METHODS

The TPM-silica colloids studied here, which have laboratory code "SA6(2) TPM", have been described in reference [144]. Though synthesized approximately 26 years prior to this study, these dispersions are still stable. These particles have a hydrodynamic radius a of 90 nm as determined by dynamic light scattering (DLS) with a polydispersity of 8 % as determined from electron microscopy, and they have a density of 1.6 g cm^{-3}. A stock dispersion was deionized with resin (BioRad, AG 501-X8 20-50 mesh (D)) and the weight fraction was determined by drying a known amount of dispersion and weighing the residue (1.67 ± 0.04 %-wt). Deionized ethanol was prepared from resin and ethanol (p.a.). All dispersions were prepared by mixing weighed amounts of silica dispersion, deionized ethanol, and a solution of $LiNO_3$ in deionized ethanol. The deionized ethanol and $LiNO_3$ in deionized ethanol were filtered prior to use with a Minisart NY25 0.20 μm filter (Sartorius Stedim).

Electrophoretic mobilities were measured with a Malvern Zetasizer Nano and a dip cell (PCS1115) as probe. The Malvern Zetasizer Nano uses phase analysis light scattering (PALS) [13] to measure the electrophoretic mobility. The dip cell was sonicated in ethanol for 15 minutes before use. All samples were measured at 20.0 ^{o}C and at least 48 hours after preparation of the dispersion

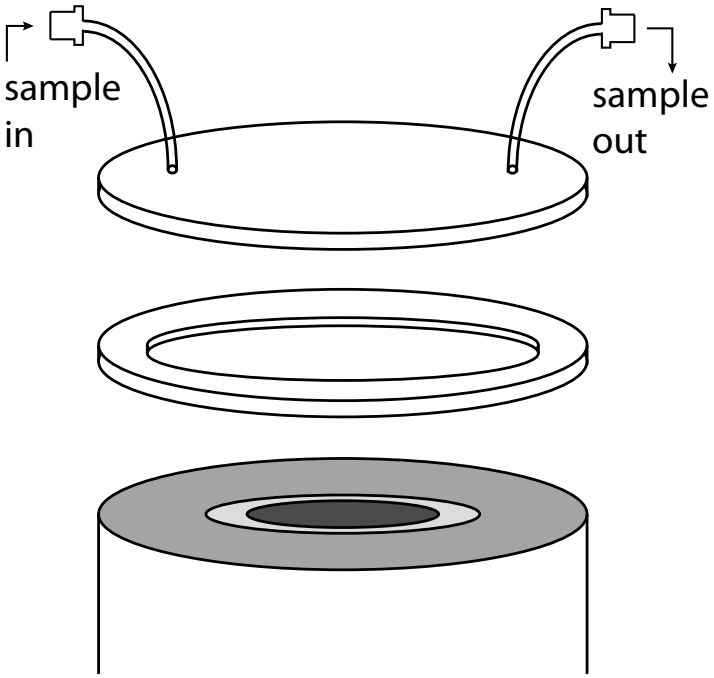

FIGURE 5.1. Illustration of the 0.9 mL homebuilt cell, consisting of a glass plate with two tubes, separated from the DT-310 probe by a Teflon ring.

to allow the dispersion to equilibrate. A voltage of 7.5 V was applied to obtain symmetric phase plots. Each sample was measured seven times, with a two or three minute interval between each measurement of 50 data points. The results of seven measurements were averaged.

Electroacoustic measurements were performed with a DT-310 (Dispersion Technology, Inc., Mt. Kisco, New York) in a thermostated room at 21 °C. This device applies $800 - 1.6 \cdot 10^6$ sound pulses at a frequency of 3.3 MHz and measures electric pulses. The electric signal can be converted to CVI using a geometrical constant, which can be found by calibration with a colloidal dispersion of known zeta potential. More details of this device can be found in reference 139.

Measurements can be performed by placing the probe in a beaker with dispersion. However, this method requires much dispersion. Alternatively, a plastic cap which is delivered with the device can be placed on top of the probe and can be filled with 9 mL dispersion. If less dispersion is used, the signal depends on the volume of the dispersion. To use even less dispersion, a homemade cell was used to measure on small volumes of dispersion (0.9 mL) and to ensure measurement on the same volume during each measurement. The cell (Fig. 5.1) consists of glass plate (with the same diameter as the electroacoustic probe of 32 mm, and 2 mm in thickness), separated from the probe by two teflon rings (outer diamater 32 mm, inner diameter 16 mm, 2 mm thickness). Two flexible 1 mm diameter

teflon tubes are glued in two small holes in the glass plate to fill the cell with dispersion. A plastic holder keeps the cell on the probe to prevent leakage of dispersion.

The device was calibrated prior to use with an aqueous 10%-wt Ludox silica dispersion from Quantachrome, with a known zeta potential of 38 mV. Test measurements with our homemade cell were performed with diluted aqueous Ludox HS-40 dispersions. Supernatant for background measurements was obtained through centrifugation of the dispersions with a Beckmann centrifuge at 2095 g for 16-20 hours.

Calculations of dynamic and electrophoretic mobilities were performed with the software package Dynamic Mobility and Conductivity v1.0 (Colloid Consulting Group), which uses the theory described in references 142, 158–161. Dispersion properties used for the calculations were volume fraction ϕ = 0.01 %, temperature T = 20 °C, ethanol dielectric constant ϵ_s = 25.45, particle dielectric constant ϵ_p = 3.9, ethanol viscosity η = 1.144 mPa·s, ethanol density ρ_s = 0.789 kg L^{-1}, particle density ρ_p = 1.6 kg L^{-1}, particle radius a = 90 nm, and limiting ionic conductivities $\Lambda_{0,H^+} = 61.3$ cm^2 Ω^{-1} mol^{-1} and $\Lambda_{0,Cl^-} = 23.0$ cm^2 Ω^{-1} mol^{-1} [162].

5.3. LASER DOPPLER ELECTROPHORESIS

Electrophoretic mobilities of the TPM-silica spheres in ethanol were measured using laser Doppler electrophoresis as a function of ionic strength and volume fraction. The electrophoretic mobility is volume fraction independent below 0.1 %; however, it decreases strongly above 0.1 % (Fig. 5.2). In the case of thin electric double layers, the mobility is proportional to $1 - \phi$ [163]. We expect that the much stronger volume fraction dependence observed here is due to multiple scattering. Therefore, measurements as a function of salt concentration were performed at a low volume fraction of 0.01 % (Fig. 5.3). The indifferent salt $LiNO_3$ was used to tune the ionic strength from 1.3 μM to 1.9 mM. The ionic strength is expressed in this work as the parameter κa, which gives the ratio between the particle radius a and the Debye length or double layer thickness κ^{-1}:

$$\kappa^{-1} = \sqrt{\frac{\epsilon_0 \epsilon_m k_B T}{\sum_i c_i N_A z_i^2 e^2}} \tag{5.2}$$

where $\epsilon_0\epsilon_m$ is the solvent permittivity, k_B is the Boltzmann constant, N_A is the Avogadro constant, T is the temperature, e is the elementary charge and c_i and z_i are the molar concentration and valency of ion i.

To obtain the correct κa, it was necessary to take into account 'background' ions still present in deionized ethanol. Assuming the presence of a symmetric monovalent 'background' salt, its concentration was estimated from the conductivity

of deionized ethanol by:

$$c_{bg} \approx \frac{\sigma}{\Lambda_{0,+} + \Lambda_{0,-}} \tag{5.3}$$

with the conductivity σ and limiting ionic mobilities $\Lambda_{0,+}$ and $\Lambda_{0,-}$. The conductivity $\sigma = 1.1 \cdot 10^{-5}\ S\ m^{-1}$ was measured with a parallel plate capacitor, and limiting ionic mobilities $\Lambda_{0,H^+} = 61.3$ cm^2 Ω^{-1} mol^{-1} and $\Lambda_{0,Cl^-} = 23.0$ cm^2 Ω^{-1} mol^{-1} [162] were assumed (both in ethanol at 25 °C). The resulting background salt concentration of $c_{bg} = 1.3$ μM was added to the $LiNO_3$ concentration for the calculation of the double layer thickness κ^{-1}. This yields a κ^{-1} of 153 nm in our deionized ethanol, and a minimum κa of 0.59 for our silica particles of 90 nm. On this basis, we estimate that in each dispersion the salt concentration is at least 200 times larger than the concentration of counterions.

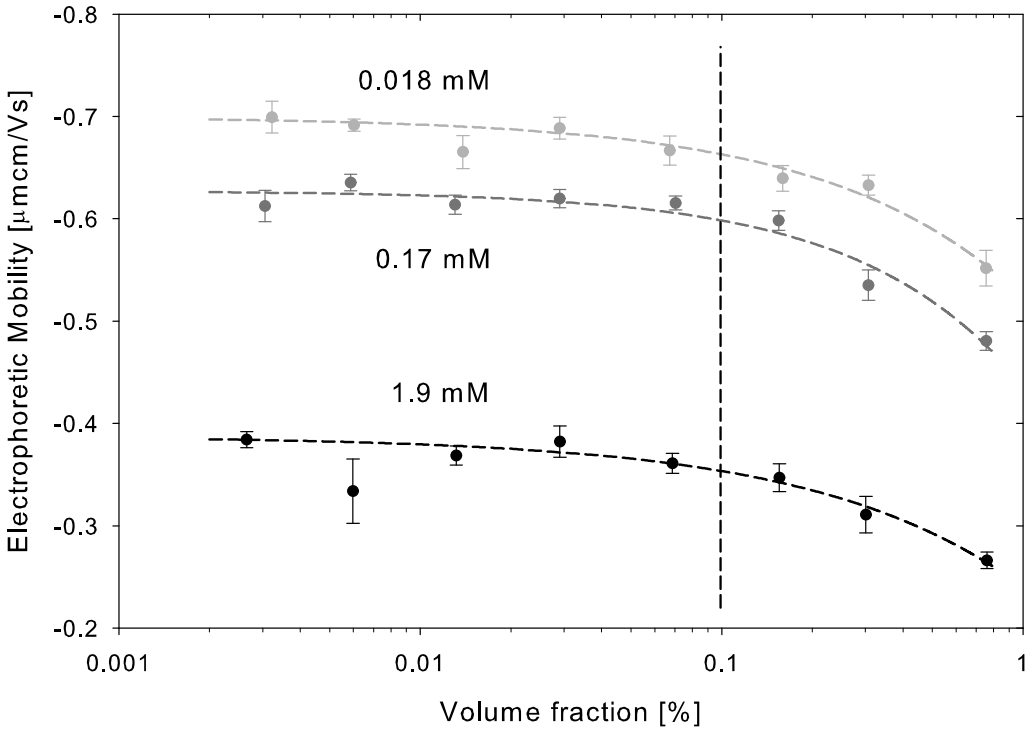

FIGURE 5.2. Electrophoretic mobility as a function of volume fraction for three different concentrations of $LiNO_3$: 0.018 mM ($\kappa a = 2.3$; light grey), 0.17 mM ($\kappa a = 6.9$; dark grey), 1.9 mM ($\kappa a = 22.8$; black). The dashed lines are guides to the eye. Below a volume fraction of ≈ 0.1 %, indicated by the vertical line, the mobility is considered volume fraction independent. The error bars represent the standard deviation of multiple measurements.

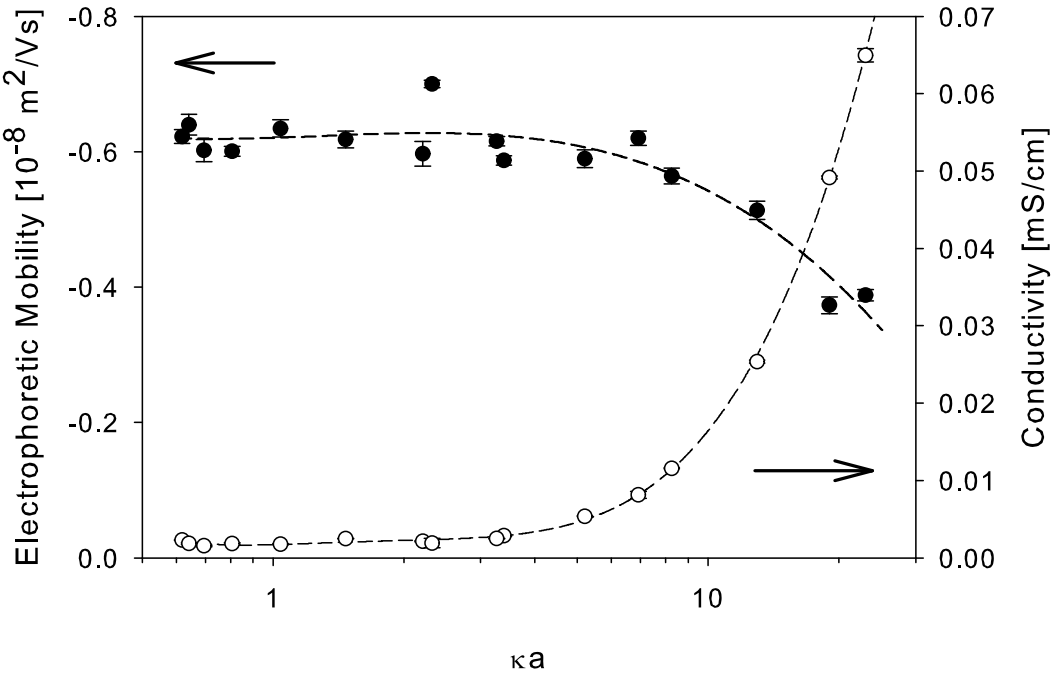

FIGURE 5.3. Mobility (black) and conductivity (white) of 90 nm radius silica spheres in ethanol at different concentrations of $LiNO_3$ at 0.01 % vol. Dashed lines are guides to the eye. The error bars represent the standard deviation of multiple measurements.

5.4. ELECTROACOUSTICS

As stated in the experimental methods section, measurements with the DT-300 setup can be performed by placing the probe in a beaker with dispersion, but this method requires much dispersion. To use as little dispersion as possible, we performed measurements with a homemade cell, which can be placed on top of the probe (shown in Fig. 5.1), and requires only 0.9 mL. Electroacoustic measurements on aqueous Ludox silica dispersions at various volume fractions, measured with (≈ 0.9 mL) and without (≈ 9 mL) the homemade cell, justify the use of this cell. The dynamic mobilities obtained with both methods agree very well, as shown in Fig. 5.4, with a maximum error of 6% for the highest volume fraction. Therefore, this 0.9 mL cell was used for the measurements in this work.

The primary measured physical quantity measured is the total vibration current (TVI), which is a complex quantity. In principle, the TVI has contributions from the colloidal vibration current (CVI) and the ionic vibration current (IVI), because both charged colloids and ions, respectively, respond to the ultrasonic wave: $\mathrm{TVI} = \mathrm{CVI} + \mathrm{IVI}$. The mobility of the charged colloids determines the magnitude of the CVI, while the sign of their charge determines the phase. Usually the CVI is much larger than the IVI, hence the IVI can be neglected. However,

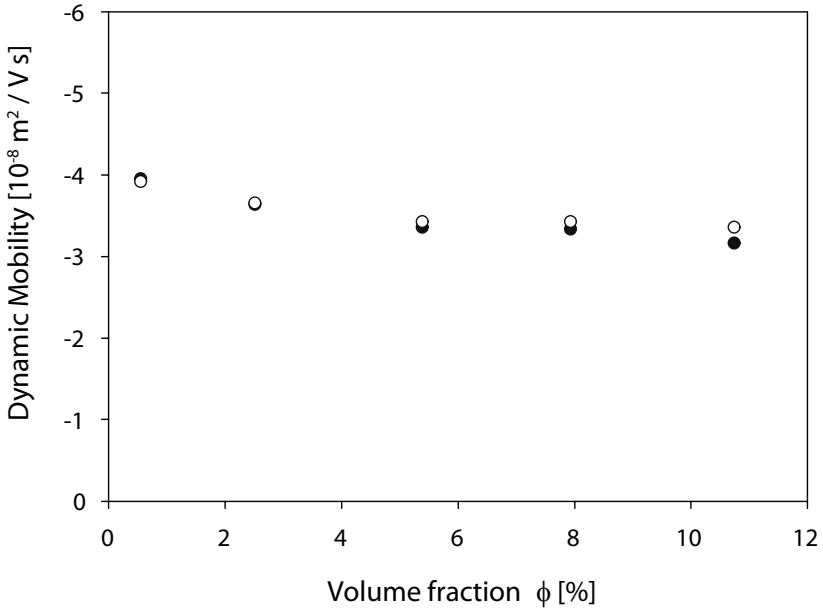

FIGURE 5.4. Dynamic mobility of Ludox silica particles in water as function of volume fraction, measured electroacoustically with the commercial 9 mL cell (•) and the smaller homebuilt 0.9 mL cell (○).

this is not necessarily the case if the volume fraction of colloids is low, if the conductivity is high, if there is only a small density difference between colloid and solvent or if the particle size is large.

Dispersions of TPM-coated silica particles at high and low ionic strength were measured at three different volume fractions, as well as the supernatant of the same centrifuged dispersions. The electroacoustic signal from the supernatant hardly varied with the concentration of $LiNO_3$. Furthermore the same signal was obtained for $LiNO_3$ solutions in ethanol, pure toluene and pure hexanol. Therefore, it is believed that the signal of the supernatant it not the IVI signal, but a condenser microphone effect [140, 164] that is insensitive to the ion concentration or the dielectric constant of the solvent. We corrected our TVI results by subtracting this background signal vectorially [140] (Fig. 5.5 and 5.6). The magnitude of the resulting CVI neatly scales linearly with volume fraction and through the origin at both high and low ionic strength (Fig. (5.7)), thus the CVI signal was successfully extracted using this measurement method. Furthermore, the linearity indicates negligible interparticle interactions and double layer overlap, at least up to 0.8 %-vol. This is as expected, since the average center-to-center separation at 0.8 %-vol $r_{av} \approx n^{-1/3}$ = 725 nm (with n the colloid number density) is larger than two times $(a + \kappa^{-1})$. Therefore, the dynamic mobility and electrophoretic mobility can be directly compared, despite being measured at different volume fractions. Although of little significance for the

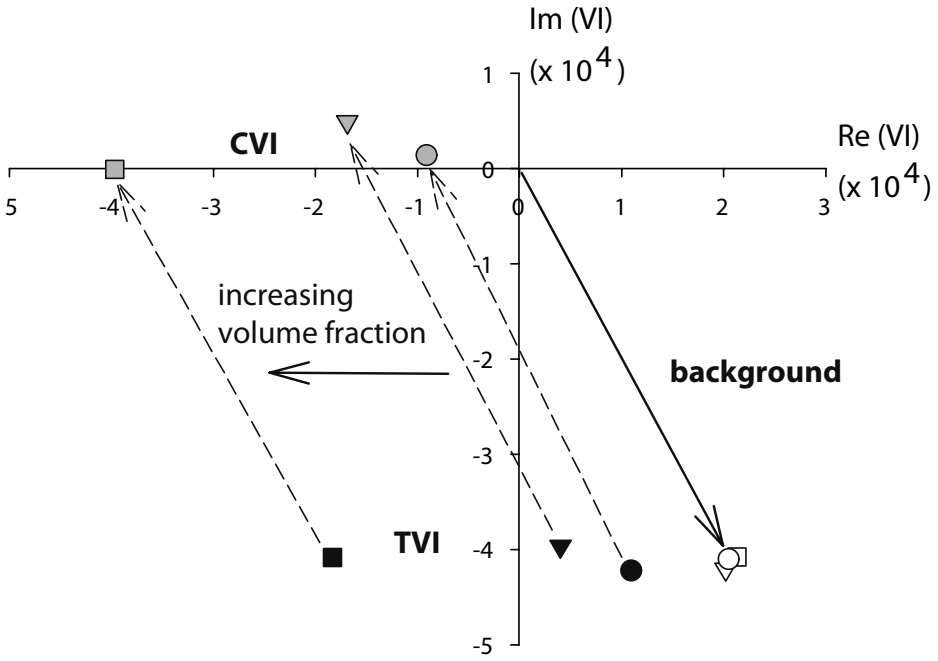

FIGURE 5.5. Real and imaginary parts (units: [mV$*\sqrt{s/g}$]) of TVI (black), CVI (grey) and background (white) for silica dispersions in ethanol with 1.9 mM $LiNO_3$, for volume fractions of 0.15 % (○), 0.31 % (▽) and 0.74 % (□).

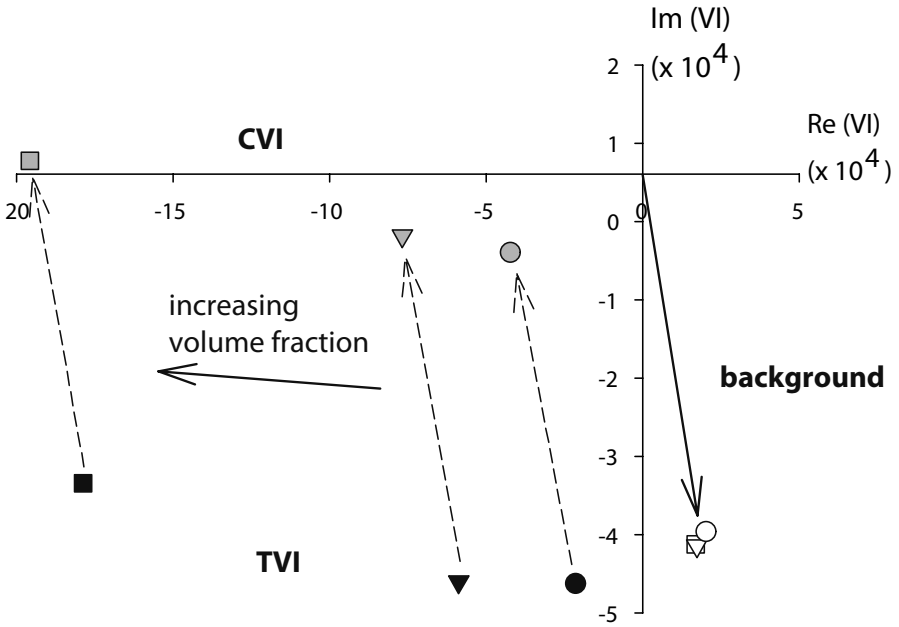

FIGURE 5.6. Real and imaginary parts (units: [mV$*\sqrt{s/g}$]) of TVI (black), CVI (grey) and background (white) for silica in deionized ethanol (0.0013 mM), for volume fractions of 0.17 % (○), 0.33 % (▽) and 0.83 % (□).

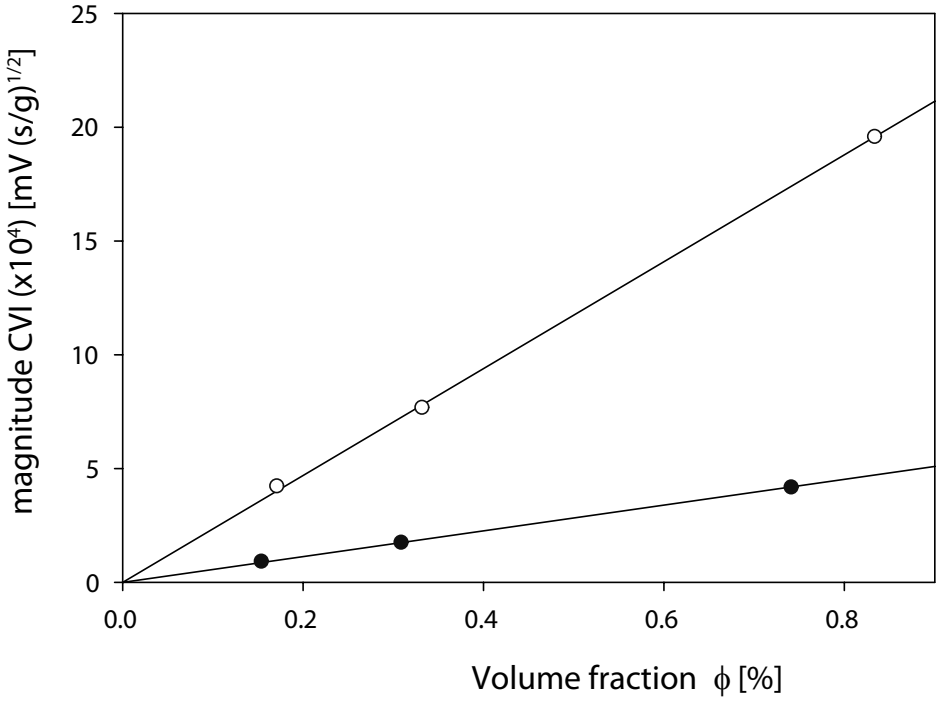

FIGURE 5.7. Magnitude CVI as function of silica volume fraction for deionized ethanolic dispersions (○) and with 1.9 mM $LiNO_3$ (●); solid lines are fits.

low volume fractions in this study, it should be mentioned that the volume fraction dependencies of μ_e and μ_d as determined here are expected to be different. While the electrophoretic mobility μ_e is expected to be proportional to $1-\phi$ due to back flow of the solvent [163] (since the mobility is measured relative to the laboratory frame of reference), the dynamic mobility in equation 5.1 is defined relative to the fluid velocity [165] and it is not expected to show the $1-\phi$ volume fraction dependence, in absence of interparticle interactions. Furthermore, it must be noted that inertia effects at high frequencies, described by the G term in reference 137, hardly influence μ_d for the small particles in this work ($G = 0.99$).

There is, however, a large difference in the CVI between high and low ionic strength. Dispersions at several ionic strengths were measured at a volume fraction of 0.5 %. The dynamic mobility was calculated using equation 5.1. The dynamic mobilities are plotted in Fig. 5.8 and these results are discussed in the next section. The difference between μ_d and μ_e is accompanied by a negative phase shift of the mobility, as shown in Fig. 5.9. The DT-310 setup does not measure an absolute value for the phase of the mobility, but it only compares the measured phase with the calibration value to obtain the sign of the mobility. Therefore, a relative phase shift was calculated, with the phase at the highest ionic strength set to zero.

5.5. DISCUSSION

Both the electrophoretic mobility μ_e in the low frequency limit and the dynamic mobility μ_d at 3.3 MHz were measured as a function of ionic strength for dilute dispersions in absence of interparticle interactions, allowing a direct comparison. The ratio between μ_d and μ_e strongly increases from ≈ 1 at high ionic strength to ≈ 5 at low ionic strength (Fig. 5.8). Since any effects of double layer overlap, interparticle interactions, or inertia have been excluded in the previous section, the difference between dynamic and electrophoretic mobilities must be ascribed to the difference in frequency at which the mobilities are measured, suggesting effects of double layer relaxation. In an electric field or sound wave of low frequency, the double layer relaxes to a stationary asymmetric distribution, reducing the particle mobility, while the double layer remains symmetric at very high frequencies, as schematically illustrated in Fig. 5.10. In the case of electroacoustics, the amplitude of the oscillating motion of the particle was smaller than 1 nm, as calculated in the appendix (section 5.8). Double layer relaxation occurs either through conduction, the Maxwell-Wagner relaxation with a typical relaxation frequency of $\omega_{\mathrm{MW}} \approx \sigma/\epsilon_0\epsilon_m \approx D\kappa^2$, or through diffusion, the α relaxation with a typical relaxation frequency of $\omega_\alpha \approx D/(\kappa^{-1}+a)^2$ [11, 12, 166]. Since analytical expressions for the mobility are only available in limiting cases, a software package was used to calculate dynamic mobility as a function of frequency.

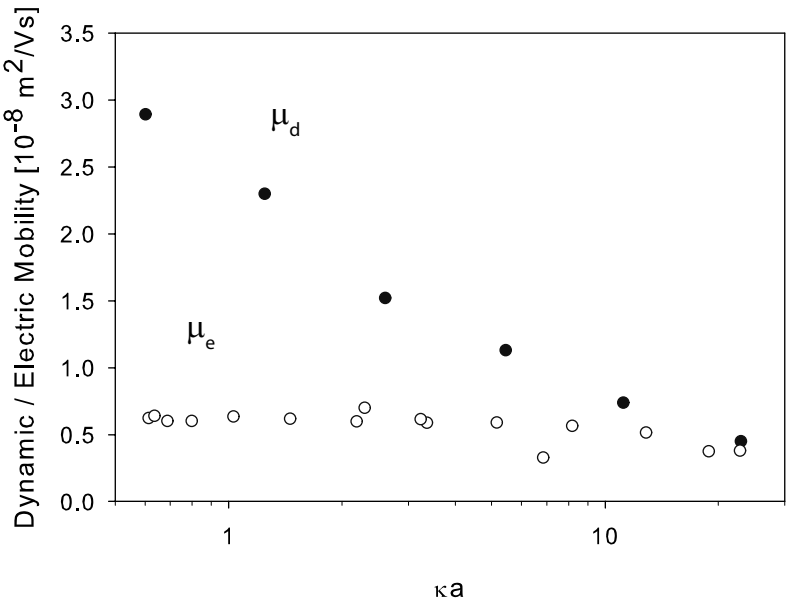

FIGURE 5.8. Dynamic (black) and electrophoretic mobility (white) as a function κa, the ratio between the particle radius a and the Debye length κ^{-1}.

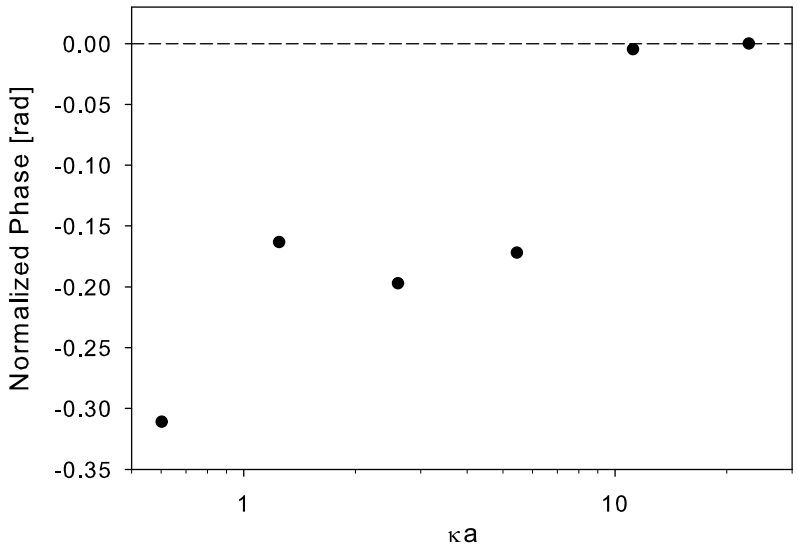

FIGURE 5.9. The phase of the dynamic mobility, normalized with the phase of the highest ionic strength set to zero.

This software uses cell theory as described in references 142, 158–161, solving the hydrodynamic and electrostatic equations for a spherical charged particle with a smooth surface. We performed calculations of the mobility as a function of frequency for a zeta potential of 50 mV and ionic strengths corresponding to κa = 0.6, 5.0 and 22 (producing electrophoretic mobilities equal to or slightly larger than our experimental values; other dispersion parameters used are mentioned in the experimental methods section). The results (Fig. 5.11) correctly predict an increasing mobility with increasing frequency, but the magnitude of the ratio μ_d/μ_e does not exceed 1.1, much smaller than for our experimental data. Small parameter adjustments did not result in significantly better agreement with the data. Other studies show electroacoustic evidence for these relaxations in more concentrated dispersions [142, 167]; however, in these studies the zeta potential was used as a fitting parameter and a quantitative comparison of the dynamic and electrophoretic mobilities in these studies was not made.

Large dynamic mobilities were recently reported for spherical polyelectrolyte brushes [168, 169], consisting of large polyelectrolyte chains grafted on a polystyrene core. These measurements were complemented with an electrokinetic model for these polyelectrolyte brushes as a polyelectrolyte shell in which both the volume charge density and the friction force are assumed to decay in the shell from the rigid core following r^{-2}. This inhomogeneous brush leads to very large double layer relaxation amplitudes.

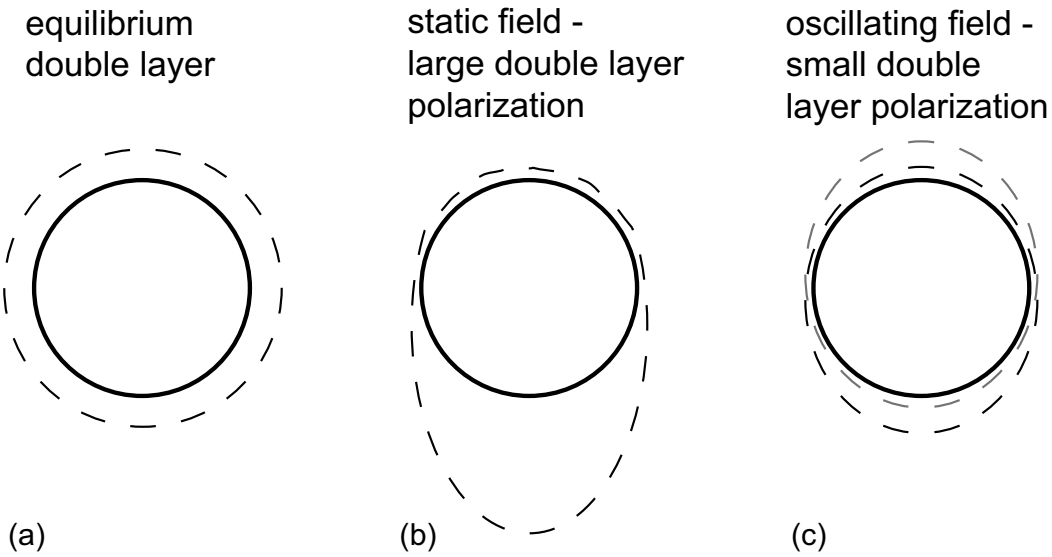

FIGURE 5.10. Schematic illustrations of (a) an equilibrium double layer, (b) large double layer polarization in a static field, and (c) small double layer polarization in an oscillating field.

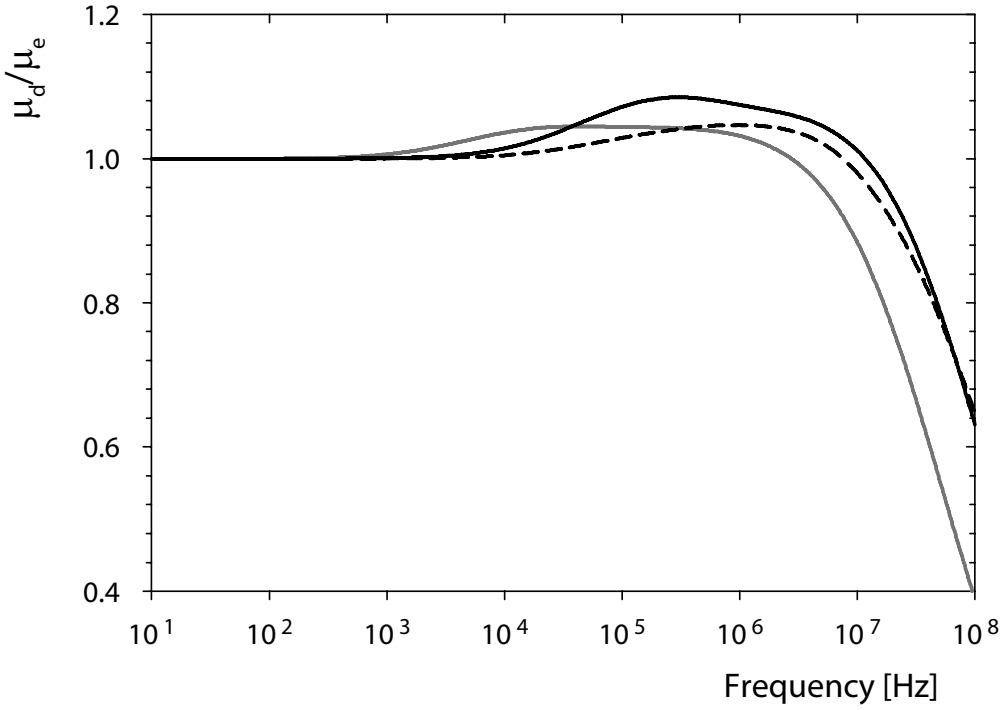

FIGURE 5.11. The ratio μ_d/μ_e as a function of frequency, produced by software calculations for a zeta potential of 50 mV and ionic strengths corresponding to κa = 0.6 (grey solid line), 5.0 (black solid line), and 22 (black dashed line).

The findings for polyelectrolyte brushes and our electrophoretic and electroacoustic measurements suggest that one should reconsider the view of the silica colloid as having a charged, smooth surface. Instead, a better picture may be that it is a fairly rigid, but rough and porous sponge with a TPM multilayer. This view is supported by the relatively low density of our silica particles of 1.6 g cm^{-3}, compared to other silicas ($\geq$ 2 g cm^{-3}) [170]. Additionally, it has been reported that our kinds of silica particles are not fully condensed, hence silanol groups that may dissociate to SO^- are present inside the particles [171].

Streaming potential measurements are expected to provide more insight in the structure of the double layer, independent of the techniques employed here. These measurements are currently being planned.

5.6. CONCLUSIONS

We measured a large difference in dynamic and electrophoretic mobility of charged silica spheres in ethanol at low ionic strength. This behavior is not to be expected for charged smooth spheres; instead, it more resembles that of polyelectrolyte brushes [168]. This spongy behavior was not found in other studies of these TPM coated silica particles [91, 145, 146], employing methods (DLS, SLS, sedimentation) where the dynamic characteristics of the double layer do not become apparent. As a follow-up, streaming potential measurements are planned to further elucidate the mobility ratio at low ionic strength.

5.7. ACKNOWLEDGEMENTS

I would like to acknowledge Hans Lyklema for stimulating discussions.

5.8. APPENDIX

The amplitude is calculated of the motion of a particle with radius a in an acoustic wave with a wavelength λ much larger than the particle radius $\lambda \gg a$ [140]. It is assumed that a particle is able to reach its steady state velocity much faster than the time of an acoustic oscillation, and charges are neglected. In this case, the Stokes friction force is balanced by the dynamic reaction:

$$6\pi\eta a(u_p - u_s) = \frac{4}{3}\pi a^3(\rho_p - \rho_s)\frac{-du_s}{dt} \tag{5.4}$$

where u_p is the particle velocity, u_s is the fluid velocity, η is the solvent viscosity, ρ_p the particle density, and ρ_s the solvent density. The fluid velocity is given by:

$$u_s = Ue^{i(\omega t)} \tag{5.5}$$

with the amplitude U:

$$U = \frac{P}{c\rho_s} \tag{5.6}$$

where c is the sound velocity and P is the pressure amplitude, which is related to the sound intensity I:

$$I = \frac{P^2}{2c\rho_s} \tag{5.7}$$

The velocity of the particle relative to the fluid is:

$$(u_p - u_s) = -i\omega\frac{2a^2}{9\eta}(\rho_p - \rho_s)Ue^{i\omega t} \tag{5.8}$$

If the relative displacement is given by $x = X_0e^{i\omega t}$, and $|u_p - u_s| = |dx/dt| = |\omega x|$, then the amplitude of the relative particle motion is:

$$|X| = U/\omega = \frac{2a^2}{9\eta}(\rho_p - \rho_s)\sqrt{\frac{2I}{\rho_s c}} \tag{5.9}$$

A sound wave is applied with an intensity of 1 W per 0.1 cm^2 (neglecting intensity losses in the probe), the sound velocity in ethanol is 1144 m/s, particle radius a = 90 nm, ethanol viscosity η = 1.144 mPa·s, particle density ρ_p = 1.6 kg L^{-1}, ethanol density ρ_s = 0.789 kg L^{-1}. Then, an amplitude of the particle oscillation is obtained of 0.7 nm, much smaller than the smallest Debye length in this study.

Bibliography

[1] A. P. Alivisatos, *Perspectives on the physical chemistry of semiconductor nanocrystals,* J. Phys. Chem. **100**, 13226-13239 (1996).

[2] L. E. Brus, *Electron electron and electron-hole interactions in small semiconductor crystallites - the size dependence of the lowest excited electronic state,* J. Chem. Phys. **80**, 4403-4409 (1984).

[3] M. G. Bawendi, M. L. Steigerwald, and L. E. Brus, *The Quantum-Mechanics of Larger Semiconductor Clusters (Quantum Dots),* Annu. Rev. Phys. Chem. **41**, 477-496 (1990).

[4] D. V. Talapin, J. S. Lee, M. V. Kovalenko, and E. V. Shevchenko, *Prospects of colloidal nanocrystals for electronic and optoelectronic applications,* Chem. Rev. **110**, 389-458 (2010).

[5] C. B. Murray, D. J. Norris, and M. G. Bawendi, *Synthesis and characterization of nearly monodisperse CdE (E = S, Se, Te) semiconductor nanocrystallites,* J. Am. Chem. Soc. **115**, 8706-8715 (1993).

[6] C. de Mello Donega, P. Liljeroth, and D. Vanmaekelbergh, *Physicochemical evaluation of the hot-injection method, a synthesis route for monodisperse nanocrystals,* Small **1**, 1152-1162 (2005).

[7] J. N. Israelachvili, *Intermolecular and surfaces forces*. Academic Press, (2011).

[8] J. Macdonald, *Impedance Spectroscopy*. New York: John Wiley & Sons, Inc., (1987).

[9] B. V. Derjaguin and L. Landau, *Theory of the stability of strongly charged lyophobic sols and of the adhesion of strongly charged particles in solutions of electrolytes,* Acta Physiochim. **14**, 633 (1941).

[10] E. J. W. Verwey and J. T. G. Overbeek, *Theory of the stability of lyophobic colloids*. New York: Dover, (1999).

[11] J. Lyklema, *Fundamentals of interface and colloid science (Volume II)*. Amsterdam: Academic Press, (1995).

[12] A. V. Delgado, F. González-Caballero, R. J. Hunter, L. K. Koopal, and J. Lyklema, *Measurement and interpretation of electrokinetic phenomena,* J. Colloid Interface Sci. **309**, 194-224 (2007).

[13] J. F. Miller, K. Schatzel, and B. Vincent, *The determination of very small electrophoretic mobilities in polar and nonpolar colloidal dispersions using phase-analysis light-scattering,* J. Colloid Interface Sci. **143**, 532-554 (1991).

[14] P. Debye, *A method for the determination of the mass of electrolytic ions,* J. Chem. Phys. **1**, 13-16 (1933).

[15] S. A. Empedocles and M. G. Bawendi, *Quantum-confined stark effect in single CdSe nanocrystallite quantum dots,* Science **278**, 2114-2117 (1997).

[16] M. Klokkenburg, A. J. Houtepen, R. Koole, J. W. J. de Folter, B. H. Erné, E. van Faassen, and D. Vanmaekelbergh, *Dipolar structures in colloidal dispersions of PbSe and CdSe quantum dots,* Nano Lett. **7**, 2931-2936 (2007).

[17] J. van Rijssel, B. H. Erné, J. D. Meeldijk, M. Casavola, D. Vanmaekelbergh, A. Meijerink, and A. P. Philipse, *Enthalpy and entropy of nanoparticle association from temperature-dependent cryo-TEM,* Phys. Chem. Chem. Phys. **13**, 12770-12774 (2011).

[18] S. Ahmed and K. M. Ryan, *Centimetre scale assembly of vertically aligned and close packed semiconductor nanorods from solution,* ChemComm, 6421-6423 (2009).

[19] S. A. Blanton, R. L. Leheny, M. A. Hines, and P. Guyot-Sionnest, *Dielectric dispersion measurements of CdSe nanocrystal colloids: Observation of a permanent dipole moment,* Phys. Rev. Lett. **79**, 865-868 (1997).

[20] M. Shim and P. Guyot-Sionnest, *Permanent dipole moment and charges in colloidal semiconductor quantum dots,* J. Chem. Phys. **111**, 6955-6964 (1999).

[21] A. D. Hollingsworth and D. A. Saville, *A broad frequency range dielectric spectrometer for colloidal suspensions: cell design, calibration, and validation,* J. Colloid Interface Sci. **257**, 65-76 (2003).

[22] V. L. Colvin and A. P. Alivisatos, *CdSe nanocrystals with a dipole-moment in the 1st excited-state,* J. Chem. Phys. **97**, 730-733 (1992).

[23] L. S. Li and A. P. Alivisatos, *Origin and scaling of the permanent dipole moment in CdSe nanorods,* Phys. Rev. Lett. **90**, 097402 (2003).

[24] M. Cirillo, F. Strubbe, K. Neyts, and Z. Hens, *Thermal charging of colloidal quantum dots in apolar solvents: a current transient analysis,* ACS Nano **5**, 1345-1352 (2011).

[25] E. V. Shevchenko, D. V. Talapin, N. A. Kotov, S. O'Brien, and C. B. Murray, *Structural diversity in binary nanoparticle superlattices,* Nature **439**, 55-59 (2006).

[26] T. D. Krauss and L. E. Brus, *Charge, polarizability, and photoionization of single semiconductor nanocrystals,* Phys. Rev. Lett. **83**, 4840-4843 (1999).

[27] J. P. Runt and J. J. Fitzgerald, *Dielectric spectroscopy of polymeric materials*. American Chemical Society, (1997).

[28] R. Pethig, *Protein-water interactions determined by dielectric methods,* Annu. Rev. Phys. Chem. **43**, 177-205 (1992).

[29] A. D. Hollingsworth and D. A. Saville, *Dielectric spectroscopy and electrophoretic mobility measurements interpreted with the standard electrokinetic model,* J. Colloid Interface Sci. **272**, 235-245 (2004).

[30] F. Kremer and M. Arndt, *Broadband dielectric measurement techniques*, pp. 67–79. Dielectric Spectroscopy of Polymeric Materials, Fundamentals and Applications, American Chemical Society, (1997).

[31] P. Hedvig, *Dielectric spectroscopy of polymers*. Dielectric Spectroscopy of Polymers, Bristol: Adam Hilger Ltd., (1977).

[32] L. Callegaro, *On strategies for automatic bridge balancing,* Instrumentation **54**, 529 (2005).

[33] M. Dutta, A. Chatterjee, and A. Rakshit, *Intelligent phase correction in automatic digital ac bridges by resilient backpropagation neural network,* Measurement **39**, 884-891 (2006).

[34] N. K. Das, T. Jayakumar, and B. Raj, *Noniterative digital AC bridge balance,* IEEE Trans. Instrument. Meas. **59**, 3058 (2010).

[35] R. Richert, *A simple current-to-voltage interface for dielectric relaxation measurements in the range 10^{-3} to 10^{7} Hz,* Rev. Sci. Instrum. **67**, 3217-3221 (1996).

[36] B. W. M. Kuipers, I. A. Bakelaar, M. Klokkenburg, and B. H. Erné, *Complex magnetic susceptibility setup for spectroscopy in the extremely low-frequency range,* Rev. Sci. Instrum. **79**, 013901 (2008).

[37] Signal Recovery, Technical Report AN 1001, *Input offset reduction using the model 7265 / 7260 / 7225 / 7220 synchronous oscillator / demodulator monitor output*, 2008.

[38] C. M. van der Wel, R. J. Kortschot, I. A. Bakelaar, B. H. Erné, and B. W. M. Kuipers, *Note: Rapid offset reduction of impedance bridges taking into account instrumental damping and phase shifting,* Rev. Sci. Instrum. **84**, 036109 (2013).

[39] CRC Handbook of Chemistry and Physics, 93rd edition, 2012-2013, "Permittivity (Dielectric Constant) of Liquids" (http://www.hbcpnetbase.com/, accessed 2012).

[40] H. P. Schwan, *Electrode polarization impedance and measurements in biological materials,* Ann. N.Y. Acad. Sci. **148**, 191 (1968).

[41] J. C. Dyre, P. Maass, B. Roling, and D. L. Sidebottom, *Fundamental questions relating to ion conduction in disordered solids,* Rep. Prog. Phys. **72**, 046501 (2009).

[42] M. M. Springer, A. Korteweg, and J. Lyklema, *The relaxation of the double-layer around colloid particles and the low-frequency dielectric-dispersion .2. experiments,* J. Electroanal. Chem. **153**, 55-66 (1983).

[43] M. Winter and R. J. Brodd, *What are batteries, fuel cells, and supercapacitors?,* Chem. Rev. **104**, 4245-4269 (2004).

[44] B. Comiskey, J. D. Albert, H. Yoshizawa, and J. Jacobson, *An electrophoretic ink for all-printed reflective electronic displays,* Nature **394**, 253-255 (1998).

[45] A. R. Minerick, R. H. Zhou, P. Takhistov, and H. C. Chang, *Manipulation and characterization of red blood cells with alternating current fields in microdevices,* Electrophoresis **24**, 3703-3717 (2003).

[46] I. Wolff, *A study of polarization capacity over a wide frequency band,* Phys. Rev. **27**, 755-763 (1926).

[47] R. Fricke, *The theory of electrolytic polarization,* Philos. Mag. **14**, 310-318 (1932).

[48] W. Scheider, *Theory of frequency dispersion of electrode polarization - topology of networks with fractional power frequency-dependence,* J. Phys. Chem. **79**, 127-136 (1975).

[49] G. J. Brug, A. L. G. van den Eeden, M. Sluyters-Rehbach, and J. H. Sluyters, *The analysis of electrode impedances complicated by the presence of a constant phase element,* J. Electroanal. Chem. **176**, 275-295 (1984).

[50] K. S. Cole and R. H. Cole, *Dispersion and absorption in dielectrics I. Alternating current characteristics,* J. Chem. Phys. **9**, 341-351 (1941).

[51] A. K. Jonscher, *A new understanding of the dielectric-relaxation of solids,* J. Mater. Sci. **16**, 2037-2060 (1981).

[52] J. R. Macdonald, *Note on the parameterization of the constant-phase admittance element,* Solid State Ionics **13**, 147-149 (1984).

[53] P. Zoltowski, *On the electrical capacitance of interfaces exhibiting constant phase element behaviour,* J. Electroanal. Chem. **443**, 149-154 (1998).

[54] G. Lang and K. E. Heusler, *Remarks on the energetics of interfaces exhibiting constant phase element behaviour,* J. Electroanal. Chem. **457**, 257-260 (1998).

[55] A. Sadkowski, *On the ideal polarisability of electrodes displaying CPE-type capacitance dispersion,* J. Electroanal. Chem. **481**, 222-226 (2000).

[56] G. Lang and K. E. Heusler, *Comments on the ideal polarisability of electrodes displaying CPE-type capacitance dispersion,* J. Electroanal. Chem. **481**, 227-229 (2000).

[57] P. Zoltowski, *Comments on the paper 'On the ideal polarisability of electrodes displaying CPE-type capacitance dispersion' by A. Sadkowski,* J. Electroanal. Chem. **481**, 230-231 (2000).

[58] A. Sadkowski, *Response to the 'Comments on the ideal polarisability of electrodes displaying CPE-type capacitance dispersion' by G. Lang, K.E. Heusler,* J. Electroanal. Chem. **481**, 232-236 (2000).

[59] J. R. Macdonald, *Theory of AC space-charge polarization effects in photoconductors, semiconductors, and electrolytes,* Phys. Rev. **92**, 4-17 (1953).

[60] J. R. Macdonald, *Utility of continuum diffusion models for analyzing mobile-ion immittance data: electrode polarization, bulk, and generation-recombination effects,* J. Phys.: Condens. Matter **22**, 495101 (2010).

[61] J. R. Macdonald, *Electrical response of materials containing space charge with discharge at electrodes,* J. Chem. Phys. **54**, 2026-2050 (1971).

[62] A. D. Hollingsworth, *Remarks on the determination of low-frequency measurements of the dielectric response of colloidal suspensions,* Curr. Opin. Colloid Interface Sci. **18**, 157-159 (2013).

[63] R. Coelho, *On the relaxation of a space-charge,* Rev. Phys. Appl. **18**, 137-146 (1983).

[64] R. Coelho, *On the static permittivity of dipolar and conductive media - an educational-approach,* J. Non-Cryst. Solids **131**, 1136-1139 (1991).

[65] J. R. Macdonald, L. R. Evangelista, E. K. Lenzi, and G. Barbero, *Comparison of impedance spectroscopy expressions and responses of alternate anomalous Poisson-Nernst-Planck diffusion equations for finite-length situations,* J. Phys. Chem. C **115**, 7648-7655 (2011).

[66] B. S. Krumgalz, *Dimensions of tetra-alkyl(aryl)onium ions,* J. Chem. Soc., Faraday Trans. I **78**, 437-449 (1982).

[67] C. Valeriani, P. J. Camp, J. W. Zwanikken, R. van Roij, and M. Dijkstra, *Ion association in low-polarity solvents: comparisons between theory, simulation, and experiment,* Soft Matter **6**, 2793-2800 (2010).

[68] H. S. Harned and B. B. Owen, *The physical chemistry of electrolyte solutions*. New York: Reinhold Publishing Corporation, (1950).

[69] M. Tomsic, M. Bester-Rogac, A. Jamnik, R. Neueder, and J. Barthel, *Conductivity of magnesium sulfate in water from 5 to 35 degrees C and from infinite dilution to saturation,* J. Solution Chem. **31**, 19-31 (2002).

[70] G. D. Parfitt and A. L. Smith, *Conductance of silver, potassium and lithium nitrates in ethanol-water mixtures,* Trans. Faraday Soc. **59**, 257 (1963).

[71] C. Chassagne, D. Bedeaux, J. P. M. van der Ploeg, and G. J. M. Koper, *Theory of electrode polarization: application to parallel plate cell dielectric spectroscopy experiments,* Colloid Interfaces A **210**, 137-145 (2002).

[72] C. Chassagne, D. Bedeaux, J. P. M. van der Ploeg, and G. J. M. Koper, *Polarization between concentric cylindrical electrodes,* Physica A **326**, 129-140 (2003).

[73] S. Uemura, *Low-frequency dielectric behavior of poly(vinylidene fluoride),* J. Polym. Sci., Part B: Polym. Phys. **12**, 1177-1188 (1974).

[74] S. Murakami, H. Iga, and H. Naito, *Dielectric properties of nematic liquid crystals in the ultralow frequency regime,* J. Appl. Phys. **80**, 6396-6400 (1996).

[75] P. A. Cirkel, J. P. M. van der Ploeg, and G. J. M. Koper, *Electrode effects in dielectric spectroscopy of colloidal suspensions,* Physica A **235**, 269-278 (1997).

[76] A. Sawada, *Internal electric fields of electrolytic solutions induced by space-charge polarization,* J. Appl. Phys. **100**, 074103 (2006).

[77] L. Onsager, *Deviations from Ohm's law in weak electrolytes,* J. Chem. Phys. **2**, 599-615 (1934).

[78] G. Barbero, *Influence of adsorption phenomenon on the impedance spectroscopy of a cell of liquid,* Phys. Rev. E **71**, 062201 (2005).

[79] R. de Levie, *The influence of surface roughness of solid electrodes on electrochemical measurements,* Electrochim. Acta **10**, 113-130 (1965).

[80] A. Le Mehaute and G. Crepy, *Introduction to transfer and motion in fractal media - the geometry of kinetics,* Solid State Ionics **9-10**, 17-30 (1983).

[81] L. Nyikos and T. Pajkossy, *Fractal dimension and fractional power frequency-dependent impedance of blocking electrodes,* Electrochim. Acta **30**, 1533-1540 (1985).

[82] J. B. Bates, Y. T. Chu, and W. T. Stribling, *Surface-topography and impedance of metal-electrolyte interfaces,* Phys. Rev. Lett. **60**, 627-630 (1988).

[83] T. Pajkossy, *Impedance of rough capacitive electrodes,* J. Electroanal. Chem. **364**, 111-125 (1994).

[84] Z. Kerner and T. Pajkossy, *Impedance of rough capacitive electrodes: the role of surface disorder,* J. Electroanal. Chem. **448**, 139-142 (1998).

[85] T. Pajkossy, *Impedance spectroscopy at interfaces of metals and aqueous solutions - Surface roughness, CPE and related issues,* Solid State Ionics **176**, 1997-2003 (2005).

[86] J. M. Liu, J. S. de Groot, J. P. Matte, T. W. Johnston, and R. P. Drake, *Measurements of inverse bremsstrahlung absorption and non-Maxwellian electron velocity distributions,* Phys. Rev. Lett. **72**, 2717-2720 (1994).

[87] J. A. S. Lima, R. Silva, and J. Santos, *Plasma oscillations and nonextensive statistics,* Phys. Rev. E **61**, 3260-3263 (2000).

[88] J. L. Du, *Nonextensivity in nonequilibrium plasma systems with Coulombian long-range interactions,* Phys. Lett. A **329**, 262-267 (2004).

[89] K. Ito, H. Yoshida, and N. Ise, *Void structure in colloidal dispersions,* Science **263**, 66-68 (1994).

[90] A. E. Larsen and D. G. Grier, *Like-charge attractions in metastable colloidal crystallites,* Nature **385**, 230-233 (1997).

[91] A. P. Philipse and G. H. Koenderink, *Sedimentation-diffusion profiles and layered sedimentation of charged colloids at low ionic strength,* Adv. Colloid Interface Sci. **100**, 613-639 (2003).

[92] R. Metzler and J. Klafter, *The random walk's guide to anomalous diffusion: a fractional dynamics approach,* Phys. Rep. **339**, 1-77 (2000).

[93] E. K. Lenzi, L. R. Evangelista, and G. Barbero, *Fractional diffusion equation and impedance spectroscopy of electrolytic cells,* J. Phys. Chem. B **113**, 11371-11374 (2009).

[94] L. R. Evangelista, E. K. Lenzi, G. Barbero, and J. R. Macdonald, *Anomalous diffusion and memory effects on the impedance spectroscopy for finite-length situations,* J. Phys.: Condens. Matter **23**, 485005 (2011).

[95] F. Beunis, F. Strubbe, K. Neyts, and A. R. M. Verschueren, *Power-law transient charge transport in a nonpolar liquid,* Appl. Phys. Lett. **90**, 182103 (2007).

[96] F. Beunis, F. Strubbe, M. Marescaux, J. Beeckman, K. Neyts, and A. R. M. Verschueren, *Dynamics of charge transport in planar devices,* Phys. Rev. E **78**, 011502 (2008).

[97] G. Barbero and A. L. Alexe-Ionescu, *Role of the diffuse layer of the ionic charge on the impedance spectroscopy of a cell of liquid,* Liq. Cryst. **32**, 943-949 (2005).

[98] S. Das, *Functional fractional calculus*. eBook: Springer-Verlag, (2011).

[99] M. E. Schmidt, S. A. Blanton, M. A. Hines, and P. Guyot-Sionnest, *Polar CdSe nanocrystals: Implications for electronic structure,* J. Chem. Phys. **106**, 5254-5259 (1997).

[100] B. Diaconescu, L. A. Padilha, P. Nagpal, B. S. Swartzentruber, and V. I. Klimov, *Measurement of electronic states of PbS nanocrystal quantum dots using scanning tunneling spectroscopy: the role of parity selection rules in optical absorption,* Phys. Rev. Lett. **110**, 127406 (2013).

[101] G. Nootz, L. A. Padilha, P. D. Olszak, S. Webster, D. J. Hagan, E. W. Van Stryland, L. Levina, V. Sukhovatkin, L. Brzozowski, and E. H. Sargent, *Role of symmetry breaking on the optical transitions in lead-salt quantum dots,* Nano Lett. **10**, 3577-3582 (2010).

[102] J. M. Schins, M. T. Trinh, A. J. Houtepen, and L. D. A. Siebbeles, *Probing formally forbidden optical transitions in PbSe nanocrystals by time- and energy-resolved transient absorption spectroscopy,* Phys. Rev. B **80**, 035323 (2009).

[103] A. Franceschetti, J. W. Luo, J. M. An, and A. Zunger, *Origin of one-photon and two-photon optical transitions in PbSe nanocrystals,* Phys. Rev. B **79**, 241311 (2009).

[104] M. T. Trinh, A. J. Houtepen, J. M. Schins, J. Piris, and L. D. A. Siebbeles, *Nature of the second optical transition in PbSe nanocrystals,* Nano Lett. **8**, 2112-2117 (2008).

[105] P. Liljeroth, P. A. Z. van Emmichoven, S. G. Hickey, H. Weller, B. Grandidier, G. Allan, and D. Vanmaekelbergh, *Density of states measured by scanning-tunneling spectroscopy sheds new light on the optical transitions in PbSe nanocrystals,* Phys. Rev. Lett. **95**, 086801 (2005).

[106] T. Nann and J. Schneider, *Origin of permanent electric dipole moments in wurtzite nanocrystals,* Chem. Phys. Lett. **384**, 150-152 (2004).

[107] C. Noguera, *Polar oxide surfaces,* J. Phys.: Condens. Matter **12**, R367-R410 (2000).

[108] J. Goniakowski, F. Finocchi, and C. Noguera, *Polarity of oxide surfaces and nanostructures,* Rep. Prog. Phys. **71**, 016501 (2008).

[109] J. Goniakowski and C. Noguera, *Polarity at the nanoscale,* Phys. Rev. B **83**, 115413 (2011).

[110] E. Rabani, B. Hetenyi, B. J. Berne, and L. E. Brus, *Electronic properties of CdSe nanocrystals in the absence and presence of a dielectric medium,* J. Chem. Phys. **110**, 5355-5369 (1999).

[111] E. Rabani, *Structure and electrostatic properties of passivated CdSe nanocrystals,* J. Chem. Phys. **115**, 1493-1497 (2001).

[112] S. Shanbhag and N. A. Kotov, *On the origin of a permanent dipole moment in nanocrystals with a cubic crystal lattice: Effects of truncation, stabilizers, and medium for CdS tetrahedral homologues,* J. Phys. Chem. B **110**, 12211-12217 (2006).

[113] Z. Zhang, Z. Tang, N. A. Kotov, and S. C. Glotzer, *Simulations and analysis of self-assembly of CdTe nanoparticles into wires and sheets,* Nano Lett. **7**, 1670-1675 (2007).

[114] P. W. Avraam, N. D. M. Hine, P. Tangney, and P. D. Haynes, *Factors influencing the distribution of charge in polar nanocrystals,* Phys. Rev. B **83**, 241402 (2011).

[115] Y. Luo and L. W. Wang, *Electronic structures of the CdSe/CdS core-shell nanorods,* ACS Nano **4**, 91-98 (2010).

[116] S. Dag, S. Wang, and L. W. Wang, *Large surface dipole moments in ZnO nanorods,* Nano Lett. **11**, 2348-2352 (2011).

[117] K. S. Cho, D. V. Talapin, W. Gaschler, and C. B. Murray, *Designing PbSe nanowires and nanorings through oriented attachment of nanoparticles,* J. Am. Chem. Soc. **127**, 7140-7147 (2005).

[118] D. V. Talapin, E. V. Shevchenko, C. B. Murray, A. V. Titov, and P. Kral, *Dipole-dipole interactions in nanoparticle superlattices,* Nano Lett. **7**, 1213-1219 (2007).

[119] K. Butter, P. H. H. Bomans, P. M. Frederik, G. J. Vroege, and A. P. Philipse, *Direct observation of dipolar chains in iron ferrofluids by cryogenic electron microscopy,* Nature Mater. **2**, 88-91 (2003).

[120] M. Klokkenburg, C. Vonk, E. M. Claesson, J. D. Meeldijk, B. H. Erné, and A. P. Philipse, *Direct Imaging of zero-field dipolar structures in colloidal dispersions of synthetic magnetite,* J. Am. Chem. Soc. **126**, 16706-16707 (2004).

[121] B. H. Erné, K. Butter, B. W. M. Kuipers, and G. J. Vroege, *Rotational diffusion in iron ferrofluids,* Langmuir **19**, 8218-8225 (2003).

[122] M. Klokkenburg, B. H. Erné, V. Mendelev, and A. O. Ivanov, *Magnetization behavior of ferrofluids with cryogenically imaged dipolar chains,* J. Phys.: Condens. Matter **20**, 204113 (2008).

[123] P. Debye, *Polar molecules*. New York: Dover Publications, (1929).

[124] C. J. F. Böttcher, *Theory of Electric Polarization*. Amsterdam: Elsevier, (1973).

[125] M. M. Tirado and J. Garcia de la Torre, *Translational friction coefficients of rigid, symmetric top macromolecules - application to circular-cylinders,* J. Chem. Phys. **71**, 2581-2587 (1979).

[126] M. M. Tirado and J. Garcia de la Torre, *Rotational-dynamics of rigid, symmetric top macromolecules - application to circular-cylinders,* J. Chem. Phys. **73**, 1986-1993 (1980).

[127] J. Garcia de la Torre, M. C. Lopez Martinez, and M. M. Tirado, *Dimensions of short, rodlike macromolecules from translational and rotational diffusion-coefficients - study of the gramicidin dimer,* Biopolymers **23**, 611-615 (1984).

[128] M. V. Kovalenko, D. V. Talapin, M. A. Loi, F. Cordella, G. Hesser, M. I. Bodnarchuk, and W. Heiss, *Quasi-seeded growth of ligand-tailored PbSe nanocrystals through cation-exchange-mediated nucleation,* Angew. Chem. Int. Ed. **47**, 3029-3033 (2008).

[129] L. H. Qu, Z. A. Peng, and X. G. Peng, *Alternative routes toward high quality CdSe nanocrystals,* Nano Lett. **1**, 333-337 (2001).

[130] I. Moreels, K. Lambert, D. De Muynck, F. Vanhaecke, D. Poelman, J. C. Martins, G. Allan, and Z. Hens, *Composition and size-dependent extinction coefficient of colloidal PbSe quantum dots,* Chem. Mat. **19**, 6101-6106 (2007).

[131] C. de Mello Donegá and R. Koole, *Size dependence of the spontaneous emission rate and absorption cross section of CdSe and CdTe quantum dots,* J. Phys. Chem. C **113**, 6511-6520 (2009).

[132] D. S. Viswanath, T. K. Ghosh, D. H. L. Prasad, N. V. K. Dutt, and K. Y. Rani, *Viscosity of liquids: theory, estimation, experiment, and data*. Dordrecht: Springer, (2007).

[133] C. H. Ben-Porat, O. Cherniavskaya, L. Brus, K. S. Cho, and C. B. Murray, *Electric fields on oxidized silicon surfaces: Static polarization of PbSe nanocrystals,* J. Phys. Chem. A **108**, 7814-7819 (2004).

[134] L. W. Wang and A. Zunger, *Pseudopotential calculations of nanoscale CdSe quantum dots,* Phys. Rev. B **53**, 9579-9582 (1996).

[135] J. van Rijssel, *Colloidal Interactions of Quantum Dots in Apolar Liquids*. PhD thesis, Utrecht University, (2013).

[136] P. Schapotschnikow, M. A. van Huis, H. W. Zandbergen, D. Vanmaekelbergh, and T. J. H. Vlugt, *Morphological transformations and fusion of PbSe nanocrystals studied using atomistic simulations,* Nano Lett. **10**, 3966-3971 (2010).

[137] R. W. O'Brien, *Electro-acoustic effects in a dilute suspension of spherical particles,* J. Fluid Mech. **190**, 71-86 (1988).

[138] R. W. O'Brien, A. Jones, and W. N. Rowlands, *A new formula for the dynamic mobility in a concentrated colloid,* Colloid Surface A **218**, 89-101 (2003).

[139] A. S. Dukhin, V. N. Shilov, H. Ohshima, and P. J. Goetz, *Electroacoustic phenomena in concentrated dispersions: New theory and CVI experiment,* Langmuir **15**, 6692-6706 (1999).

[140] B. J. Marlow, D. Fairhurst, and H. P. Pendse, *Colloid vibration potential and the electrokinetic characterization of concentrated colloids,* Langmuir **4**, 611-626 (1988).

[141] R. W. O'Brien, B. R. Midmore, A. Lamb, and R. J. Hunter, *Electroacoustic Studies of Moderately Concentrated Colloidal Suspensions,* Faraday Discuss. **90**, 301-312 (1990).

[142] S. Ahualli, A. V. Delgado, S. J. Miklavcic, and L. R. White, *Use of a cell model for the evaluation of the dynamic mobility of spherical silica suspensions,* J. Colloid Interface Sci. **309**, 342-349 (2007).

[143] J. Van Tassel and C. A. Randall, *Surface chemistry and surface charge formation for an alumina powder in ethanol with the addition of HCl and KOH,* J.Colloid Interface Sci. **241**, 302-316 (2001).

[144] A. P. Philipse and A. Vrij, *Preparation and properties of nonaqueous model dispersions of chemically modified, charged silica spheres,* J. Colloid Interface Sci. **128**, 121-136 (1989).

[145] A. P. Philipse and A. Vrij, *Determination of static and dynamic interactions between monodisperse, charged silica spheres in an optically matching, organic-solvent,* J. Chem. Phys. **88**, 6459-6470 (1988).

[146] D. M. E. Thies-Weesie, A. P. Philipse, G. Nägele, B. Mandl, and R. Klein, *Nonanalytical concentration-dependence of sedimentation of charged silica spheres in an organic-solvent - experiments and calculations,* J. Colloid Interface Sci. **176**, 43-54 (1995).

[147] G. Nägele, O. Kellerbauer, R. Krause, and R. Klein, *Hydrodynamic effects in polydisperse charged colloidal suspensions at short times,* Phys. Rev. E **47**, 2562-2574 (1993).

[148] J. K. Phalakornkul, A. P. Gast, R. Pecora, G. Nägele, A. Ferrante, B. Mandl-Steininger, and R. Klein, *Structure and short-time dynamics of polydisperse charge-stabilized suspensions,* Phys. Rev. E **54**, 661-675 (1996).

[149] J. S. van Duijneveldt, J. K. G. Dhont, and H. N. W. Lekkerkerker, *Expansion and crystallization of a sediment of charged colloidal spheres,* J. Chem. Phys. **99**, 6941-6949 (1993).

[150] P. Jiang, J. F. Bertone, K. S. Hwang, and V. L. Colvin, *Single-crystal colloidal multilayers of controlled thickness,* Chem. Mat. **11**, 2132-2140 (1999).

[151] K. L. Smith and G. G. Fuller, *Electric-field induced structure in dense suspensions,* J. Colloid Interface Sci. **155**, 183-190 (1993).

[152] M. Rasa and A. P. Philipse, *Evidence for a macroscopic electric field in the sedimentation profiles of charged colloids,* Nature **429**, 857-860 (2004).

[153] M. Rasa, B. H. Erné, B. Zoetekouw, R. van Roij, and A. P. Philipse, *Macroscopic electric field and osmotic pressure in ultracentrifugal sedimentation-diffusion equilibria of charged colloids,* J. Phys.: Condens. Matter **17**, 2293-2314 (2005).

[154] Y. D. Yan, J. K. G. Dhont, C. Smits, and H. N. W. Lekkerkerker, *Oscillatory-shear-induced order in nonaqueous dispersions of charged colloidal spheres,* Physica A **202**, 68-80 (1994).

[155] Y. D. Yan and J. K. G. Dhont, *Shear-induced structure distortion in nonaqueous dispersions of charged colloidal spheres via light-scattering,* Physica A **198**, 78-107 (1993).

[156] J. E. Martin, D. Adolf, and T. C. Halsey, *Electrorheology of a model colloidal fluid,* J. Colloid Interface Sci. **167**, 437-452 (1994).

[157] J. E. Martin, J. Odinek, and T. C. Halsey, *Evolution of structure in a quiescent electrorheological fluid,* Phys. Rev. Lett. **69**, 1524-1527 (1992).

[158] S. Ahualli, A. V. Delgado, S. J. Miklavcic, and L. R. White, *Dynamic electrophoretic mobility of concentrated dispersions of spherical colloidal particles. On the consistent use of the cell model,* Langmuir **22**, 7041-7051 (2006).

[159] B. H. Bradshaw-Hajek, S. J. Miklavcic, and L. R. White, *Frequency-dependent electrical conductivity of concentrated dispersions of spherical colloidal particles,* Langmuir **24**, 4512-4522 (2008).

[160] B. H. Bradshaw-Hajek, S. J. Miklavcic, and L. R. White, *Dynamic dielectric response of concentrated colloidal dispersions: Comparison between theory and experiment,* Langmuir **25**, 1961-1969 (2009).

[161] B. H. Bradshaw-Hajek, S. J. Miklavcic, and L. R. White, *High-frequency behavior of the dynamic mobility and dielectric response of concentrated colloidal dispersions,* Langmuir **26**, 1656-1665 (2010).

[162] G. Kortüm, *Treatise on electrochemistry*. Amsterdam: Elsevier, (1965).

[163] C. F. Zukoski and D. A. Saville, *Electrokinetic properties of particles in concentrated suspensions,* J. Colloid Interface Sci. **115**, 422-436 (1987).

[164] R. Zana and E. Yeager, *Ultrasonic vibration potentials,* Mod. Aspects Electrochem. **14**, 1-60 (1982).

[165] A. S. Dukhin, H. Ohshima, V. N. Shilov, and P. J. Goetz, *Electroacoustics for concentrated dispersions,* Langmuir **15**, 3445-3451 (1999).

[166] V. N. Shilov, A. V. Delgado, F. González-Caballero, J. Horno, J. J. López-García, and C. Grosse, *Polarization of the electrical double layer. Time evolution after application of an electric field,* J. Colloid Interface Sci. **232**, 141-148 (2000).

[167] S. E. Gibb and R. J. Hunter, *Dynamic mobility of colloidal particles with thick double layers,* J. Colloid Interface Sci. **224**, 99-111 (2000).

[168] M. L. Jiménez, A. V. Delgado, S. Ahualli, M. Hoffmann, A. Witteman, and M. Ballauff, *Giant permittivity and dynamic mobility observed for spherical polyelectrolyte brushes,* Soft Matter **7**, 3758-3762 (2011).

[169] S. Ahualli, M. Ballauff, F. J. Arroyo, A. V. Delgado, and M. L. Jiménez, *Electrophoresis and dielectric dispersion of spherical polyelectrolyte brushes,* Langmuir **28**, 16372-16381 (2012).

[170] R. K. Iler, *The chemistry of silica: solubility, polymerization, colloid and surface properties, and biochemistry*. New York: Wiley, (1979).

[171] A. van Blaaderen and A. P. M. Kentgens, *Particle morphology and chemical microstructure of colloidal silica spheres made from alkoxysilanes,* J. Non-Cryst. Solids **149**, 161-178 (1992).

Summary

This thesis deals with the measurement of the permanent electric dipole moment and net charge of colloidal quantum dots (QDs) in apolar liquids. Their electric properties are essential for understanding their optical properties, colloidal interactions, and electric field directed assembly. In view of the optical sensitivity of QDs, a non-optical measurement technique was chosen: dielectric spectroscopy.

Chapter 2 describes a dielectric spectroscopy setup that was built specifically for the study of quantum dot dispersions in this thesis. High sensitivity is required, especially to detect the dipolar relaxation. This was achieved by a differential circuit, whose output could be nullified by a software-controlled phase-adjusted compensating voltage in the absence of nanoparticles, such that after they are added to the liquid, nanoparticle response is measured at the highest sensitivity. This made it possible to detect QDs at volume fractions down to 0.1 %-vol.

The effect of electrode polarization, which typically occurs at low frequencies in dielectric spectroscopy measurements, was investigated in **Chapter 3** for simple electrolytes. The response at moderate ionic strength (> 0.25 mM) is in good agreement with the Poisson-Nernst-Planck (PNP) equations. However, deviations from these PNP equations were observed at lower ionic strengths. In terms of an equivalent electronic circuit, all data was well described by a constant phase element (CPE) as model for the double layer capacity, with the CPE exponent as the only fit parameter. Surprisingly, when this exponent was plotted against the Debye length, all studied systems follow the same trend. Double layer dynamics at low ionic strength are possibly influenced by the long-range nature of the Coulomb interaction.

Dispersions of PbSe and CdSe quantum dots are studied in **Chapter 4**. Dipolar relaxation was detected in dilute dispersions at a characteristic frequency corresponding to Brownian rotation of single particles, from which the dipole moments of both PbSe and CdSe quantum dots could be determined. The dipole moment of PbSe QDs is reported for the first time. In more concentrated dispersions, structures of a few QDs are present, indicated by a slower dipolar relaxation. Until now, structure formation had been neglected in the interpretation of dielectric spectroscopy of QD dispersions. Here, the relaxation was modeled by accounting for the presence of chains due to a net attraction between the

QDs. A coupling free energy of -2 to -4 kT was calculated, which is in quantitative agreement with yet unpublished values recently found by independent techniques: cryo-TEM, SAXS, and analytical ultracentrifugation. In disagreement with past speculations, the permanent dipole moment is too weak to explain this net attraction. Additionally, it was found that a small fraction of 1% of the QDs carries a net charge of $\pm$ 1 e.

In **Chapter 5**, a second non-optical technique, electroacoustics, was explored to study charged colloidal particles. A well studied model system of surface modified silica particles in ethanol has been used to compare electroacoustics with a better known technique, laser Doppler electrophoresis. While these techniques measure the same mobility in the case of thin double layers, a large difference was found in the dynamic and the electrophoretic mobility in the case of thick double layers. This effect turns out to be much larger than the existing theories for smooth particles predict.

In conclusion, dielectric spectroscopy has revealed the influence of structure formation on the dipolar relaxation of colloidal quantum dots in apolar liquids. Measurements of both the electric double layer dynamics in dielectric spectroscopy measurements and the electrophoretic and electroacoustic motion of charged colloidal particles at low ionic strength point to insufficient development of the theoretical basis of the techniques. As a result, their physical interpretation remains a challenge.

Samenvatting voor Iedereen

Quantum Dots

Quantum dots zijn nanodeeltjes van halfgeleidermateriaal. Deze nanodeeltjes hebben een grootte van een paar nanometer, en bestaan uit een paar duizend atomen. Ter vergelijking: een watermolecuul heeft een grootte van ongeveer 0,2 nanometer (dat is 0,0000002 millimeter) en een menselijke haar heeft een dikte van ongeveer 50000 nanometer (of 0,05 millimeter). Een halfgeleider is een materiaal dat stroom kan geleiden, al kan het dat niet zo goed als een metaal, maar de geleiding is wel te manipuleren door de samenstelling een beetje te veranderen of door de temperatuur te variëren. Om deze reden worden halfgeleiders gebruikt voor bijvoorbeeld computerchips. Daarnaast kunnen halfgeleiders ook licht absorberen en dit licht weer uitzenden (fluorescentie).

Het bijzondere aan quantum dots, is dat ze zo klein zijn, dat de kleur licht die wordt uitgezonden niet alleen afhangt van de soort halfgeleider, maar ook van de grootte van het deeltje. Deze eigenschap maakt ze zeer interessant voor allerlei toepassingen. Hun vermogen om licht te absorberen, bijvoorbeeld, maakt ze geschikt voor zonnecellen, en hun vermogen om licht met een specifieke kleur uit te zenden maakt ze geschikt voor LED lampen. Daarnaast kunnen quantum dots ook worden gestapeld tot kristallen van quantum dots. Ook deze quantum dot kristallen bieden nieuwe mogelijkheden tot toepassingen. De eigenschappen van quantum dots kunnen worden gevarieerd door kleine variaties in materiaalsamenstelling, of door het oppervlak van het deeltje te manipuleren.

Het onderzoek naar de eigenschappen van quantum dots, dat is beschreven in dit proefschrift, is van fundamentele aard, maar het is dus ook van praktisch belang om de eigenschappen in detail te begrijpen.

Colloïden

Andere deeltjes, die ook in dit proefschrift worden beschreven, zijn silica colloïden. In dit geval gaat het niet specifiek om de eigenschappen van silica, zoals de 'halfgeleider-eigenschappen' van belang zijn voor de quantum dots, maar het gaat om de eigenschappen van colloïdale dispersies. Colloïden zijn vaste of vloeibare deeltjes met een afmeting van 1 tot 1000 nanometer, en een colloïdale dispersie is een vloeistof waarin colloïden zijn 'gedispergeerd'.

Alledaagse voorbeelden van colloïdale dispersies zijn bloed, melk en verf. Ook dispersies van quantum dots vallen in deze categorie.

Colloïden hebben de neiging om aan elkaar te plakken, en in veel gevallen, zoals bijvoorbeeld voor bloed, is dat zeer ongewenst. Er zijn twee manieren om dit te voorkomen. Eén mogelijkheid is om de colloïden te bedekken met een beschermende laag van moleculen. Zo'n beschermende laag wordt bijvoorbeeld gebruikt bij de quantum dots. Een tweede mogelijkheid is bescherming met lading. De silica deeltjes in dit proefschrift zijn negatief geladen. Rond dit deeltje vormt zich een wolk van positieve ionen die zich in de vloeistof bevinden. Het is deze ionenwolk die voorkomt dat de colloïden aan elkaar blijven plakken. Geladen colloïden worden ook toegepast in bijvoorbeeld e-readers, waarin pixels door (geladen) pigment deeltjes met behulp van een elektrisch veld worden aan- of uitgeschakeld.

Dit proefschrift

Terug naar de quantum dots. Dit proefschrift beschrijft de metingen van het dipool moment van quantum dots, en de gebruikte meettechniek heet diëlektrische spectroscopie. Een dipool moment betekent dat het deeltje aan een kant van het deeltje een beetje positief is geladen, en aan de andere kant een beetje negatief, hoewel het totale deeltje netto niet geladen is. Diëlektrische spectroscopie maakt gebruik van het feit dat deeltjes met een dipool moment uitlijnen in een elektrisch veld (net zoals een kompasnaald uitlijnt in het magneetveld van de aarde). De metingen worden uitgevoerd met een wisselend elektrisch veld. In een wisselend veld met een lage frequentie draaien de deeltjes mee met het elektrische veld, maar bij hoge frequentie kunnen de deeltjes het veld niet meer volgen. De rotatie is dus frequentie afhankelijk en ieder deeltje heeft een karakteristieke frequentie, waarbij het deeltje het elektrische veld slechts met veel moeite kan volgen. Deze karakteristieke frequentie van een deeltje hangt af van zijn grootte en van de viscositeit van de vloeistof. Het dipool moment kan dan worden bepaald door de elektrische stroom bij verschillende frequenties te meten, zowel boven als onder de karakteristieke frequentie.

Bij het ronddraaien van deeltjes met een dipool moment komt ook een klein beetje warmte vrij. Juist bij de karakteristieke frequentie is de hoeveelheid warmte die vrijkomt maximaal. Op dit principe berust ook de werking van de magnetron om voedsel op te warmen. Voedsel bestaat voor een groot deel uit water en watermoleculen hebben ook een dipool moment. Met behulp van een elektrisch veld dat een frequentie heeft die karakteristiek is voor de rotatie van watermoleculen, namelijk microgolven, kan dus voedsel worden opgewarmd.

De elektrische stroom als gevolg van de roterende quantum dots in een vloeistof is echter zeer klein ten opzicht van de totaal gemeten stroom. Om toch nauwkeurig deze stroom te bepalen, is speciaal hiervoor een elektrische opstelling gebouwd. Deze opstelling is beschreven in Hoofdstuk 2. Het elektronische circuit van deze opstelling is zo geschakeld dat de 'achtergrond' stroom gecompenseerd wordt, waardoor alleen de stroom van het dipool moment wordt gemeten.

In Hoofdstuk 4 worden de diëlektrische metingen aan quantum dots beschreven. Het rotatie effect werd gemeten, en bij een lage quantum dot concentratie blijkt dat de karakteristieke frequentie is zoals te verwachten valt op basis van de grootte van de deeltjes. Op basis hiervan kon het dipool moment van loodselenide en cadmiumselenide quantum dots worden bepaald.

Bij hogere concentraties blijkt de karakteristieke frequentie te verschuiven naar lagere frequenties. Het was al bekend dat quantum dots in een vloeistof, ondanks een beschermende laag, aan elkaar kunnen plakken en hierbij kleine ketens kunnen vormen. Bij hogere concentraties zijn er ook meer ketens aanwezig. Met een model dat de aanwezigheid van deze ketens kan voorspellen, kon het rotatie effect bij hoge concentraties precies worden beschreven. Hiermee kon ook worden bepaald hoe sterk de wisselwerking tussen de quantum dots in een vloeistof is. Hoewel het dipool moment kan zorgen voor een attractie tussen de quantum dots, blijkt dat, in tegenstelling tot wat vaak gesuggereerd wordt, het dipool moment niet verantwoordelijk is voor de wisselwerking tussen quantum dots.

Bij de diëlektrische metingen treedt, naast het roteren van de quantum dots, nog een effect op. Ladingen bewegen onder invloed van het elektrisch veld naar de elektroden toe. Net zoals geladen colloïden een ionenwolk van tegengestelde lading hebben, zo ontstaan deze ionenwolken ook aan de elektroden. De frequentie-afhankelijkheid van dit effect is in meer detail onderzocht in Hoofdstuk 3, door verschillende zoutoplossingen te meten. Bij een hoge zoutconcentratie blijken de meetresultaten in overeenstemming te zijn met de verwachtingen, echter niet bij lagere zoutconcentratie. De waargenomen afwijking kon desondanks op een empirische manier worden beschreven.

In Hoofdstuk 5 zijn twee methoden onderzocht om de lading van silica colloïden te bepalen door de beweeglijkheid van deze deeltjes te meten. De eerste methode is elektroakoestiek. Deze techniek maakt gebruik van geluidsgolven, die zorgen dat de dispersie gaat trillen. De silica deeltjes zijn echter zwaarder dan de vloeistof, waardoor de deeltjes vertraagt bewegen ten opzicht van de vloeistof. De positieve ionen die zich in een wolk rond het deeltje bevinden worden door de

vloeistof los getrokken van het negatieve deeltje. Dit resulteert in een elektrische stroom die gemeten kan worden.

De tweede methode is laser Doppler elektroforese. Deze techniek meet de snelheid van geladen deeltjes in een elektrisch veld met behulp van een laser. De laserbundel wordt door het deeltje verstrooid, waarbij ook de frequentie (kleur) van het laser licht verandert. Deze frequentieverschuiving heet het Doppler effect (dit effect verklaart ook waarom het geluid van een tegemoetkomende sirene anders klinkt dan een weggaande sirene).

De metingen in Hoofdstuk 5, met behulp van de twee genoemde meetmethoden, zijn uitgevoerd bij verschillende zout concentraties. Bij een hoge zout concentratie is de ionenwolk, die zich rond het deeltje bevindt, heel dun. In dit geval gaven beide technieken hetzelfde resultaat. Echter, bij lage zout concentratie is de ionenwolk veel dikker. In dit geval blijkt dat de beweeglijkheid van de deeltjes, zoals gemeten met elektroakoestiek, veel groter is dan de beweeglijkheid zoals gemeten met laser Doppler elektroforese. Dit effect is veel sterker dan wordt voorspeld door bestaande theorieën, die aannemen dat de colloïden gladde bollen zijn. In werkelijkheid gaat het om deeltjes met een ruw oppervlak, wat invloed heeft op de beweeglijkheid.

Dankwoord

Onderzoek doen is zeer interessant en uitdagend, maar het is niet altijd makkelijk en het vergt ook veel geduld. Gelukkig ben ik hierbij geholpen door een aantal mensen, die ik hierbij graag wil bedanken.

Allereerst wil ik mijn co-promotor Ben Erné bedanken. Ben, jij bent zeer betrokken geweest bij mijn onderzoek. Jouw deur stond altijd open om zaken te bespreken en resultaten en manuscripten werden zeer aandachtig gelezen en becommentarieerd. Hartelijk dank voor jou betrokkenheid. Ik wil ook graag mijn promotor Albert Philipse bedanken. Ik heb jouw interesse en nuttige suggesties bij alle gevoerde discussie zeer gewaardeerd. Ook bedankt voor de mogelijkheid om aan jou TPM bollen te meten.

Bij de ontwikkeling van de diëlektrische opstelling was de kennis en hulp van Bonny Kuipers en Emile Bakelaar onmisbaar. Hartelijk dank voor jullie inzet. Ernst van Faassen, jouw hulp bij de eerste impedantie metingen heb ik ook erg gewaardeerd. Casper van der Wel, het was me een genoegen om jou als gemotiveerde bachelorstudent te begeleiden en bedankt voor jouw bijdrage aan dit proefschrift. De quantum dots in dit proefschrift zijn gemaakt door Relinde van Dijk-Moes, hartelijk dank hiervoor. Also thanks to Esther Groeneveld, Sander de Brouwer en Francesca Pietra for providing quantum dots, even though they did not make it to this thesis, unfortunately. Jos van Rijssel, het was fijn dat ook jij je in onze groep met quantum dots bezig hield. Hartelijk bedankt voor alle discussies die we daarover hebben gevoerd. Hans Lyklema, bedankt voor de interesse en de hulp bij de interpretatie van elektroakoestische metingen, en ook Leo Vleugels en Remco Tuinier voor de poging deze metingen verder te begrijpen. Voor nuttige discussies en suggesties wil ik ook graag Daniël Vanmaekelbergh, Andrew Hollingsworth, René van Roij, Andrei Petukhov, Jan Groenewold en Alwin Verschueren bedanken.

Hartelijk dank aan mijn kamergenoten in N710 voor de gezelligheid: Esther van den Pol, Bob Luigjes (en voor alle koffie!), Susanne van Berkum en Roel Baars. Dank aan Dominique, Kanvaly, Marina voor hulp op het lab en met administratieve zaken. Ik heb het altijd erg naar mijn zin gehad op het Van 't Hoff Laboratorium, daarvoor ook dank aan alle andere collega's: Willem, Gert-Jan, Hans, Henk, Anke, Janne-Mieke, Joost, Sonja, Chris, Bas, Mark, Ping, Yong, Nina, Mikal, Julius, Sandra, Maurice, Lia, Laura, Jan, Andrei, Agnieska, Dima, Tian Hui, Raja, Dzina, Rocio, Antara, Stefan, en alle studenten. Ook het contact

met collega's van de Soft Condensed Matter en Condensed Matter and Interfaces groepen heb ik gewaardeerd.

Voor de interesse en de nodige afleiding van buiten het lab wil ik ook graag vrienden en familie bedanken. In het bijzonder bedankt voor de vriendschap van de afgelopen jaren: Menno, Jos, Sjoerd, Michiel, Reinout, Bob, Iwan, Tim, Laura, Eva, Hedwig, Nienke, Hanna, Julia, Suzanne, Dirk, Lucy en Sabine. Menno en Jos, leuk dat jullie mijn paranimfen willen zijn. Ook wil ik graag mijn oud-huisgenootjes van de Nassaustraat noemen, Fritsies bedankt! Marianne, ook jij bedankt.

Hartelijk dank aan mijn familie, und auch Wolfgang und Ursula will ich gerne meinen Dank aussprechen. In het bijzonder heel veel dank aan mijn ouders en Marlijn, voor jullie onvoorwaardelijke steun, dat was en is mij ontzettend veel waard. Daniela, hartelijk dank voor de leuke tijd met jou, en je steun en begrip bij het afronden van dit proefschrift. Vielen Dank für deine Geduld und Liebe.

List of Publications

This thesis is based on the following publications:

- R.J. Kortschot, I.A. Bakelaar, B.H. Erné and B.W.M. Kuipers, *A Differential Dielectric Spectroscopy Setup to Measure the Electric Dipole Moment and Net Charge of Colloidal Quantum Dots*, submitted. (Chapter 2)
- R.J. Kortschot, and B.H. Erné, *Influence of Ionic Strength on the Frequency Dispersion of Electrode Polarization*, in preparation. (Chapter 3)
- R.J. Kortschot, J. van Rijssel, R.J.A. van Dijk-Moes, and B.H. Erné, *Dielectric Spectroscopy of PbSe and CdSe Colloidal Quantum Dots*, in preparation. (Chapter 4)
- R.J. Kortschot, J. Lyklema, A.P. Philipse, and B.H. Erné, *Comparative Study of Electrophoretic and Dynamic Mobilities of Model Silica Colloids in Ethanol*, in preparation. (Chapter 5)

Other papers by the author:

- C.M. van der Wel, R.J. Kortschot, I.A. Bakelaar, B.H. Erné, and B.W.M. Kuipers, *Note: Rapid offset reduction of impedance bridges taking into account instrumental damping and phase shifting*, Review of Scientific Instruments 84, 036109 (2013).
- M. Marechal, R.J. Kortschot, A.F. Demirörs, A. Imhof, and M. Dijkstra, *Phase Behavior and Structure of a New Colloidal Model System of Bowl-Shaped Particles*, Nano Letters 10, 1907-1911 (2010).

Curriculum Vitae

Rob Kortschot was born on the 25th of June 1985 in Gorinchem. After graduation from the Gymnasium Camphusianum in Gorinchem in 2003, he started his chemistry studies at Utrecht University. He obtained his bachelor after finishing his bachelor thesis on dipolar structures in colloidal dispersions of bidisperse magnetite at the Van 't Hoff Laboratory for Physical and Colloid Chemistry under supervision of Mark Klokkenburg. His research for his master thesis on self-organisation of colloidal hemispherical caps was performed in the Soft Condensed Matter group under supervision of Arnout Imhof, Ahmet Demirörs, and Carmen Zoldesi. Also, a six-month internship was performed on the intrinsic stability of dye-sensitized solar cells at the Energy Research Centre of the Netherlands (ECN) under supervision of Paul Sommeling. After obtaining the masters degree (Nanomaterials: Chemistry and Physics) in 2009, he started as a PhD researcher at the Van 't Hoff Laboratory for Physical and Colloid Chemistry under supervision of Ben Erné and Albert Philipse. The results of this research are published in this thesis.